

Remote sensing of solar-induced chlorophyll fluorescence (SIF) in vegetation: 50 years of progress

Gina H. Mohammed^{a*}, Roberto Colombo^b, Elizabeth M. Middleton^c, Uwe Rascher^d,
Christiaan van der Tol^e, Ladislav Nedbal^d, Yves Goulas^f, Oscar Pérez-Priego^g,
Alexander Damm^{h,i}, Michele Meroni^j, Joanna Joiner^c, Sergio Cogliati^b,
Wouter Verhoef^e, Zbyněk Malenovsky^k, Jean-Philippe Gastellu-Etchegorry^l,
John R. Miller^m, Luis Guanterⁿ, Jose Moreno^o, Ismael Moya^f, Joseph A. Berry^p,
Christian Frankenberg^q, and Pablo J. Zarco-Tejada^{i,r,s,t}

^a*P&M Technologies, Sault Ste. Marie, Ontario, Canada*

^b*Remote Sensing of Environmental Dynamics Lab., University of Milano - Bicocca, Milan, Italy*

^c*NASA/Goddard Space Flight Center, Greenbelt, Maryland, United States*

^d*Forschungszentrum Jülich, Institute of Bio- and Geosciences, IBG-2: Plant Sciences, Jülich, Germany*

^e*University of Twente, Faculty of Geo-Information Science and Earth Observation,
Enschede, The Netherlands*

^f*CNRS, Laboratoire de Météorologie Dynamique (LMD), Ecole Polytechnique, Palaiseau, France*

^g*Department of Biogeochemical Integration, Max Planck Institute for Biogeochemistry, Jena, Germany*

^h*Department of Geography, University of Zurich, Zurich, Switzerland*

ⁱ*Eawag, Swiss Federal Institute of Aquatic Science and Technology, Dübendorf, Switzerland*

^j*European Commission, Joint Research Centre (JRC), Ispra (VA), Italy*

^k*Department of Geography and Spatial Sciences, School of Technology, Environments and Design,
College of Sciences and Engineering, University of Tasmania, Hobart, Australia*

^l*Centre d'Etudes Spatiales de la Biosphère – UPS, CNES, CNRS, IRD,
Université de Toulouse, Toulouse, France*

^m*Department of Earth and Space Science and Engineering, York University, Toronto, Canada*

ⁿ*German Research Center for Geosciences (GFZ), Remote Sensing Section, Potsdam, Germany*

^o*Department of Earth Physics and Thermodynamics, University of Valencia, Valencia, Spain*

^p*Department of Global Ecology, Carnegie Institution of Washington, Stanford, California, United States*

^q*Jet Propulsion Laboratory, California Institute of Technology, Pasadena, California, United States*

^r*Instituto de Agricultura Sostenible (IAS), Consejo Superior de Investigaciones
Científicas (CSIC), Córdoba, Spain*

^s*Department of Infrastructure Engineering, Melbourne School of Engineering,
University of Melbourne, Melbourne, Victoria, Australia*

^t*School of Agriculture and Food, Faculty of Veterinary and Agricultural Sciences,
University of Melbourne, Melbourne, Victoria, Australia*

38 *Correspondence: gina.mohammed@pmtech.ca
39 Revision-1 Submitted to: *Remote Sensing of Environment, 50th Anniversary Special Issue—*
40 *Marvin Bauer. 08 February 2019*

41 **Abstract**

42 Remote sensing of solar-induced chlorophyll fluorescence (SIF) is a rapidly advancing front in
43 terrestrial vegetation science, with emerging capability in space-based methodologies and
44 diverse application prospects. Although remote sensing of SIF – especially from space – is seen
45 as a contemporary new specialty for terrestrial plants, it is founded upon a multi-decadal history
46 of research, applications, and sensor developments in active and passive sensing of chlorophyll
47 fluorescence. Current technical capabilities allow SIF to be measured across a range of
48 biological, spatial, and temporal scales. As an optical signal, SIF may be assessed remotely using
49 highly-resolved spectral sensors and state-of-the-art algorithms to distinguish the emission from
50 reflected and/or scattered ambient light. Because the red to far-red SIF emission is detectable
51 non-invasively, it may be sampled repeatedly to acquire spatio-temporally explicit information
52 about photosynthetic light responses and steady-state behaviour in vegetation. Progress in this
53 field is accelerating with innovative sensor developments, retrieval methods, and modelling
54 advances. This review distills the historical and current developments spanning the last several
55 decades. It highlights SIF heritage and complementarity within the broader field of fluorescence
56 science, the maturation of physiological and radiative transfer modelling, SIF signal retrieval
57 strategies, techniques for field and airborne sensing, advances in satellite-based systems, and
58 applications of these capabilities in evaluation of photosynthesis and stress effects. Progress,
59 challenges, and future directions are considered for this unique avenue of remote sensing.

60 **Keywords**

61 (1) Sun-induced fluorescence; (2) Steady-state photosynthesis; (3) Stress detection; (4) Radiative
62 transfer modelling; (5) SIF retrieval methods; (6) Satellite sensors; (7) Airborne instruments;
63 (8) Applications; (9) Terrestrial vegetation; (10) Passive techniques; (11) Review.

64 **Table of contents**

65 Abstract..... 2
66 Keywords 3
67 1. Introduction 5
68 2. Steady-state chlorophyll fluorescence and vegetation physiology..... 9
69 2.1. Fluorescence basics..... 9
70 2.2. Methodological advances in measuring steady-state fluorescence under controlled
71 conditions 12
72 2.3. Transitioning from lab to field..... 15
73 2.4. Lessons from the laboratory for remote sensing of SIF 16
74 3. Early evidence of steady-state chlorophyll fluorescence effects on leaf and canopy spectra... 18
75 4. Modelling the effects of chlorophyll fluorescence through the canopy 24
76 4.1. Fundamentals of chlorophyll fluorescence modelling 24
77 4.2. Leaf physiological models of steady-state fluorescence 26
78 4.3. Leaf radiative transfer models for fluorescence 28
79 4.4. Canopy radiative transfer models for fluorescence 30
80 4.5. Integrated canopy fluorescence and photosynthesis models 35
81 4.6. Lessons learned using these models..... 36
82 4.7. Challenges and future directions in modelling 39
83 5. SIF estimation methods..... 41
84 5.1. General strategies..... 41
85 5.2. Retrieval of SIF at selected absorption bands 45
86 5.2.1. Oxygen absorption bands 47
87 5.2.2. Fraunhofer lines 48
88 5.3. Retrieval of the full SIF spectrum..... 49

89	5.3.1. Spectrum fitting.....	49
90	5.3.2. Model-inversion methods	50
91	5.4. Atmospheric correction, illumination, and surface anisotropy.....	51
92	5.5. Assessment of SIF retrieval accuracy	54
93	5.6. Challenges and future directions in SIF retrieval	55
94	6. SIF measurement technologies – Field and airborne systems.....	57
95	6.1. Technological overview	57
96	6.2. Hand-held leaf instrumentation	58
97	6.3. Top-of-canopy spectrometers	59
98	6.4. Airborne systems	62
99	6.4.1. Low-altitude systems – Unmanned aerial vehicles.....	62
100	6.4.2. Medium- or high-altitude systems	64
101	6.5. Adapting theory to the ‘real world’	68
102	6.6. Challenges and future directions in field and airborne sensing of SIF	70
103	7. SIF measurement technologies – Satellite systems	71
104	7.1. Technological overview	71
105	7.2. The FLuorescence EXplorer (FLEX): A tandem mission with Sentinel-3.....	72
106	7.3. Atmospheric chemistry satellites used for SIF retrieval	74
107	7.4. Factors affecting SIF retrieval accuracy of satellite data.....	79
108	7.5. Challenges and future directions in satellite sensing of SIF.....	81
109	8. Applications of remotely sensed SIF	83
110	8.1. Overview of application areas	83
111	8.2. Research uses and lessons learned.....	85
112	8.2.1. Ground-based canopy studies	85
113	8.2.2. Airborne-based studies	89
114	8.2.3. Satellite-based studies	92
115	8.3. Summary of SIF drivers and influential factors	95
116	8.4. Challenges and future directions.....	97
117	9. Conclusion.....	100
118	Acknowledgements	101
119	Acronyms and abbreviations.....	103
120	References	105
121		

122 **1. Introduction**

123 The first recorded observation of solar-induced fluorescence (SIF) was made almost two
124 centuries ago when Sir David Brewster, a Scottish preacher, discovered that a beam of sunlight
125 striking a green alcoholic extract of laurel leaves elicited a brilliant red light (Brewster, 1834).
126 He also noted that, as the light passed through successive ‘thicknesses’ of the extract, the
127 emission changed colour from red to orange to yellow – this transition possibly being the first
128 evidence of re-absorption by chlorophyll (Govindjee, 1995). Professor G.G. Stokes (1852) later
129 coined the term ‘fluorescence’ to describe the emission. The likelihood of a link between the
130 emission and photosynthetic assimilation was suggested by Müller (1874), and this idea was
131 confirmed in the seminal work of Kautsky and Hirsch (1931), who revealed the kinetics of
132 chlorophyll-*a* fluorescence (CF) emission in dark-adapted, suddenly illuminated leaves. Using
133 only their eyes to track the initial fluorescence peak and its prompt decay to a lower steady-state
134 level, they correlated this signature with the time course of CO₂ assimilation.

135 The theme of covariation between CF and photosynthesis was studied by McAlister and Myers
136 (1940), who described two processes, one involving an inverse relation between rate of CO₂
137 uptake and intensity of fluorescence, the other a direct relationship. The key to this dual response
138 was offered by Duysens and Sweers (1963), who pioneered the use of modulated excitation light
139 – as is used in modern-day pulse-amplitude modulation (PAM) fluorimetry – and were the first
140 to describe the active regulation of fluorescence yield by the process we now call “non-
141 photochemical quenching” (Krause and Weis, 1991; Weis and Berry, 1987). The Duysens and
142 Sweers (1963) approach was used to establish a quantitative relationship between fluorescence
143 yield and the rate of electron transport (Genty et al., 1989; Weis and Berry, 1987).

144 These pioneers prepared the stage for analysis of CF to become an established protocol in
145 photosynthesis research and applications in forestry, crop science, horticulture, and
146 ecophysiology (reviews by Baker and Rosenqvist, 2004; DeEll and Toivonen, 2003; Govindjee,
147 2004; Krause and Weis, 1991, 1984; Lichtenthaler, 1989; Lichtenthaler and Rinderle, 1988;
148 Mohammed et al., 1995; Papageorgiou and Govindjee, 2004). PAM fluorimetry is now used
149 routinely to monitor photosynthetic responses. CF is informative about the light reactions of
150 Photosystem II (PSII) especially, and is non-invasive, rapidly performed, and field-portable
151 (Duysens, 1963; Franck and Herzfeld, 1941; Franck et al., 1941; Papageorgiou and Govindjee,
152 2004; Porcar-Castell et al., 2014; Schreiber, 2004; Schreiber et al., 1986). The catch is that PAM
153 requires active manipulation of the light environment, limiting the approach to small scale (e.g.,
154 single leaf) applications.

155 As an optical signal, CF can be remotely sensed. This generally relies on passive measurement of
156 SIF instead of active techniques using artificial excitation light. Remote sensing of fluorescence,
157 already well-established in aquatic science since the early 1960s (reviews by Blondeau-Patissier
158 et al., 2014; Gower, 2016), is a more recent endeavour in terrestrial science (reviews by
159 Frankenberg and Berry, 2018; Malenovský et al., 2009; Meroni et al., 2009; Middleton et al.,
160 2018; Moya and Cerovic, 2004; Moya et al., 1992; Zhang et al., 2009). Passive airborne sensors
161 for fluorescence assessment include hyperspectral imaging systems able to retrieve discrete
162 emission bands and potentially the full SIF emission spectrum, with high spatial granularity for
163 field applications (e.g., Damm et al., 2011; Frankenberg et al., 2018; Meroni et al., 2009;
164 Rascher et al., 2015; Zarco-Tejada et al., 2018, 2013b).

165 Atmospheric satellite sensors from several missions have been used to measure far-red SIF in
166 terrestrial vegetation. They include: the Greenhouse gases Observing SATellite (GOSAT) –
167 Thermal And Near-infrared Sensor for carbon Observation Fourier Transform Spectrometer
168 (TANSO-FTS); the Meteorological Operational satellite (MetOp) – Global Ozone Monitoring
169 Experiment-2 (GOME-2) sensor; the Environmental Satellite (EnviSat) – SCanning Imaging
170 Absorption spectroMeter for Atmospheric CHartographY (SCIAMACHY), and MEidium
171 Resolution Imaging Spectrometer (MERIS); the Orbiting Carbon Observatory (OCO-2); the
172 Sentinel-5 Precursor (S-5P) – TROPOspheric Monitoring Instrument (TROPOMI); and the
173 Carbon Dioxide Observation Satellite (TanSat) – Atmospheric Carbon dioxide Grating
174 Spectrometer (ACGS) (Du et al., 2018; Frankenberg et al., 2011b; Guanter et al., 2007; Joiner et
175 al., 2012, 2011; Köhler et al., 2018a; Sun et al., 2018). Applications of this satellite data are
176 being studied for estimation of photosynthesis and stress effects (e.g., He et al., 2017; Köhler et
177 al., 2018b; Li et al., 2018b; MacBean et al., 2018; Middleton et al., 2018; Qiu et al., 2018; Smith
178 et al., 2018; Verma et al., 2017). None of those satellite systems were intended originally for
179 measuring SIF, and only recently was the first global mission approved that is designed
180 specifically for SIF measurement in terrestrial vegetation – the FLuorescence EXplorer (FLEX)
181 (Drusch et al., 2017).

182 The vision to utilize remotely-detected fluorescence for ecological purposes is not entirely new.
183 Almost 30 years ago, Krause and Weis (1991) presciently speculated that “...extension of
184 fluorescence measurements to large-scale spectroscopy may be useful in basic and applied
185 environmental research, such as mapping of the photosynthetic activity of terrestrial and marine
186 vegetation.” Progress in that direction was realized when chlorophyll fluorescence was shown

187 experimentally and analytically to be a signal superimposed upon apparent reflectance spectra in
188 leaves and canopies (Zarco-Tejada et al., 2000a, 2000b). Later, Moya and Cerovic (2004)
189 commented that “...it is surprising that, even after a quarter of a century of research on satellite
190 detection of chlorophyll fluorescence, no operational system has yet even been developed” (a
191 situation they considered true to some extent for airborne systems as well). Today, there are
192 exceptional breakthroughs on these fronts – in SIF sensor technologies, retrieval algorithms, and
193 the modelling of leaf and canopy fluorescence and photosynthesis (Cogliati et al., 2015b; Damm
194 et al., 2014; Frankenberg et al., 2012; Gastellu-Etchegorry et al., 2017; Hernández-Clemente et
195 al., 2017; Joiner et al., 2016; Pedrós et al., 2010; Van der Tol et al., 2014, 2009a, 2009b; Verhoef
196 et al., 2018; Vilfan et al., 2016; Zarco-Tejada et al., 2013b, 2006; Zhao et al., 2016). Much has
197 occurred in fluorescence science since Brewster recorded that first observation! Now,
198 fluorescence may be ‘viewed’ at multiple and complementary scales, even from space.

199 This review synthesizes developments in terrestrial SIF remote sensing over the last 50 years. It
200 covers essential fluorescence basics, historical progress delineating fluorescence effects upon
201 leaf and canopy reflectance spectra, advances in modelling, SIF retrieval methods, remote
202 sensing technologies, and applications. As a synoptic overview, it complements recent reviews
203 focused more specifically on fluorescence-photosynthesis linkages, SIF retrieval methods,
204 applications, and/or instrumentation (Ač et al., 2015; Frankenberg and Berry, 2018; Garbulsky et
205 al., 2014a, 2014b; Malenovský et al., 2009; Meroni et al., 2009; Middleton et al., 2018; Porcar-
206 Castell et al., 2014; Zhang et al., 2009).

207 This paper is dedicated to Dr. Marvin Bauer, who was pivotal for the communication of
208 scientific advances on remote sensing of chlorophyll fluorescence during his tenure as Senior

209 Editor of *Remote Sensing of Environment*. Dr. Bauer engaged this emerging specialty with
210 curiosity and caution, weighing its application and relevance to the field of remote sensing.
211 Subsequent reporting of fluorescence science in this journal (and others) over the decades attests
212 to his willingness to debut many advances in this field.

213 **2. Steady-state chlorophyll fluorescence and vegetation physiology**

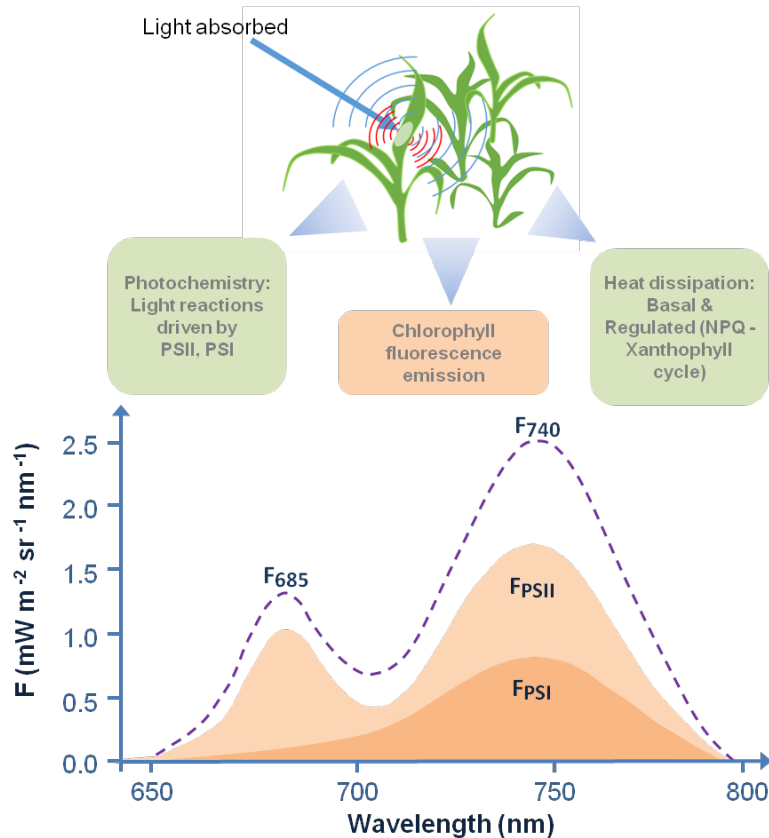
214 **2.1. Fluorescence basics**

215 The CF spectral emission spans approximately 650-800 nm in intact leaves, with two maxima –
216 one in the red spectral region around 685-690 nm (F_{685}) and the other a shoulder in the far-red
217 (near-infrared) around 730-740 nm (F_{740}). Two photosystems are involved: PSII, which emits in
218 both the red and far-red regions of the spectrum, and PSI, which emits mainly in the far-red
219 (Boardman et al., 1966; Govindjee, 1995; Pfündel, 1998) (**Figure 1**). Emission of CF is one of
220 the pathways by which plants dissipate excitation energy absorbed from Photosynthetically
221 Active Radiation (PAR), the others being photochemical electron transport, and two types of
222 thermal energy dissipation – constitutive (i.e., internal conversions at the level of the chlorophyll
223 molecule that operate over the longer term or seasonally), and regulated (i.e., photosystem and
224 molecular processes that respond rapidly to short-term changes in light intensity) (Hendrickson
225 et al., 2004; Krause and Weis, 1991; Lichtenthaler and Rinderle, 1988; Papageorgiou and
226 Govindjee, 2004; Porcar-Castell et al., 2014).

227 The dynamic nature of fluorescence emission from plants – evident in response to varying light
228 intensity or, in the extreme, to sudden dark-light transition – is due to changing photochemical
229 and non-photochemical quenching in the photosystem. The term quenching may be used to

230 represent all processes that reduce fluorescence emission (Krause and Weis, 1991).
231 Photochemical quenching (PQ) indicates the availability of open PSII reaction centers for
232 photochemistry. In dark-adapted foliage that is suddenly exposed to strong light, PQ is quickly
233 saturated, causing fluorescence to rise to a maximum (F_{\max}); concomitantly, non-photochemical
234 processes are triggered to harmlessly dissipate absorbed excessive light energy until PQ is re-
235 established and allowing fluorescence to decline to a 'steady-state' level after a few minutes of
236 illumination (Demmig-Adams et al., 2012). Outdoors, steady-state fluorescence is dynamically
237 tuned by the balance of photochemical and non-photochemical processes responding to light
238 intensities and other environmental conditions. CF quantum yield *in vivo* usually is less than
239 10%, with typical values of 0.5-3% under steady-state illumination (Porcar-Castell et al., 2014,
240 and references therein).

241 Steady-state fluorescence is sometimes called terminal or stationary fluorescence (in Kautsky
242 induction kinetics) and denoted as F_T , F_t , or F_S (Maxwell and Johnson, 2000; Van Kooten and
243 Snel, 1990). Specific metrics quantify F_T , F_t , or F_S (Toivonen and Vidaver, 1984; Schreiber et
244 al., 1986); PSII maximal or effective quantum yield (Genty et al., 1989); amplitude of the
245 individual emission peaks, or their ratio (Agati et al., 1995; Campbell et al., 2007; Kuckenberget
246 al., 2009; Lichtenthaler and Rinderle, 1988); fluorescence lifetime (Cerovic et al., 1996); spectral
247 wavelength position of the peaks (Kancheva et al., 2007); fluorescence band width (Subhash and
248 Mohanan, 1997); area under the spectral emission curve (Srivastava and Pandey, 2012; Subhash,
249 1995); and fluorescence spatial patterns (Lichtenthaler and Rinderle, 1988).



250
251

252 **Figure 1.** Distribution of absorbed light energy in leaves under steady-state conditions. Absorbed
 253 light may be used for photochemistry, dissipated thermally, or re-emitted as chlorophyll
 254 fluorescence. Lower graph: Conceptual figure of leaf fluorescence emission, with maxima in the
 255 red and far-red spectral regions, and arising from photosystems PSII and PSI. PSII contributes to
 256 both red and far-red emissions, and PSI mainly to the far-red region. In healthy green leaves the
 257 red peak typically is lower than the far-red one, due to greater re-absorption of red fluorescence
 258 by chlorophyll during the transit of fluorescence to the leaf surface. (Plant drawing courtesy of
 259 C. van der Tol; lower graph courtesy of U. Rascher, and adapted.)

260 Sensitivity of PSII reactions to abiotic and biotic stresses results in impairments of
 261 photochemical electron transport capacity, often readily echoed in changes to the fluorescence
 262 emission (Ač et al., 2015). Strategies for photoprotection are thus needed and involve multiple
 263 mechanisms in addition to thermal dissipation. These include scavenging of reactive oxygen
 264 species, regulation of light absorption via leaf or chloroplast movements, redistribution of light
 265 energy between PSII and PSI via state transitions (migration of light harvesting complexes), and

266 adjustments in photosystem stoichiometry (relative amounts of PSII and PSI) (Dall'Osto et al.,
267 2014; Demmig-Adams et al., 2012; Krause and Weis, 1991). Although these are 'non-
268 photochemical' in a generic sense, the more specific, regulated thermal dissipation is usually
269 intended by the term 'non-photochemical quenching' (NPQ), which is assessed by active
270 fluorescence sensors (albeit imperfectly as they cannot exclude all the other forms of
271 photoprotection during measurement). Two NPQ mechanisms are the xanthophyll cycle
272 involving interconversion of violaxanthin, antheraxanthin, and zeaxanthin pigments (Demmig-
273 Adams et al., 2012; Goss and Lepetit, 2015), and the xanthophyll lutein-epoxide cycle
274 (Matsubara et al., 2007).

275 By the time fluorescence emission reaches a remote sensor, it has been subjected to the
276 influences of diverse drivers in the vegetation, environment, and atmosphere, which can affect
277 quenching, light absorption, re-absorption and scattering of fluorescence signals [see also
278 **Sections 4 and 8**]. Disentangling the effects and importance of the various factors in a given
279 situation is a focus of mechanistic interpretation of fluorescence data [**Section 4**] and is relevant
280 to the effective usage of fluorescence as an optical proxy for photosynthesis and associated stress
281 effects (Ac et al., 2015; Paul-Limoges et al., 2018; Verrelst et al., 2016, 2015b).

282 **2.2. Methodological advances in measuring steady-state fluorescence under** 283 **controlled conditions**

284 Fluorescence assessment in the laboratory, growth chamber, or greenhouse has utilized a suite of
285 measurement devices, including fluorescence microscopes, spectroscopic or spectrofluorimetric
286 devices, portable fluorometers, and imaging tools (Kalaji et al., 2012; Mohammed et al., 1995).

287 These have allowed study of fluorescence induction kinetics and steady-state behaviour scales
288 ranging from isolated photosystems to small vegetation canopies (**Table 1**) (reviews by Bolhàr-
289 Nordenkampf et al., 1989; Fernandez-Jaramillo et al., 2012; Kalaji et al., 2012; Mohammed et
290 al., 1995), and visualization of leaf fluorescence to better understand ultrastructural influences on
291 light absorption, scattering, transmission, and fluorescence re-absorption (Kalaji et al., 2012).
292 They have been helpful for examining spatial distribution of fluorescence in the leaf, and non-
293 chlorophyll fluorophores and absorbers in leaf tissues (Bornman et al., 1991; Buschmann et al.,
294 2000; Chappelle and Williams, 1987; Kalaji et al., 2012; Vogelmann and Evans, 2002).

295 Imaging reveals spatial and temporal heterogeneities in CF on leaf or plant surfaces due to biotic
296 and abiotic stress factors (Barón et al., 2016; Buschmann et al., 2009; Donaldson and Williams,
297 2018; Gorbe and Calatayud, 2012; Nedbal and Whitmarsh, 2004; Nedbal et al., 2000;
298 Oxborough, 2004; Rascher and Lüttge, 2002; Rascher et al., 2001). Imaging techniques have also
299 been combined with other methods like gas exchange or infrared thermography for
300 comprehensive details on spatial distribution of photosynthetic variables, stomatal function, and
301 water use efficiency (Chaerle et al., 2007; Lawson, 2009; Murchie and Lawson, 2013).

302

303 **Table 1.** Laboratory technologies to measure steady-state fluorescence. Symbols: ✓ standard
 304 feature, ⊙ requires specialized configuration, ◇ provides mainly qualitative information.

Technology type	Steady-state CF feature							
	Location within leaf	Amplitude (intensity)	Quenching analysis	Life-time	Red, far-red, full emission	Integrated CF over branch / plant	Effective PSII quantum yield	Heterogeneity of CF over leaf / plant
fluorescence microscopes [1]	✓	◇	-	-	-	-	-	✓
cryo-F-microscopes [2]	✓	✓	⊙	-	⊙	-	⊙	-
confocal & two-photon microscopes [3]	✓	◇	⊙	-	-	-	-	-
fiber-optic microprobes [4]	✓	✓	-	-	-	-	-	-
imaging systems (PAM etc.) [5]	-	✓	✓	-	-	✓	✓	✓
high-resolution spectrometers (spectroradiometers) [6]	-	✓	-	-	-	-	-	-
spectro-fluorimeters [7]	-	✓	-	-	✓	-	-	✓
continous excitation fluorometers [8]	-	✓	-	-	-	-	-	-
integrating- sphere fluorometer [9]	-	✓	-	-	-	✓	-	-
laser-induced fluorescence (LIF) systems [10]	✓	✓	✓	-	✓	-	-	✓
τ-LIDARs [11]	-	-	-	✓	-	-	-	-
PAM systems (excluding imaging) [12]	-	✓	✓	-	-	-	✓	-
laser-induced fluorometers measuring fluorescence transients, PSII effective antenna size [13]	-	-	-	-	-	-	✓	-

305 [1] Buurman et al., 1992; Kalaji et al., 2012; Murchie and Lawson, 2013. [2] Vácha et al., 2007. [3] Benediktyová
 306 and Nedbal, 2009; Osmond et al., 1999. [4] Bornman et al., 1991. [5] Aldea et al., 2006; Calatayud et al., 2006;
 307 Genty and Meyer, 1995; Gorbe and Calatayud, 2012; Nedbal et al., 2000; Oxborough, 2004. [6] Dobrowski et al.,
 308 2005; Julitta et al., 2016; Magney et al., 2017; Zarco-Tejada et al., 2003, 2001, 2000a, 2000b. [7] Boardman et al.,
 309 1966; Gitelson et al., 1998; Govindjee, 1995; Mohanty et al., 1972; Papageorgiou, 1975.
 310 [8] Bolhár-Nordenkamp et al., 1989*; Mohammed et al., 1995*; Öquist and Wass, 1988; Strasser et al., 1995.
 311 [9] Toivonen and Vidaver, 1984. [10] Buschmann and Lichtenthaler, 1998; Buschmann et al., 2000; Cecchi et al.,
 312 1994; Lichtenthaler and Rinderle, 1988*; Omasa et al., 2007; Ounis et al., 2001; Rosema et al., 1991; Stober et al.,
 313 1994; Szabò et al., 1992. [11] Cerovic et al., 1996; Moya et al., 1995. [12] Magney et al., 2017; Schreiber, 2004;
 314 Schreiber et al., 1986. [13] Keller et al., 2018; Kolber and Falkowski, 1993; Kolber et al., 1998; Nedbal et al., 1999.
 315 *Review papers.

316 Laboratory spectroscopic methods have allowed examination of fluorescence induction and
317 decay kinetics, derivation of excitation-emission matrices (Louis et al., 2006), and
318 discrimination of PSII and PSI fluorescence bands (Franck et al., 2002; Palombi et al., 2011;
319 Papageorgiou, 1975; Vácha et al., 2007). They have also supported the development of leaf and
320 canopy fluorescence models (Pedrós et al., 2010, 2008; Van der Tol et al., 2009a, 2009b).
321 Combinations and special configurations of various devices have also been used – such as a
322 PAM fluorometer with a spectroradiometer to probe changes in the green spectral region related
323 to NPQ (Gamon et al. 1997, 1992, 1990; Wong and Gamon, 2015); a fluorescence spectrometer
324 and an integrating sphere to quantify fluorescence re-absorption by chlorophyll (Gitelson et al.,
325 1998); an integrating sphere with spectral detectors to study CF in whole plants or branches
326 (Toivonen and Vidaver, 1984) or fluorescence effects on apparent reflectance (Zarco-Tejada et
327 al., 2003, 2000a, 2000b); and passive with active sensors to follow induction kinetics (Moya et
328 al., 2004), spectrally-resolved fluorescence emission signatures, quenching parameters, and other
329 photosynthetic variables (Magney et al., 2017; Wyber et al., 2017).

330 **2.3. Transitioning from lab to field**

331 Since the late 1980s, portable devices increasingly dominated laboratory and field-based CF
332 science. The PAM systems have been used extensively for leaf-level work (Schreiber, 2004;
333 Schreiber et al., 1986) (e.g., from Heinz Walz GmbH, Germany; Hansatech Instruments Ltd.,
334 UK; Photon Systems Instruments, Czech Republic; Opti-Sciences, USA). Some systems also
335 measure gas exchange, chlorophyll content, and other spectral characteristics (e.g., from PP
336 Systems, USA; LI-COR, USA; PhotosynQ, USA). Fluorescence lifetime has also been analyzed,
337 as it is correlated with CF yield and feasible for short-distance assessments (e.g., a few meters)

338 (Cerovic et al., 1996; Moya and Cerovic, 2004; Moya et al., 1995; Terjung, 1998). Micro-lidars
339 have been used in short-range work (1-10 meters) (Flexas et al., 2000; Ounis et al., 2001), but
340 delivering high intensity light pulses from great distances in order to saturate photosynthesis has
341 been technically challenging. LIFT methods (Kolber et al., 2005) use fast repetition of high-
342 power laser diode pulses to partially reduce the plastoquinone pool and can allow distances up to
343 50 m. A recent refinement is smaller and still allows a full suite of active fluorescence
344 parameters and canopy reflectance in a fast scanning mode (Keller et al. in press).

345 Airborne lasers for excitation of fluorescence generally require high-peak-power sources
346 (Chekalyuk et al., 2000; Hoge and Swift, 1981; Kim, 1973) that can pose risks to eye safety.
347 However, Ounis et al. (2016) found that eye safety is achievable with appropriate operational
348 conditions using an airborne platform for laser-induced fluorescence (LIF), SIF, reflectance, and
349 waveform analysis of the backscattered laser signal – thereby deriving a multiple set of
350 vegetation variables to help disentangle the various SIF drivers.

351 **2.4. Lessons from the laboratory for remote sensing of SIF**

352 Research into fluorescence-photosynthesis relationships, stress effects, and confounding factors
353 has been greatly facilitated by the variety of measurement tools and the use of controlled studies.
354 Such studies have been helpful for development and refinement of models representing
355 fluorescence-photosynthesis linkages in different vegetation types, radiative transfer of
356 fluorescence in leaves and small canopies, and fluorescence superimpositional effects upon
357 reflectance [Sections 3 & 4]. Key messages have emerged from such research. First, steady-state
358 fluorescence is influenced not only by PQ and NPQ, but also light absorption by chlorophyll,

359 environmental conditions, structural traits, and stress factors (Buschmann, 2007; Cecchi et al.,
360 1994; Chappelle and Williams, 1987; Stober et al., 1994; Valentini et al., 1994). Therefore –
361 ancillary information is needed to reduce sources of error in interpretation of fluorescence
362 changes and for parameterization of models (Mohammed et al., 2016, 2003, 1995). Second, since
363 re-absorption reduces the visible fluorescence below that initially produced by the photosystems
364 (e.g., Gitelson et al., 1998; Lichtenthaler and Rinderle, 1988), quantification of the re-absorption
365 effect requires radiative transfer theory [**Section 4**] and understanding of leaf anatomical effects
366 on light penetration, scattering, transmission, and re-absorption. Third, it can be advantageous to
367 measure more than one fluorescence variable. Having both red and far-red fluorescence has been
368 shown empirically to be advantageous for studying fluorescence-photosynthesis associations,
369 stress effects, and influences due to vegetation type (Chappelle and Williams, 1987; Valentini et
370 al., 1994). Several steady-state fluorescence indicators have been identified from fundamental
371 studies and are relevant for the design of future remote sensors and associated ground-based
372 activities (Drusch et al., 2017; Fernandez-Jaramillo et al., 2012; Maxwell and Johnson, 2000;
373 Mohammed et al., 2003, 1995; Roháček et al., 2008).

374 Transferability of lab-based fluorescence results to field situations, and of active to passive
375 methods, is subject to caveats. Laboratory results might not mirror in-situ behaviour due to
376 differences in growing environment, sampling protocols, and sensor operating conditions
377 (Maxwell and Johnson, 2000; Stober et al., 1994). Data from active and passive techniques might
378 not be consistently comparable (Goulas et al., 2017; Porcar-Castell et al., 2014; Rascher et al.,
379 2009), and this continues to be investigated (Ač et al., 2015; Cecchi et al., 1994; Magney et al.,
380 2017; Wyber et al., 2017). Artificial excitation light sources differ from sunlight in spectral

381 composition, intensity and directionality (affecting light penetration, emission wavelength, and
382 re-absorption) (Cerovic et al., 1999). Portable fluorometers using red excitation light can be
383 biased toward the far-red region of the emission (to avoid overlap between excitation and emitted
384 light) (Kalaji et al., 2014; Porcar-Castell et al., 2014), whereas blue light stimulates the full CF
385 emission but mainly from superficial leaf layers. A helpful approach is to analyze excitation-
386 emission matrices to reveal illumination effects (Corp et al., 2003; Louis et al., 2006; Middleton
387 et al., 2008). Further comparative work is warranted, and assumptions must be well understood
388 (Porcar-Castell et al., 2014).

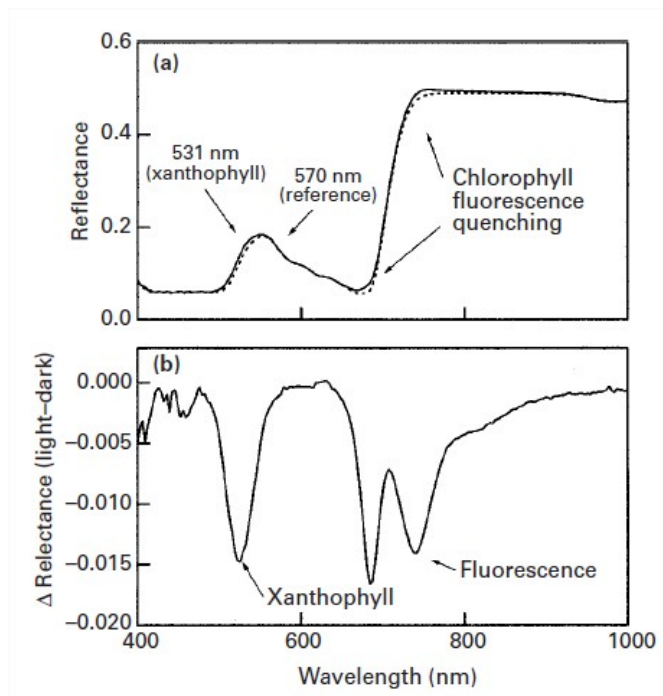
389 Recognizing those caveats, future lab-scale or controlled-environment trials can support SIF
390 remote sensing activities in several ways: (i) creation of spectral-fluorescence-physiology
391 databases and libraries to support calibration, modelling and interpretation of remotely sensed
392 SIF; (ii) elucidation of confounding factors for interpretation of SIF changes; (iii) identification
393 of ancillary data types needed for airborne or space-based missions; (iv) prototyping and
394 refinement of remote sensor specifications and spatio-temporal sampling protocols; (v) testing of
395 field sensors to be used in ground-truthing and validation; and (vi) determination of confidence
396 margins and constraints for applications, based on vegetational and environmental variables.

397 **3. Early evidence of steady-state chlorophyll fluorescence effects on leaf and** 398 **canopy spectra**

399 Before the year 2000, measurement technology was limited in its capacity to provide convincing
400 evidence that for vegetation in natural light the very small upwelling fluorescence signal could
401 be reliably distinguished in the presence of the dominant reflected radiance signal.

402 Consequently, first references on the topic were qualitative or tentative. Buschmann and
403 Lichtenthaler (1988) inspected reflectance and fluorescence signatures using the Visible Infrared
404 Reflectance Absorbance Fluorescence (VIRAF) spectrometer and concluded that the
405 fluorescence emission could probably influence the red edge spectral region – in particular
406 around 750 nm. McFarlane et al. (1980) and Carter et al. (1996, 1990) used a Fraunhofer Line
407 Radiometer and the Fraunhofer Line Depth (FLD) measurement principle to study fluorescence
408 in the H α line (656 nm) and the O₂-B absorption band (687 nm), revealing changes in SIF from
409 leaves or canopies with treatments of herbicide, water stress, or light regime. Later, other studies
410 evaluated relationships between reflectance indices and fluorescence, especially the trends
411 obtained between the PRI vs. fluorescence-based indicators of PSII photochemical efficiency in
412 the context of radiation-use-efficiency estimations (Gamon et al., 1997; Peñuelas et al., 1998,
413 1997). Using calculations of reflectance-difference spectra between dark-adapted and light-
414 adapted leaves, Gamon and Surfus (1999) showed that xanthophyll pigment de-epoxidation and
415 CF emission affected the reflectance signatures of vegetation after exposure to white light
416 (**Figure 2**). Nevertheless, the main focus of this work was on the PRI, and particularly its relative
417 increment (Δ PRI) as a direct indicator of xanthophyll cycle pigment activity. As yet, no
418 quantitative assessments were carried out to demonstrate the reliability of the fluorescence
419 emission extracted from the leaf spectral radiance or apparent spectral reflectance.

420 After these first qualitative demonstrations of the potential effects of chlorophyll fluorescence
421 superimposed on the apparent reflectance, a series of laboratory-based experiments were
422 undertaken aimed at its quantitative assessment both at the leaf level (Zarco-Tejada et al., 2000a,
423 1999a) and at the canopy level using the Compact Airborne Spectrographic Imager (CASI)



424

425 **Figure 2.** Leaf reflectance spectra of *Helianthus annuus* (sunflower), (a) in the dark state (solid
 426 line) and after 10 minutes of exposure to light (dotted line); (b) reflectance-difference calculation
 427 (dark-state minus light-state), showing the effects due to xanthophyll pigment de-epoxidation in
 428 the green region, and chlorophyll fluorescence quenching in the red-edge region. (Source:
 429 Gamon and Surfus, 1999.)

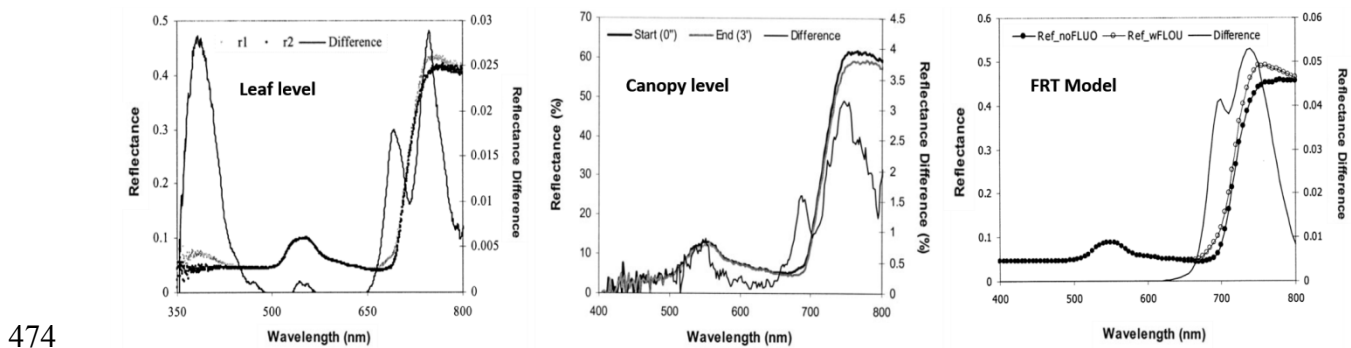
430 (Zarco-Tejada et al., 2000b, 1999b). Experiments were conducted with an integrating sphere to
 431 examine the leaf optical properties with and without a cut-off bandpass filter (<695 nm),
 432 allowing leaves to be illuminated thereby without and with fluorescence-exciting radiation
 433 (**Figure 3**, left). These experiments were also carried out with the CASI to acquire imagery over
 434 plant seedlings (**Figure 3**, centre), which enabled the quantitative demonstration at the image
 435 level (i.e., canopy level) of a fluorescence signal superimposed upon the apparent reflectance.
 436 These results were further validated via the development of a leaf radiative transfer model
 437 (RTM), named the Fluorescence–Reflectance–Transmittance (FRT) model, based on the
 438 doubling method that accounted for the within-leaf fluorescence signal (Zarco-Tejada et al.,
 439 2000a) (**Figure 3**, right). These leaf- and canopy-level experiments, along with the physical

440 modelling approach, served as a quantitative demonstration that the fluorescence emission could
441 be extracted and, more importantly, that the observed fluorescence signal effects on the apparent
442 reflectance agreed with independently acquired fluorescence data using the PAM-2000
443 instrument. It was further demonstrated that the experimental protocols used to extract the
444 fluorescence signal from the leaf reflectance spectra were consistent with basic radiative transfer
445 theory.

446 Those experiments and the modelling work proved that the SIF emission was superimposed upon
447 the apparent reflectance acquired by the “*narrow-band*” imaging spectrometers of that time (i.e.,
448 imagers with spectral resolution, SR, in the range of 2.5 to 10 nm full-width-at-half-maximum,
449 FWHM). Further efforts attempted to quantify the fluorescence signal under natural illumination
450 (Zarco-Tejada et al., 2002, 2001) using CASI imagery acquired over *Acer saccharum* M. (sugar
451 maple) sites in Canada. Flights conducted over the course of diurnal experiments under natural
452 light conditions and over forest sites with different levels of stress demonstrated that the SIF
453 signal could be extracted by reflectance subtraction methods. Reflectance differences calculated
454 between early and midday imagery acquired by CASI showed spectral differences that at the
455 time were associated with the diminution of the fluorescence emission as a function of stress
456 over the course of the diurnal cycle. Moreover, the derivative reflectance calculated from
457 canopy-level CASI airborne imagery showed a peak at the 700-730 nm region which was
458 experimentally shown to relate to stress conditions and potentially to be caused by fluorescence
459 emission and chlorophyll content changes in vegetation under stress.

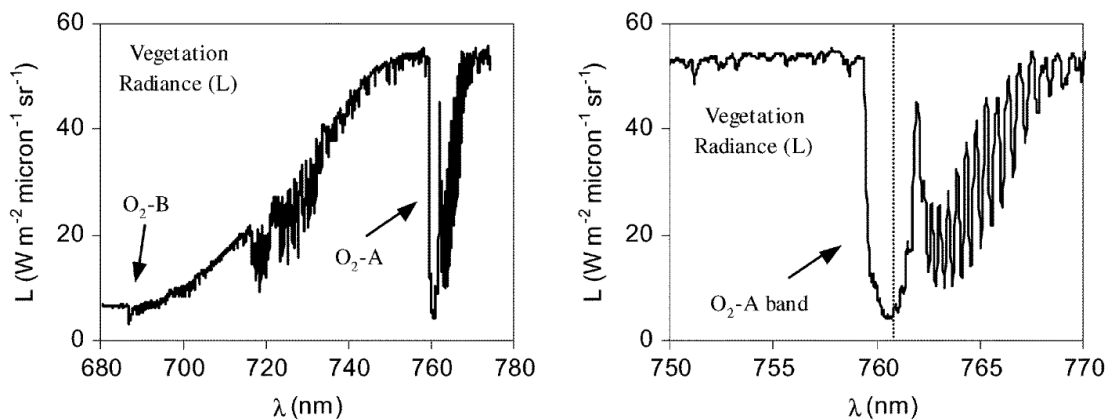
460 The derivative-based peak feature discussed in Zarco-Tejada et al. (2002), which responded as a
461 function of forest health condition, was further investigated in a series of laboratory experiments

462 (Dobrowski et al., 2005; Zarco-Tejada et al., 2003). The studies of this feature, observed on the
 463 derivative reflectance with heat- and light-induced stress in growth chambers, demonstrated that
 464 the diurnal dynamics of the chlorophyll fluorescence emission could be tracked at the canopy
 465 level, mimicking the dynamics of the steady-state fluorescence measured concurrently and
 466 corresponding with induced stress levels. Dobrowski et al. (2005) successfully extracted the
 467 fluorescence signal in diurnal experiments designed to induce stress, analyzing the dynamics of
 468 the recovery from stress in the reflectance spectra. They proved the link between the
 469 fluorescence variables extracted from canopy reflectance and plant photosynthesis measured at
 470 the same time. Later, Campbell et al. (2008) showed the contribution of CF to the apparent
 471 reflectance of corn leaves in time-resolved laboratory measurements using a solar simulator and
 472 blocking filters (which blocked incoming light in the PAR region to prevent fluorescence
 473 excitation, similarly to what was done by Zarco-Tejada et al., 2000a).



474
 475 **Figure 3.** Reflectance differences between a dark-adapted and light-adapted leaf of *Acer*
 476 *saccharum* (sugar maple) showing the spectral differences in the blue region, in the green region
 477 due to the xanthophyll pigment dynamics, and in the red edge region due to the fluorescence
 478 emission (**left**). Canopy level reflectance of dark-adapted seedlings after illumination with white
 479 light, showing the fluorescence signal extracted by spectral subtraction using the CASI imager
 480 after three minutes (**centre**). First attempts of fluorescence simulation by radiative transfer with
 481 the Fluorescence–Reflectance–Transmittance model to simulate leaf reflectance accounting for
 482 the fluorescence emission (**right**). (Source: Zarco-Tejada et al., 2000a, 2000b.)

483 New experiments to extract chlorophyll fluorescence signals using the FLD principle with the
484 oxygen absorption feature became possible with spectrometers able to provide sub-nanometer
485 resolutions [Section 5] (Meroni and Colombo, 2006; Pérez-Priego et al., 2005). In water stress
486 experiments conducted under natural light and field conditions, Pérez-Priego et al. (2005)
487 demonstrated that the radiance in-filling within the O₂-A feature was related to steady-state
488 fluorescence, an indicator of the water stress dynamics over the course of diurnal experiments.
489 More importantly, they proved experimentally that sub-nanometer spectrometers could be used
490 to understand the radiance variations embedded in the O₂-B and O₂-A absorption bands
491 (Figure 4). This approach would be used several years later, along with narrow-band
492 spectrometers, as standard protocols for validation of fluorescence results. The FLD principle has
493 been successfully applied to leaf radiance spectra track changes in the photosynthetic apparatus
494 of herbicide-treated vegetation (Meroni and Colombo, 2006), demonstrating the feasibility of the
495 oxygen features for fluorescence quantification using high-resolution spectrometers [Section 5].



496
497 **Figure 4.** Canopy radiance measured from *Olea europaea* (olive) trees under water stress levels
498 using a sub-nanometer spectrometer covering the O₂-B and O₂-A regions (left) and the detailed
499 absorption features observed (right). (Source: Pérez-Priego et al., 2005.)

500 The experiments described here were critical for the understanding of the fluorescence emission
501 effects on apparent reflectance and for convincing the scientific community of the feasibility of
502 measuring fluorescence from passive reflectance spectra. (Although now widely accepted,
503 doubts still existed until the late 1990s.) The initial qualitative descriptions by Buschmann and
504 Lichtenthaler (1988) followed by Gamon and Surfus (1999) served to encourage further progress
505 on the quantitative assessments as part of detailed experiments carried out in the laboratory and
506 under natural light conditions, both at the leaf and at the canopy levels (Zarco-Tejada et al.,
507 2000a, 2000b). The conclusions of these studies seeded the development of the first robust
508 RTMs to account for the fluorescence emission at both the leaf and canopy levels, and stimulated
509 an in-depth analysis of more advanced methodologies for the retrieval of chlorophyll
510 fluorescence using the FLD principle – widely used currently, but poorly understood at the
511 beginning of the millennium.

512 **4. Modelling the effects of chlorophyll fluorescence through the canopy**

513 **4.1. Fundamentals of chlorophyll fluorescence modelling**

514 The development of technologies and retrieval algorithms to evaluate fluorescence has
515 progressed hand in hand with model developments. Measurement of active chlorophyll
516 fluorescence in plant leaves, often combined with analysis of gas exchange [**Section 2**], has
517 played a crucial role in fundamental research on plant photosynthesis and has supported the
518 development of mathematical models for leaf photosynthesis (Farquhar et al., 1980). . These
519 models have been implemented in global land surface models for climate research (for a review,
520 see Pitman, 2003), which has entailed upscaling of modelled photosynthetic processes from the

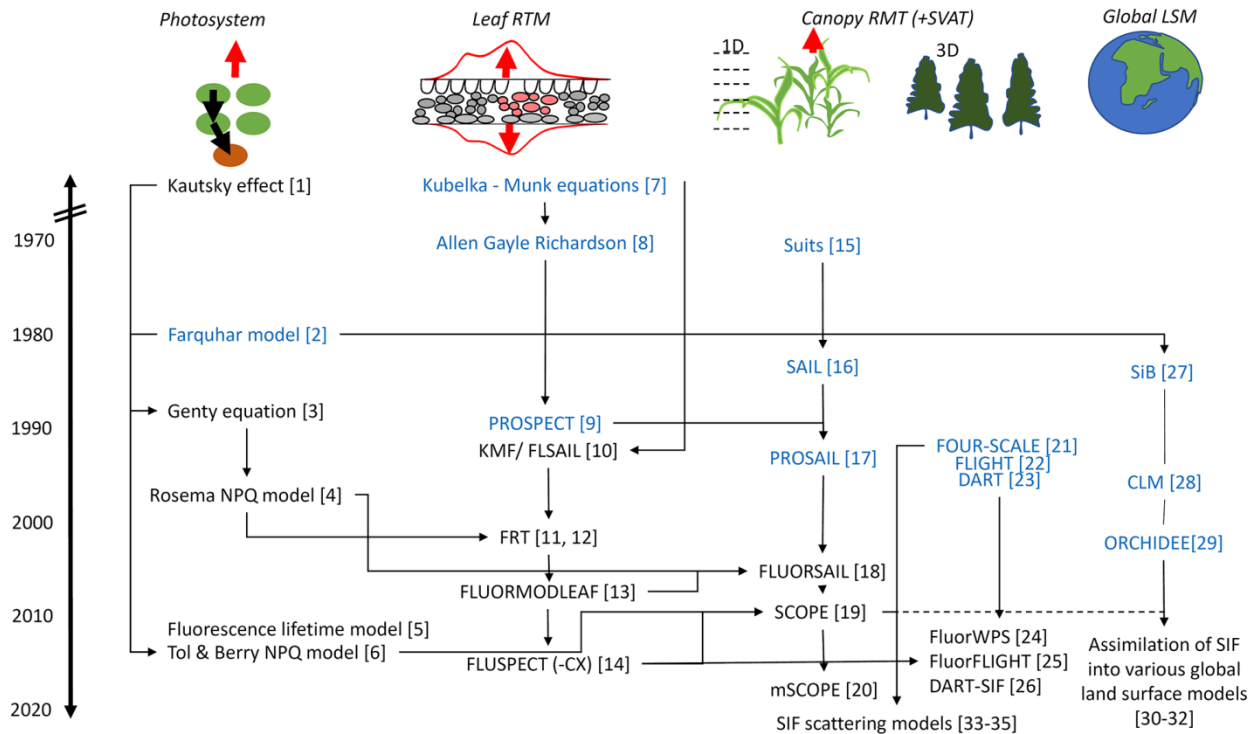
521 leaf to the stand level (or ‘vegetation canopy’) and differentiation between sunlit and shaded
522 leaves (De Pury and Farquhar, 1997). In general, two-stream (simulating direct and diffuse
523 fluxes) RTMs have been implemented in dynamic vegetation models such as the Boreal
524 Ecosystems Productivity Simulator (BEPS) (Liu et al., 1997), Biome-BGC (Chen et al., 1999),
525 and land surface models such as CLM2 (Dai et al., 2004), CLM4 (Bonan et al., 2011), and the
526 Breathing Earth System Simulator (BESS) (Ryu et al., 2011). Contemporary analyses of airborne
527 and satellite fluorescence have further stimulated the development of models as scaling tools.

528 In contrast to measurements of conducted on individual leaves, SIF retrieved from Top-of-
529 Canopy (TOC) data is subject to complexities of canopy structure and coverage, solar
530 illumination angle, soil brightness, stem and branch effects, leaf pigments, and other drivers
531 [Sections 2, 8] (Fournier et al., 2012; Middleton et al., 2018; Porcar-Castell et al., 2014; Rosema
532 et al., 1991). Quantitative modelling of such effects allows a way to integrate them and to use
533 SIF in parameterizing terrestrial vegetation traits in land surface models (Lee et al., 2015;
534 Norton et al., 2018).

535 In essence, models for canopy photosynthesis describe light absorption and utilization, whereas a
536 canopy-level model for fluorescence describes three key processes: (i) the absorption of incident
537 radiation; (ii) the subsequent emission as fluorescence; and (iii) the scattering and re-absorption
538 of fluorescence through the canopy after emission.

539 Knowledge about the relationships between fluorescence, electron transport and photochemistry
540 in leaves (e.g., Schreiber et al., 1995) did not include the variability caused by the canopy
541 structure on absorption and scattering. These aspects have been addressed in a different
542 disciplinary field, using radiative transfer theory (Jacquemoud et al., 2009). During the last two

543 decades, that work has resulted in models that quantify the key processes and their
 544 interdependencies (**Figure 5**).



545

546 **Figure 5.** History of leaf physiological and radiative transfer models of leaves and canopy for
 547 fluorescence. Relevant models that do not include fluorescence are shown in blue.
 548 [1] Kautsky and Hirsch, 1931. [2] Farquhar et al., 1980. [3] Genty et al., 1989. [4] Rosema et al.,
 549 1998. [5] Zaks et al., 2012. [6] Van der Tol et al., 2014. [7] Kubelka and Munk, 1931. [8] Allen
 550 et al., 1970. [9] Jacquemoud and Baret, 1990. [10] Rosema et al., 1991. [11] Zarco-Tejada et al.,
 551 2000a. [12] Zarco-Tejada et al., 2000b. [13] Pedrós et al., 2010. [14] Vilfan et al., 2016.
 552 [15] Suits, 1972. [16] Verhoef, 1984. [17] Jacquemoud, 1993. [18] Miller et al., 2005. [19] Van
 553 der Tol et al., 2009b. [20] Yang et al., 2017. [21] North, 1996. [22] Gastellu-Etchegorry et al.,
 554 1996. [23] Zhao et al., 2014. [24] Hernández-Clemente et al., 2017. [25] Gastellu-Echegorry et
 555 al., 2017. [26] Sellers et al., 1996. [27] Bonan, 1996. [28] Krinner et al., 2005. [29] Lee et al.,
 556 2015. [30] Lee et al., 2015. [31] MacBean et al., 2018. [32] Norton et al., 2018. [33] He et al.,
 557 2017. [34] Yang and Van der Tol., 2018. [35] Köhler et al., 2018b.

558 4.2. Leaf physiological models of steady-state fluorescence

559 Leaf physiological models have aimed to quantify the partitioning of absorbed radiation to the
 560 pathways of photochemical and non-photochemical quenching [**Section 2**]. To overcome the

561 lack of modulated light and saturating flashes (available with active methods), predictive models
562 for the relationship between PQ and NPQ were needed. To that end, Andries Rosema and co-
563 workers developed the Laser Environmental Active Fluorosensor (LEAF-NL), which they used
564 to acquire active and passive fluorescence and to develop a quantitative model for steady-state
565 fluorescence that describes NPQ as a function of irradiance with two empirical parameters
566 (Rosema et al., 1998). Their measurements on poplar seedlings and their modelling results
567 showed that NPQ causes a positive relationship between fluorescence emission and
568 photochemistry efficiency at high light intensities, which challenged a common perception that a
569 fluorescence increase generally implies a reduction in photochemistry (McFarlane et al., 1980) –
570 although Rosema’s findings were consistent with the comments of McAlister and Myers (1940)
571 regarding the existence of both an inverse and a direct relationship [**Section 1**].

572 The values of the fitting parameters in Rosema’s model appeared to depend not only on
573 irradiance but also on the temperature and water stress status of the plants, which was consistent
574 with studies on PAM fluorescence showing positive correlation of steady-state fluorescence
575 with actual photosynthesis rate as assessed via gas exchange. Flexas et al. (2002), for instance,
576 observed drought effects on NPQ and gas exchange, confirming feedback mechanisms between
577 actual photosynthesis and NPQ (Bilger and Björkman, 1990). Van der Tol et al. (2009a)
578 modelled this feedback by introducing the fluorescence emission, the pH-gradient across the
579 thylakoid membrane, and NPQ, into the photosynthesis model of Farquhar et al. (1980). Later
580 Lee et al. (2013) and Van der Tol et al. (2014), on the initiative of Joe Berry, parameterized and
581 calibrated a simpler model for this feedback, using a calibrated non-linear relationship between

582 NPQ and the relative light saturation of photosynthesis. This relative light saturation is the ratio
583 of the actual over the theoretical maximum electron transport.

584 These models are fairly simple and can easily be implemented in canopy-level or global-scale
585 models, but they still rely on empirical coefficients and lack a mechanistic process description of
586 the feedback mechanism. Zaks et al. (2012), Bennett et al. (2018), and Morris and Fleming
587 (2018) developed a dynamic (time-resolved) model that simulates the pools of excited
588 chlorophyll and the concentrations of the quenchers zeaxanthin and antheraxanthin using the rate
589 coefficients of the involved processes in a more mechanistic way. Such mechanistic
590 representations could be used in remote sensing models for satellite fluorescence as well.

591 All of the models for fluorescence, photochemistry and NPQ quantify the initial emission of
592 fluorescence after incident photons have been captured by photosystems. They do not answer the
593 questions of ‘how much light is absorbed by the photosystems in the first place?’, nor ‘what
594 happens to the fluorescence after emission by the photosystems?’. These questions have been
595 addressed with RTMs, for both individual leaves and vegetation canopies.

596 **4.3. Leaf radiative transfer models for fluorescence**

597 The absorption of incident light and the (re-)absorption of emitted fluorescence inside leaves has
598 been described in detail by Gitelson et al. (1999, 1998) and Buschmann (2007). A part of the
599 incident light is reflected by the leaf surface before entering the leaf. The remaining light
600 penetrates into the leaf – where it may be absorbed by different pigments, including chlorophyll
601 – or scattered. When fluorescence is produced, a certain part is (re-)absorbed by pigments on its
602 way out of the leaf. The absorption of the incident light and thus the emission of fluorescence

603 increases asymptotically with chlorophyll content of the leaf. But as the fluorescence emission
604 spectrum (~650-800 nm) overlaps with the chlorophyll absorption spectrum (~400-720 nm),
605 some of the emitted fluorescence is re-absorbed by chlorophyll again. This absorption by
606 chlorophyll is strong in the red region, thus red fluorescence quickly saturates and then decreases
607 with increase in leaf chlorophyll content. As the leaf is far less absorbent in the far-red region,
608 the saturation of fluorescence is much lower there. Gitelson et al. (1999) showed that for this
609 reason, the fluorescence peak ratio, i.e., the ratio of far-red to red fluorescence is correlated with
610 chlorophyll content. Due to the re-absorption, only a little red fluorescence (~ 690 nm) escapes
611 from the shaded (usually abaxial) side of the leaf compared to the illuminated (usually adaxial)
612 leaf side, resulting in different spectral shapes (Louis et al., 2006; Van Wittenberghe et al.,
613 2013).

614 For modelling of fluorescence it was necessary to describe these processes mathematically.
615 Several leaf RTMs (without fluorescence) had emerged already in the 1960s. Most prominent
616 was one by Allen et al. (1970, 1969), using the analogy of a pile of glass plates. An improved
617 successor is the widely used PROSPECT (from the French PROpriétés SPECTrales) model,
618 created by Jacquemoud and Baret (1990), which relaxed the number of plates to be a non-integer
619 to gain more control over the variability of mesophyll scattering properties of the modelled
620 leaves. Calibration of the specific absorption coefficients of chlorophyll, water and dry matter
621 was accomplished by numerical optimization techniques. This provided a good correspondence
622 with spectra of leaf reflectance and transmittance, which were determined for leaves of known
623 (laboratory-assayed) concentrations of leaf constituents.

624 To support the interpretation of fluorescence data from the laser-induced fluorescence instrument
625 of Rosema in the early 1990s, an early attempt was made to incorporate fluorescence in RTMs
626 for single leaves as well as vegetation canopies. Thus, the FLSAIL model was developed by
627 Rosema et al. (1991). Also called KMF ('Kubelka-Munk Fluorescence'), since it included
628 fluorescence by using the two-stream approach of Kubelka and Munk (1931), the model solved
629 the radiative transfer equations numerically using an efficient layer doubling algorithm, a variant
630 of the adding algorithm of Van de Hulst (1957; cited in Van de Hulst, 1981). The doubling
631 algorithm scales from an extremely thin layer to an optically thick layer by repeated stacking of
632 identical layers. The doubling method was used also in the FRT leaf RTM, and was developed to
633 provide theoretical support for fluorescence contribution to apparent reflectance (Zarco-Tejada et
634 al., 2000a, 2000b; see also **Section 3**). A later-published model for leaf fluorescence,
635 FluorMODleaf (Pedrós et al., 2010), was based on the PROSPECT concept of parallel plates but
636 used a different way to simulate the leaf fluorescence, calculating first the emission and
637 subsequent re-absorption of fluorescence in a plate, then the stacking of an integer number of
638 plates, and finally interpolating to a real number of plates. The more recent Fluspect model
639 (Vilfan et al., 2016) uses the doubling algorithm for fluorescence calculation, but the rest of its
640 algorithm is based entirely on PROSPECT.

641 **4.4. Canopy radiative transfer models for fluorescence**

642 To study vegetation canopy fluorescence in relation with in-situ (i.e., Bottom Of Atmosphere,
643 BOA), airborne, and satellite (i.e., Top Of Atmosphere, TOA) observations, a canopy
644 fluorescence model should simulate two types of products: (i) Canopy spectral radiative budget,
645 including fluorescence emission; and (ii) Fluorescence signal measured at any altitude. In the

646 case of canopy spectral radiative budget, depending on the spatial extent of the area and the
647 selected spatial resolution, the calculation of the three-dimensional (3D) radiative budget can be
648 very demanding in terms of computer time and memory. It must track radiation along any
649 direction, which explains the inefficiency of reverse ray tracing Monte Carlo models (Disney et
650 al., 2000) that trace sample photon paths from the sensor to the illumination sources. For
651 remotely sensed fluorescence signals at any altitude, this involves simulating radiative transfer in
652 the atmosphere in addition to the vegetation canopy. A common modelling solution is to couple a
653 canopy model and an atmospheric RTM (e.g., the MODerate resolution atmospheric
654 TRANsmission, MODTRAN) (Berk et al., 2014), or 6-S (Kotchenova et al., 2008)). But this
655 solution cannot accurately simulate the complex neighboring effects (i.e., local surface irradiance
656 depends on surrounding surfaces and topography) due to the 3D Earth-Atmosphere radiative
657 coupling.

658 Canopy fluorescence models rely on embedding a leaf fluorescence model into a canopy
659 reflectance model (Disney, 2016). One-dimensional (1D) models with the vegetation canopy
660 being simulated as homogeneous layers – such as the canopy FLSAIL model (Rosema et al.,
661 1991) – appeared first. Using the doubling approach, this model solves the four-stream
662 differential equations of radiative transfer, including bi-directional scattering terms. FLSAIL and
663 also its successors FluorSAIL (Miller et al., 2005) and the Soil-Canopy-Observation of
664 Photosynthesis and Energy fluxes (SCOPE) (Van der Tol et al., 2009b) models are all based on
665 the ‘Scattering of Arbitrarily Inclined Leaves’ (SAIL) model, in which the vegetation is
666 represented by identical leaves with stochastically described orientation that scatter the four
667 streams of incident solar light, the diffuse upward and downward fluxes and the radiance in the

668 observation direction (Verhoef, 1985, 1984). SAIL, in turn, is based on the predecessor models
669 of Allen et al. (1970) and Suits (1972). These 1D models do not simulate the effects of spatial
670 and structural heterogeneity of vegetation in the horizontal plane, such as crown shadows or row
671 culture effects, nor do they simulate effects of vertical variability of leaf types, leaf orientation
672 angles or leaf pigment concentrations, as might be present in, say, a real forest stand with an
673 understory and overstory. Although approaches exist to handle clumping in RTMs (Ni-Meister,
674 Yang and Kiang, 2010), the effect of clumping on SIF has received little attention. Modifications
675 to the four-stream radiative transfer concept have been made to overcome these limitations. For
676 example, the FluorFLIM model (Zarco-Tejada et al., 2013a), based on FluorSAIL and FLIM
677 (Rosema et al., 1992), simulates vegetation clumping (crowns), while mSCOPE (Yang et al.,
678 2017) simulates fluorescence emanating from vertically heterogeneous canopies. He et al. (2017)
679 derived a relatively simple correction for the solar-viewing geometry, in which the observed
680 signal of SIF is decomposed into contributions from sunlit and shaded fractions of the canopy.
681 Their model is based on a RTM for discrete objects with internal structures ('4-scale'), such as
682 forest stands (Chen and Leblanc, 1997). The model of He et al. (2017) should also work for
683 clumped vegetation and recent models that derive the scattering of SIF directly from reflectance
684 take effects of clumping on SIF implicitly into account via the reflectance (Köhler *et al.*, 2018b;
685 Yang and Van der Tol, 2018).

686 3D photon and flux tracing RTMs can work with realistic descriptions of actual vegetation
687 canopies, either by representing all plant parts as facets (i.e., triangles) or by discretizing
688 canopies into so-called voxels, small spatially distinct volumes filled with a turbid medium of
689 leaves, possibly with different optical properties. Several 3D models have been extended to

690 include simulation of passive fluorescence, notably FluorFLIGHT for forest canopies
691 (Hernández-Clemente et al., 2017), the Fluorescence model with Weight Photon Spread
692 (FluorWPS) for row crops (Zhao et al., 2016), and the Discrete Anisotropic Radiative Transfer
693 (DART) model for any 3D explicit vegetation architecture (Gastellu-EtcheGORRY et al., 2017). All
694 three models simulate leaf-emitted fluorescence with Fluspect, after which within-canopy
695 radiation propagation is tracked with ray or flux tracing algorithms. Their spatially detailed
696 simulations potentially can provide deep insight into interactions of fluorescence fluxes in
697 structurally complex canopies.

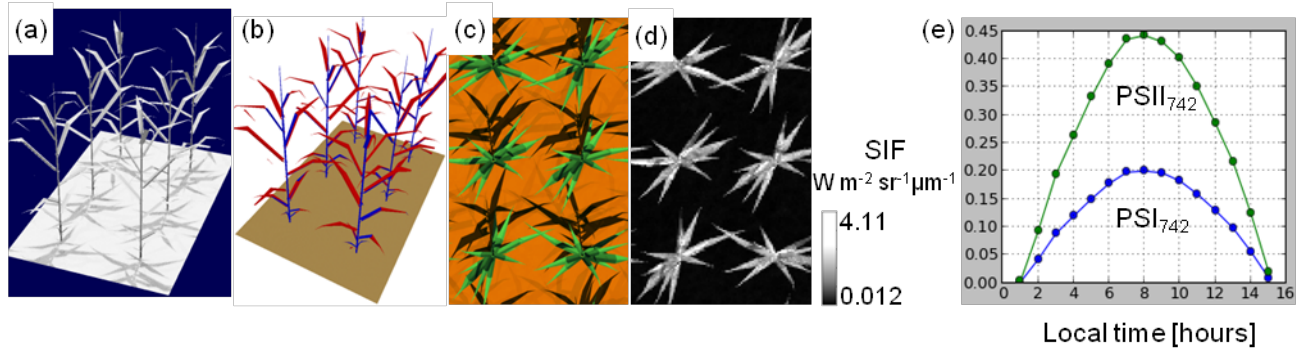
698 The DART model (Gastellu-EtcheGORRY et al., 2017, 2015, 1996) was designed to simulate both
699 the 3D radiative budget and remote sensing observations (i.e., in-situ/airborne/satellite LiDAR
700 and imaging spectrometers from visible to thermal infrared) of any urban and natural landscape
701 with any topography. The Earth-Atmosphere radiative coupling is simulated for any user-defined
702 atmosphere. Vegetation can be simulated with facets or turbid voxels. The 3D SIF emission is
703 simulated using Fluspect, based on the fluorescence quantum yield efficiencies that can be
704 specified per leaf facet or per type of leaf in relation to the leaf biochemistry and optical
705 properties. The foliage can be divided into sunlit and shaded by simulating instantaneous leaf
706 irradiance, and also into sun- and shade-adapted classes by simulating time series of scene
707 diurnal radiative budgets (e.g., simulations of multiple days with a time-step of one hour).
708 Subsequent computation of diurnal leaf irradiance integrals combined with user-specified leaf
709 irradiance thresholds determines respective duration of sun and shade exposure.

710 3D models like DART do not include an energy balance and do not work with the environmental
711 parameters (e.g., air temperature) driving apparent leaf fluorescence. Hence, for computation of

712 the emission by photosystems and the quenching mechanisms, DART imports values pre-
713 computed in SCOPE. DART chlorophyll fluorescence products, namely canopy BOA and TOA
714 SIF radiance and reflectance images and the 3D leaf radiative budget (i.e., PSI and PSII
715 fluorescence exitance and sun-scattered exitance per triangular facet), allow computation of
716 advanced outputs, such as the canopy fluorescence escape factor (Guanter et al., 2014). At this
717 time, SCOPE is the only canopy model that includes the energy balance at the leaf level and thus
718 the consistent estimation of photosynthesis and fluorescence.

719 **Figure 6** shows an example of DART-simulated BOA chlorophyll fluorescence for a maize field
720 at an early growth stage. Simulation of diurnal radiative budgets of solar irradiation (**Figure 6a**)
721 allowed for classification of the maize stand into sun and shade-adapted parts (**Figure 6b**),
722 further used for simulation of canopy reflectance (**Figure 6c**) and fluorescence (**Figures 6d**
723 **& 6e**) images. Advantages of the ray or flux tracing models are that they allow not only
724 quantification of processes leading to modelled canopy fluorescence but also their visualization.
725 Although producing more accurate results, the use of triangular facets is computationally more
726 demanding than the use of turbid voxels that represent a large set of foliar elements. (DART is
727 currently being adapted in order to simulate the fluorescence of canopies that are modelled with
728 turbid voxels.)

729



730

731 **Figure 6.** Simulation of BOA fluorescence in maize by DART: (a) Intensity of solar irradiance
 732 for a maize field in an early growth stage (39°N, 76.8°E; June 21, 2015; 13h local time); (b) 3D
 733 representation of sun- (red) and shade-adapted (blue) leaves; (c) DART true colour composite of
 734 the nadir reflectance image; (d) DART simulated PSII fluorescence radiance image; and (e) hourly
 735 evolution of the maize canopy BOA PSI and PSII fluorescence radiance at the wavelength of
 736 742.5 nm for clear sky conditions (atmosphere characterized by the USSTD 76 gas model and
 737 the Rural V23 aerosols model according to the MODTRAN gas and aerosol databases (see Berk
 738 et al., 2014).

739 4.5. Integrated canopy fluorescence and photosynthesis models

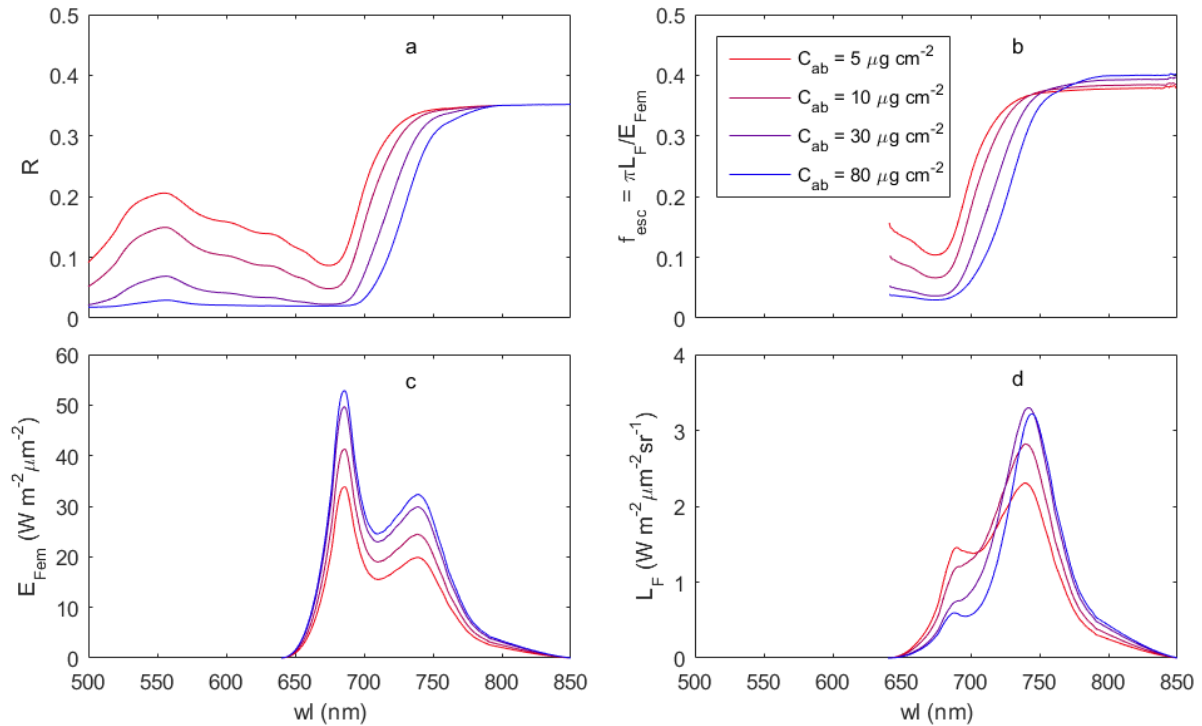
740 Interpreting fluorescence results of a canopy in terms of photosynthesis and stress requires
 741 modelling of not only the radiative fluxes but also the non-radiative energy fluxes. Non-radiative
 742 fluxes are not commonly taken into account in remote sensing observation models, but they are
 743 an important component of land surface models (Anderson, 1963; Kalma et al., 2008). Non-
 744 radiative fluxes include the energy involved in metabolism (photosynthesis and respiration), the
 745 turbulent exchange of latent and sensible heat flux, and the conduction of heat into biomass and
 746 soil. These fluxes eventually determine the temperature of the leaves and the humidity in
 747 vegetation canopies, both of which are crucial variables for stomatal aperture (Ball et al., 1987;
 748 Leuning, 1995), photosynthesis (Collatz et al., 1991) and fluorescence quenching (Bilger and
 749 Björkman, 1990). For a complete modelling of fluorescence, it was therefore considered
 750 necessary to include these processes in canopy fluorescence models.

751 Integration of radiative with non-radiative energy fluxes and photosynthesis has been a subject of
752 inquiry since the 1960s. De Wit (1965) and Goudriaan (1977) were among the first to develop
753 computer simulation models combining radiative transfer with micro-meteorology for
754 vegetation, maintaining energy and water budgets. Norman (1979) presented Cupid, a
755 comprehensive model for the soil-plant-atmosphere continuum that also simulates visible, near
756 infrared and thermal radiation. The more recent SCOPE model (Van der Tol et al.,
757 2009b) additionally simulates the fluorescence radiance spectrum for a given viewing and
758 illumination geometry (**Figure 7**). SCOPE is an extension of the FluorMOD model (Miller et al.,
759 2005), which already included a fluorescence quenching model (Rosema et al., 1998) and a
760 canopy RTM, but without considering thermal radiative transfer and non-radiative energy fluxes.
761 SCOPE has been used in a number of trials to interpret SIF in vegetation measured using field
762 devices (Migliavacca et al., 2017b; Rossini et al., 2016; Van der Tol et al., 2016) and airborne
763 sensors (Damm et al., 2015b). It has been used also for retrieval of vegetation parameters using
764 satellite sensors (Lee et al., 2013; Zhang et al., 2018a, 2014). A limitation of SCOPE is that it is
765 not valid for clumped or sparse or vegetation as it uses the original SAIL model representation
766 for radiative transfer (Verhoef, 1984).

767 **4.6. Lessons learned using these models**

768 As Porcar-Castell et al. (2014) pointed out, leaf-to-canopy scaling associated with the change
769 from active methods of fluorescence measurement to remote sensing of SIF is not just a matter of
770 application of existing models to a larger area. Rather, it has been necessary to describe all SIF-
771 relevant processes: absorption, emission, scattering, and re-absorption. The challenges in scaling

772 from leaf to canopy also present opportunities to improve understanding of photosynthesis at the
 773 canopy scale.



774

775 **Figure 7.** SCOPE model simulation of (a) reflectance R , (b) fluorescence escape probability f_{esc} ,
 776 (c) the fluorescence irradiance emitted by all photosystems E_{Fem} , and (d) the fluorescence
 777 radiance in nadir direction L_F – for four values of leaf chlorophyll content and a leaf area index
 778 of 3. Note the changes in fluorescence spectral shape as chlorophyll(a+b) mass per unit leaf
 779 surface (C_{ab}) increases, and the similarity between the fluorescence escape probability and the
 780 reflectance.

781 Various papers have reported a close correlation between far-red SIF and GPP (Cui et al., 2017a;
 782 Frankenberg et al., 2011b; Goulas et al., 2017; Guanter et al., 2012; Joiner et al., 2011; Rossini et
 783 al., 2010; Verma et al., 2017; Wagle et al., 2016; Yang et al., 2015). The question of which
 784 processes are responsible for the close correlation has been discussed in most of these studies. It
 785 is now clear that SIF and GPP rely on the incident radiation and the absorption of light by
 786 chlorophyll in the whole canopy leaf area, which are both responsible for their strong correlation

787 at diurnal and seasonal time scales (Goulas et al., 2017; Joiner et al., 2014; Yang et al., 2018b,
788 2015). The dominance of total chlorophyll absorption is confirmed by sensitivity analyses of the
789 SCOPE model (Koffi et al., 2015; Verrelst et al., 2015b).

790 Furthermore, Migliavacca et al. (2017b) evaluated changes in fluorescence of grassland
791 vegetation after fertilization, differentiating effects of canopy structure on scattering from
792 photosynthetic effects on fluorescence emission. They showed that the relative abundance of
793 species affects canopy structure and the scattering of fluorescence, and that these changes in
794 canopy structure dominate the variations in observed SIF between vegetation communities
795 observed at the same time. This confirms model sensitivity analyses demonstrating that leaf area
796 index and leaf inclination have a significant effect on SIF (Verrelst et al., 2015b), and
797 demonstrates that scattering and re-absorption can cause substantial differences in SIF among
798 various vegetation communities. A significant step in quantifying the scattering and re-
799 absorption of fluorescence in the canopy was made by Romero et al. (2018). who developed a
800 quantitative model for re-absorption in the canopy, and also performed active fluorescence
801 measurements at the canopy level, using a lamp producing blue light to obtain fluorescence
802 spectra above the tree crowns for validation. Their model confirmed the change in spectral shape
803 (the relative reduction of red fluorescence), when moving from the leaf to the canopy scale, as
804 found earlier with SCOPE.

805 Because scattering depends on the geometry of illumination and observation directions,
806 quantification of fluorescence scattering in the canopy is crucial for meaningful comparisons
807 between fluorescence observations taken under different solar and observation angles. Köhler et
808 al. (2018b) analyzed the directional scattering of fluorescence in the canopy. They showed that

809 the seasonality in SIF observed by GOME-2 is affected by the angular anisotropy of the canopy
810 fluorescence and that correction for this effect is needed. Subsequently, Liu et al. (in press) used
811 SCOPE and DART SIF simulations of vegetation canopies combined with the spectral invariant
812 theory, in the random forest machine-learning algorithm to devise a new means for scaling a
813 canopy SIF signal down to the level of single photosystems. Downscaling of SIF by correcting
814 for scattering and re-absorption appeared to be an efficient way to obtain a solar-view geometry-
815 independent measure, and a measure for the fluorescence emission at leaf level before re-
816 absorption. Yang and Van der Tol (2018) analytically compared the radiative transfer of incident
817 radiation to the radiative transfer of scattered fluorescence radiation and showed that far-red
818 fluorescence scattering in a 1D canopy is proportional to far-red reflectance normalized by the
819 leaf albedo and canopy interceptance. With this simple equation, far-red SIF can be corrected for
820 illumination and observation geometry and for re-absorption within the canopy at the same time,
821 using reflectance along with SIF.

822 Due to the similarities between reflectance and fluorescence, it makes sense to combine the two
823 together. One way of doing this is to invert quantitative RTMs and retrieve from reflectance the
824 parameters necessary to quantify the light absorption by chlorophyll and the scattering and re-
825 absorption of fluorescence. It then may be possible to estimate the efficiency of fluorescence
826 emission and the fluorescence quenching mechanisms (Van der Tol et al., 2016).

827 **4.7. Challenges and future directions in modelling**

828 Challenges and opportunities still lie ahead for modellers in the fields of remote sensing of
829 fluorescence and plant physiology.

830 One issue with current models for passive fluorescence is the empirical parameterization of NPQ
831 and the lack of quantitative mechanistic parameterizations for NPQ as a function of measurable
832 quantities. A possible strategy is to use reflectance in the region of 500-600 nm, as leaf optical
833 properties in this spectral region are affected by a number of pigments, including those involved
834 in photoprotection and non-photochemical heat dissipation (e.g., zeaxanthin). Spectral changes in
835 this region are the basis of the PRI (Gamon et al., 1997). The leaf RTM Fluspect was extended
836 recently with a more precise simulation of the reflectance and transmittance between 500 and
837 600 nm, by including spectral changes associated with NPQ (Vilfan et al., 2018). Including
838 these effects in Fluspect and SCOPE or other RTMs could help to retrieve a measure of NPQ and
839 constrain the modelled fluorescence–photosynthesis relationship. Spectrally contiguous
840 reflectance of the far-red (red edge) shoulder (700-800 nm) is also being investigated for spectral
841 absorbance features related to the pigment-pigment excitation interactions and xanthophyll
842 conversion, as possible evidence of NPQ manifestation (S. van Wittenberghe, personal
843 communication).

844 Laboratory and field experiments continue to provide new insights (**Section 2.4**), based on joint
845 acquisition of active and passive SIF and gas exchange information to examine fluorescence-
846 photosynthesis linkages, drought and ozone stress effects, and diurnal and seasonal relationships
847 between SIF and other photosynthetic parameters (Magney et al., 2017; Rosema et al., 1998;
848 Wyber et al., 2017). These data, which may be combined with the fluorescence lifetime (Sylak-
849 Glassman et al., 2016), can be helpful for better understanding of the dynamics of fluorescence
850 originating from PSI and PSII and their interdependence. This could lead to methods for
851 differentiating fluorescence from the two photosystems from retrieved SIF spectra corrected for

852 re-absorption. High spatial resolution imaging fluorescence is another promising tool, as shown
853 by Pinto et al. (2016) who set a hyperspectral camera above a vegetation canopy to retrieve
854 fluorescence images and differentiate contributions from individual leaves with different
855 insolation and orientation; this is an excellent data source for model validation.

856 Advances in computational power facilitate utilization of 3D ray and flux tracing models to
857 explore canopy structural effects (e.g., for row crops or savannah type vegetation) on
858 fluorescence, with realistic vegetation parameterizations obtained from LiDAR or orthophoto
859 data (Fawcett et al., 2018). Also the influence of landscape spatial heterogeneity – originating
860 from topographical gradients and landcover variability – on large-scale space-based SIF
861 observations is anticipated in upcoming versions of 3D RTMs. Significant progress in the use of
862 machine learning, neural networks and emulation of models (Rivera et al., 2015; Verrelst and
863 Rivera, 2017), and the development of End-to-End simulators for satellite missions (Vicent et al.,
864 2016), will bring the operational use of more complex RTMs at large spatial scales within reach.
865 This would expedite assimilation of fluorescence data into global land surface models, as has
866 been initiated by Lee et al. (2015) for the Community Land Model, Norton et al. (2018) for
867 BETHY, and MacBean et al. (2018) for the Organising Carbon and Hydrology In Dynamic
868 Ecosystems (ORCHIDEE) model.

869 **5. SIF estimation methods**

870 **5.1. General strategies**

871 Approaches used to quantify SIF emission from vegetation TOC radiance are anchored by a
872 simple equation describing the additive contributions of solar-reflected (r) and SIF radiance to

873 the total TOC radiance $L(\lambda)$ (assuming isotropic surface reflectance and neglecting canopy-
874 sensor atmospheric effects and adjacency):

$$875 \quad L(\lambda) = r(\lambda) E(\lambda)/\pi + SIF(\lambda) \quad (1)$$

876 where λ is wavelength and $E(\lambda)$ the known (measured or modelled) incident irradiance at the
877 surface (direct and diffuse). All the terms of **Equation 1** are spectrally variable, making retrieval
878 of the two unknowns challenging. Fluorescence retrieval algorithms are built mostly on the key
879 assumption that prior knowledge of the spectral shape of all terms of the equation can be
880 leveraged to estimate the unknown terms. Specifically, unlike L and E , r and SIF are smooth
881 functions of wavelength and this knowledge is exploited to retrieve SIF at specific spectral
882 absorption bands by assuming that these two variables are either constant or vary linearly over a
883 narrow wavelength range (a few nm), or vary in a more complex way over larger spectral ranges
884 (e.g., the full SIF emission spectrum).

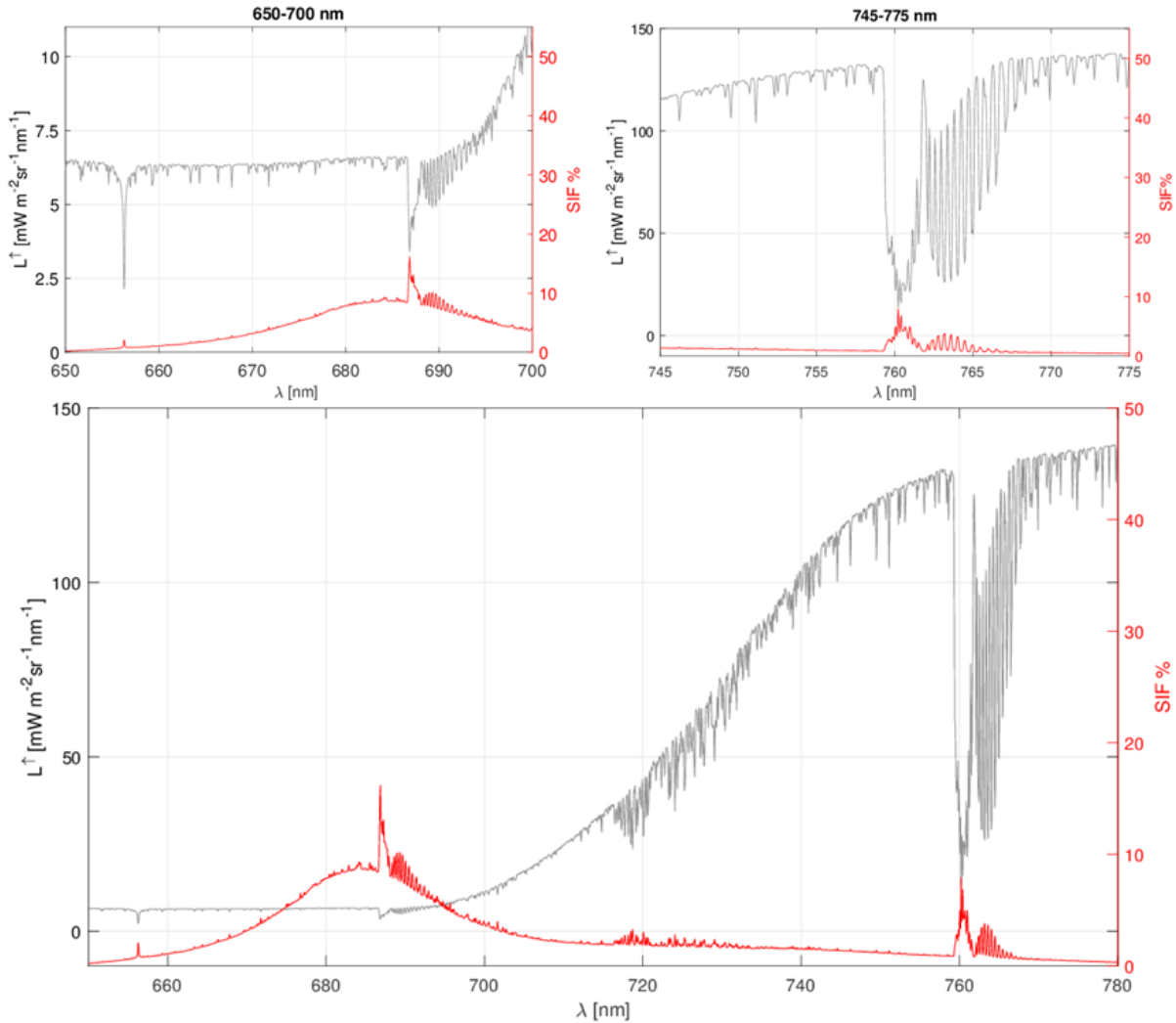
885 Retrieval methods further exploit the larger relative contribution of SIF to the total TOC radiance
886 at selected absorption bands as compared to over the whole spectrum (**Figure 8**). The
887 proportional contribution of SIF to total TOC radiance is larger for red wavelengths because,
888 despite the red fluorescence being strongly re-absorbed by chlorophyll, the canopy reflected
889 radiance is very low for the same reason. Conversely, the SIF contribution is proportionally
890 lower in the far-red where the reflected radiance is dominated mainly by canopy scattering.
891 Besides the overall effect of fluorescence in these spectral regions, it is the specific in-filling
892 effect within absorption bands that is key for retrieving SIF in most approaches. When observed
893 at high SR, the fluorescence in-filling effect within the terrestrial oxygen absorption bands (i.e.,
894 O₂-A and O₂-B at 760 nm and 687 nm, respectively) can exceed 10% (**Figure 8**). A similar

895 effect occurs in the Fraunhofer Lines (FLs), but here the fluorescence proportional contribution
896 is generally smaller as these absorption bands are less dark than oxygen bands for a given SR. In
897 contrast to the O₂ bands, absorption in the FLs does not occur in the terrestrial atmosphere, an
898 advantage in that modelling of atmospheric influence is much easier (as detailed in this section).

899 The depth of the absorption bands varies greatly over very narrow spectral ranges, hence, sensor
900 capability to accurately detect such radiance variations through fine SR and high signal-to-noise
901 ratio (SNR) is essential for SIF retrieval. Recent technological developments have produced a
902 number of high-performance spectrometers (ground, airborne, and satellite) providing
903 sufficiently high SRs and SNR for SIF retrieval [Sections 6 and 7]. For satellite instruments,
904 these features also must be balanced with spatial resolution and, in some cases, a coarse
905 resolution of several (or more) kilometers is necessary to achieve the required SNR.

906 Most retrieval algorithms can quantify fluorescence at selected absorption bands, but a novel
907 group of approaches allows derivation of the full fluorescence emission spectrum (Zhao et al.,
908 2018). This capability affords new opportunities for better understanding SIF with respect to leaf
909 composition, canopy structure and plant functional status (Verrelst et al., 2016, 2015b). Herein,
910 the methods are grouped into two main classes based on whether they allow retrieval within
911 restricted absorption bands or over the full SIF emission region (**Table 2**). Within the first class,
912 we can distinguish methods based on O₂ bands and those for FLs, and in the second class
913 methods based on parametric functions to describe $r(\lambda)$ and $SIF(\lambda)$ (i.e., spectrum fitting) are
914 distinguished from those using a full radiative transfer approach (i.e., model inversion). Most
915 retrieve SIF at different scales, from ground to satellite, using different acquisition techniques.

916



917

918 **Figure 8.** Relative contribution of solar-induced fluorescence (red curves and right axes) with
 919 respect to the total emerging radiance at top-of-canopy (grey curves and left axes) at spectral
 920 resolution of 0.1 nm, considering typical dense vegetation during summer conditions. The figure
 921 on the bottom shows the spectral range of fluorescence emission; whereas the figures on top
 922 show O₂-B (left) and O₂-A (right) details. Note the difference in radiance scales for plots.

923 For airborne and satellite observations, different physically-based or empirical approaches have
 924 been explored to account for atmospheric effects. **Table 2** also summarizes characteristics of the
 925 methods such as: capability of retrieving red, far-red, or full fluorescence; number of spectral
 926 bands employed (e.g., multispectral, hyperspectral); spectral range used in the retrieval; main

927 assumptions; use of parametric expressions vs. model-based functions; and treatment of the
928 atmospheric effect. We focus mainly on developments subsequent to the review of Meroni et al.
929 (2009), with a few earlier ones included for historical context and completeness.

930 **5.2. Retrieval of SIF at selected absorption bands**

931 The first class of retrieval methods targets restricted spectral regions associated with strong
932 absorption from gases in the terrestrial or solar atmosphere (i.e., O₂ bands or FLs, respectively).
933 Retrieval at selected wavelengths exploits the contrast between (i) spectral wavelengths where
934 the radiance signal is mostly dominated by the reflected solar flux, and (ii) narrow spectral
935 regions where the solar incident flux is largely attenuated.

936 **Table 2.** Current SIF retrieval methods and their characteristics.

Absorption band	Method	Reference	Target SIF (R=red; FR=far-red; F=full spectrum)	Scale of design (F=field; A=airborne; S=satellite; ms=model simulations)	Spectral channels (M=multispectral; H=hyperspectral)	Retrieval Spectral Range (nm)	Retrieved SIF	Assumed SIF spectral shape	Assumed r spectral shape	Model solution (A=analytical; N=numerical)	Atmospheric correction (E=empirical; D=data driven; P=physical)
<i>O₂</i> bands	FLD	Plascyk, 1975	R	A	M	486.1; 589.0; 656.3	scalar	constant	constant	A	(no correction)
	3FLD	Maier et al., 2003	FR	A	M	760	scalar	linear	linear	A	single-step (E)
	SFM	Meroni and Colombo, 2006	R, FR	F (leaf)	H	686.5–690.0; 759.0–764.0	restricted	linear	linear	N	-
	cFLD	Gómez-Chova et al., 2006	R, FR	F (leaf)	H	687; 760	scalar	adjusted with correction factor	from apparent R	A	-
	iFLD	Alonso et al., 2008	FR	F (canopy), ms	H	750-780	scalar	adjusted with correction factor	adjusted with correction factor	A	-
	SFM	Mazzoni et al., 2008	R	F (leaf)	H	686.3-691.6	restricted	polynomial	polynomial	N	-
	FLD/SFM	Guanter et al., 2010	R, FR	ms	H	677-697; 750-770	restricted	reference spectrum	linear combination of end-members	A/N	single-step (P)
	SFM	Meroni et al., 2010	R, FR	F (canopy), ms	H	686.7–691.2; 755.6–765.5	restricted	linear, polynomial, gaussian	linear, polynomial	N	-
	nFLD	Daumard et al., 2010	R, FR	F (canopy)	M	683.1-697.1; 757.9-770.5	scalar	reference spectrum	polynomial	A	-
	SFM	Mazzoni et al., 2010	R, FR	ms	H	677.0–697.0; 750.0–770.0	restricted	voigt	cubic spline	N	two-step (P)
	SFM	Mazzoni et al., 2012	FR	F (canopy), ms	H	750–770	restricted	voigt, legendre polynomial	polynomials, cubic-spline, legendre polynomial	N	-
	3FLD	Damm et al., 2014	FR	A	M	753-771	scalar	linear	linear	A	two-step (E)
	SFM	Cogliati et al., 2015a	R, FR	ms	H	750-770	restricted	gaussian, lorentzian, voigt	polynomial, cubic spline	N	two-step (P)
	iFLD	Wieneke et al., 2016	R, FR	A	M	-	scalar	adjusted with correction factor	adjusted with correction factor	A	two-step (E)
	Fraunhofer lines	-	Frankenberg et al., 2011a	FR	S, ms	H	769.5-775; 770.1 (K _i)	scalar	constant	polynomial	N
-		Joiner et al., 2011/2012	FR	S, ms	H	769.90–770.25 (K _i)	scalar	constant	constant	N	single-step (P)
SVD		Guanter et al., 2012	FR	F, ms	H	755.8-759.3; 769.2-775.2	scalar	constant	singular vectors	N	single-step (D)
PCA		Joiner et al., 2014	FR	S, ms	H	712–747; 747–783	scalar	gaussian	polynomial	N	single-step (D)
-		Köhler et al., 2015	FR	S, ms	H	720-758	scalar	constant/normalized fluorescence spectrum	linear	N	single-step (D)
DOAS		Wolanin et al., 2015	R	S	H	681.8-685.5	scalar	reference spectrum	polynomial	N	single-step (P)
-		Joiner et al., 2016	R, FR	S, ms	H	622–640; 682-692	scalar	gaussian	polynomial	N	single-step (D)
two step linearized		Grossmann et al., 2018	R, FR	F (canopy)	H	680-686; 745-758	scalar	reference spectrum	polynomial	N	-
Full Spectrum	Spectrum fitting										
	FSR	Zhao et al., 2014/2018	F	F (canopy), ms	H	640–850	spectrum	linear combination of basis spectra	-	N	-
	F-SFM	Liu et al., 2015	F	F (canopy), ms	H	645-805	spectrum	linear combination of basis spectra	linear combination of basis spectra	N	-
	SpecFit	Cogliati et al., 2015b	F	ms	H	670-780	spectrum	pseudo-voigt	piecewise cubic spline	N	two-step (P)
	Model inversion										
-	Verhoef et al., 2018	F	ms	H	400-2255	spectrum	singular vectors from SVD	physically based (RTMo)	N	two-step (P)	
-	Celesti et al., 2018	F	F (canopy), ms	H	400-900	spectrum	physically based (RTMf)	physically based (RTMo)	N	-	

937

938 5.2.1. Oxygen absorption bands

939 A classical strategy to disentangle reflected radiance and SIF contributions is to compare the
940 radiance outside and inside the O₂ absorption bands. The approach is an extension of a technique
941 originally developed for FLs, the FLD principle (Plascyk, 1975; Plascyk and Gabriel, 1975),
942 which relies on two radiance measurements – one inside and one outside the absorption feature –
943 to solve **Equation 1**. A refinement particularly relevant for red fluorescence uses more spectral
944 bands to introduce a spectral dependency of reflectance and fluorescence, as exemplified by the
945 3FLD (Maier, 2002), cFLD (Gómez-Chova et al., 2006), and iFLD (Alonso et al., 2008),
946 reviewed by Meroni et al. (2009).

947 Spectral Fitting Methods (SFMs) are a more sophisticated approach that uses all available
948 (hyper)spectral bands to quantify the spectrally variable fluorescence and reflectance
949 contribution over a restricted spectral range. The upwelling radiance spectrum is modelled over a
950 broader spectral window (i.e., ~ tens of nm) including multiple absorption lines (i.e., O₂ bands
951 and FLs), with fluorescence and reflectance as continuous parametric functions. The resulting
952 mathematical system (one equation per spectral wavelength considered) is solved to retrieve the
953 underlying unknown function parameters. Several types of functions have been proposed to
954 approximate the reflectance and fluorescence spectral behaviour within spectral windows around
955 the main oxygen absorption bands (**Table 2**). Because SFMs use all of the high-resolution
956 spectral information along the absorption region – theoretically hundreds of bands – the impact
957 of instrument noise is reduced.

958 5.2.2. Fraunhofer lines

959 In contrast to methods using oxygen absorption bands, those using solar absorption features do
960 not require complex atmospheric modelling, hence, they have been extensively applied to current
961 space-based SIF retrievals. This family of algorithms may be categorized into two main groups:
962 (i) simplified physically-based schemes applied to specific FLs, and (ii) data-driven statistical
963 approaches involving Principal Component Analysis (PCA) or Singular Value Decomposition
964 (SVD) analysis. When the retrieval is fitting only FLs (e.g., spectral windows 745-758 nm, as in
965 GOSAT, OCO-2 or S-5P), both simple physically-based (e.g., Frankenberg et al., 2011a) and
966 data-driven (e.g., Guanter et al., 2012) methods can be used. When the fitting window is wider
967 and includes atmospheric bands, as in SIF retrievals from GOME-2 data, spanning either water
968 vapor around 740 nm or O₂ in 760 nm, then data-driven approaches are the only way to avoid the
969 complex explicit modelling of atmospheric radiative transfer (e.g., Joiner et al., 2013; Köhler et
970 al., 2015). Several methods have been proposed and all these strategies have allowed
971 determination of the far-red fluorescence (**Table 2**).

972 Terrestrial SIF in the red spectral region is more difficult to detect from space using FLs as the
973 lines in the red region are not as wide, nor as deep, as those in the far-red. Also, red SIF signal
974 levels are typically lower overall than those in the far-red for healthy vegetation, because of re-
975 absorption by chlorophyll and also because the emitted red fluorescence by leaves within a
976 canopy conceivably can add to the directly emitted far-red fluorescence (i.e., the re-emission
977 phenomenon). The sharp upturn of the red edge also complicates retrievals and may necessitate
978 smaller fitting windows. Quantification of the red SIF emission was reported by Wolanin et al.
979 (2015) using SCIAMACHY and GOME-2 data and by Joiner et al. (2016).

980 Recently, FL-based methods developed for satellite sensors also are being used for ground-based
981 and airborne spectrometers operating at high SR (Grossmann et al., 2018; Frankenberg et al.,
982 2018).

983 **5.3. Retrieval of the full SIF spectrum**

984 Two main different approaches have been developed to retrieve the continuous SIF emission
985 spectrum (**Table 2**).

986 **5.3.1. Spectrum fitting**

987 Spectral fitting techniques are an evolution of SFMs to encompass the broader spectral region
988 where fluorescence emission occurs. Methods such as the Fluorescence Spectrum Reconstruction
989 (FSR) (Zhao et al., 2014), the Full-spectrum Spectral Fitting (F-SFM) (Liu et al., 2015), and the
990 advanced FSR (aFSR) (Zhao et al., 2018) are examples that use linear combinations of basis
991 spectra to model the SIF spectrum at TOC. The basis spectra are derived from PCA (Liu et al.,
992 2015) or SVD (Zhao et al., 2014) on a large dataset of SIF spectra simulated by the canopy RT
993 model SCOPE. In general, these methods are structured as follows: first, SIF is retrieved at
994 selected absorption bands (i.e., O₂ bands, H α FL, etc.) by means of a modified version of SFM;
995 then, the SIF spectrum is reconstructed as a linear combination of the basis spectra matching the
996 SIF SFM retrievals. Alternatively, the full SIF spectrum is estimated by considering
997 simultaneously all the wavelengths in the spectral window where fluorescence occurs, as in the
998 SpecFit model and using piecewise cubic spline to fit the reflectance (Cogliati et al., 2015b).

999 **5.3.2. Model-inversion methods**

1000 An emerging approach for quantifying SIF is based on numerical inversion of canopy RTMs.
1001 This route permits retrieval also of relevant biophysical parameters (e.g., chlorophyll content,
1002 leaf area index, etc.), and related variables (e.g., fraction of photosynthetically active radiation,
1003 fAPAR), as side-products of the fluorescence retrieval. This additional information is crucial for
1004 interpretation of SIF with respect to plant photosynthetic activity.

1005 An inversion approach was first developed by Verhoef et al. (2018) and is suited to the spectral
1006 and directional outputs of the tandem mission of FLEX and Sentinel-3 (S-3). The method is
1007 based on model inversion of simulated TOA radiance where the SIF and canopy parameters are
1008 retrieved simultaneously and in a consistent manner. It employs a ‘light’ version of SCOPE to
1009 generate the canopy reflectance signature; then SIF is modelled as an additional source of
1010 radiance using a linear combination of principal components (PCs). Actually, this approach
1011 represents a hybrid solution between model inversion (reflectance modelling) and the spectrum
1012 fitting methods (fluorescence modelling).

1013 A more complete canopy model-inversion procedure was recently proposed by Celesti et al.
1014 (2018) based on simulations and experimental TOC observations collected during controlled
1015 stress induction experiments. It employs both the fluorescence and reflectance SCOPE sub-
1016 routines. These routines are used to forward model the TOC apparent reflectance to be matched
1017 with spectral observations. The use of the fluorescence routine allows quantification of the
1018 fluorescence quantum yield, one of the key variables for understanding fluorescence and its link
1019 to photosynthesis. Because the work of Celesti et al. (2018) involved extreme contrasts in

1020 vegetation properties induced by a chemical treatment, the operational applicability of their
1021 approach to natural vegetation canopies or TOA satellite data remains to be studied.

1022 In the model inversion approach, Visible and Near-Infrared (VNIR) information are needed for
1023 adjusting the canopy reflectance model parameters. Unfortunately, due to current technological
1024 constraints, wide-spectral-range high-resolution spectra cannot be collected by the same
1025 spectrometer, potentially giving rise to some inconsistencies between spectral datasets with
1026 respect to spatial co-registration, radiometric intercalibration, etc. For this reason, accurate co-
1027 registration and intercalibration methods must be applied prior to fluorescence determination
1028 whenever more than one sensor is used.

1029 **5.4. Atmospheric correction, illumination, and surface anisotropy**

1030 Some of the retrieval methods require atmospheric correction before SIF retrieval (two-steps),
1031 whereas others explicitly include atmospheric correction in the design of the algorithm in a
1032 complete TOA scheme (one-step). Atmospheric effects depend on the type of absorption feature
1033 used (terrestrial vs. solar). Satellite-based FL methods explicitly include the atmospheric effect
1034 directly in a single-step algorithm design facilitated by the relatively simple behaviour of the
1035 atmosphere at these wavelengths. The assumption is that the atmospheric interference is caused
1036 mainly by scattering that, within the narrow FLs, can be considered spectrally invariant or
1037 varying as linear or polynomial functions. Thus, the simplified physically-based methods and the
1038 data-driven approaches working with FLs correct for this scattering but do not require
1039 characterization of the atmospheric status (such as aerosol optical depth or height distribution)
1040 which can strongly impact the O₂-A feature (Frankenberg et al., 2011a). By contrast, retrieval at

1041 the O₂ bands requires very accurate atmospheric modelling. High-resolution atmospheric RT
1042 codes are used to compute the spectrally-resolved atmospheric RT functions (i.e., two-way direct
1043 and diffuse transmittance, bidirectional reflectance and spherical albedo) to represent accurately
1044 the TOA reflected radiance in addition to SIF. Verhoef et al. (2018, 2014) proposed a means to
1045 couple atmospheric and surface RT at high SR based on the so-called T-18 system of
1046 atmospheric transfer functions – a method specifically designed to accommodate the finite
1047 spectral band effect. This effect concerns the fact that the atmospheric transmittance of
1048 absorption lines does not follow Beer’s Law when there are large variations of the spectral
1049 absorption within the interval (spectral band), therefore the product of two atmospheric functions
1050 (e.g., downward and upward transmittance) is not equivalent to the product of these functions
1051 convolved. This strategy has been employed in several schemes based on FLD, spectral fitting,
1052 and model inversion (Cogliati et al., 2015b; Damm et al., 2014; Mazzoni et al., 2010; Wieneke et
1053 al., 2016).

1054 The atmospheric correction at the O₂ bands may be performed either as a two-step or one-step
1055 procedure. Cogliati et al. (2015a) used a two-step approach where the TOA spectrum is
1056 converted to TOC followed by decoupling of the SIF and reflectance, based on SFM and
1057 SpecFit. A two-step approach including a more realistic atmospheric correction was presented in
1058 Sabater et al. (2017, 2015) and implemented within the FLEX End-to-End simulator (Vicent et
1059 al., 2016). A direct TOA radiance optimization approach has instead been introduced by Verhoef
1060 et al. (2018), in which at-sensor spectra are calculated by coupling a canopy model with an
1061 atmospheric RT model. The procedures described here for satellite instruments also have been
1062 adapted for airborne imaging spectrometers. For example, FL approaches have been used with

1063 the *HyPlant* airborne sensor (Colombo et al., 2018; Rossini et al., 2015) and with the novel
1064 Chlorophyll Fluorescence Imaging Spectrometer (CFIS) (Frankenberg et al., 2018) [**Section 6**].
1065 The physical methods at the O₂ bands were adapted for *HyPlant* by Cogliati et al. (2018) and a
1066 semi-empirical technique making use of fluorescence-free reference pixels (i.e., bare soils) was
1067 shown to improve characterization of the atmospheric transfer functions (Damm et al., 2014;
1068 Wieneke et al., 2016).

1069 Retrievals that rely on O₂ absorption bands are sensitive to the direct-to-diffuse ratio of the
1070 incident light and its coupled effect with canopy anisotropy. To reach the sensor, diffuse light
1071 traverses a longer pathway compared to direct light, making the depth of the absorption sensitive
1072 to the fraction of diffuse light. This effect might be confused with in-filling by fluorescence,
1073 leading to over/under-estimation of fluorescence. Evidence of such effects based on RT
1074 simulations has been reported in Fournier et al. (2014), Cogliati et al. (2015b), and Verhoef et al.
1075 (2018). Liu and Liu (2018) considered in more detail the impact of direct/diffuse radiation on the
1076 in-filling effect and SIF retrieval using simulated data. They found that this effect can have a
1077 marked impact on estimated SIF (up to 20% at the O₂-A band). These studies have been
1078 developed mainly with turbid-medium canopy RTMs, but the fluorescence angular distribution is
1079 also affected significantly by the structural arrangement of the canopy – with respect to sun and
1080 sensor viewing angles – which determines the actual fraction of illuminated and shaded leaves
1081 observed by the instrument. This is commonly observed from diurnal continuous measurements
1082 of fluorescence using ground-based and tower-mounted instruments viewing a fixed spot of the
1083 canopy. Understanding whether changes in fluorescence are related to canopy self-shadowing or
1084 to more relevant physiological processes is not trivial and still a challenge. Detailed

1085 consideration of anisotropic effects and the impact on retrieval accuracy of fluorescence was
1086 provided in Damm et al. (2015b) and Yang et al. (in press). Sensor technical characteristics (e.g.,
1087 spatial resolution, spectral range and resolution, and SNR) are relevant to such aspects and play
1088 an important role in determining the accuracy of SIF retrieval.

1089 **5.5. Assessment of SIF retrieval accuracy**

1090 Validation of SIF retrieval methods, especially for satellite-based acquisitions, is still a challenge
1091 due to issues such as large footprint sizes and instrument errors [**Section 7**]. Also, until recently
1092 there has been a lack of direct ways to observe SIF independently; however, this situation is
1093 changing with the advent of new portable sensors for leaf/canopy-scale work, platform-mounted
1094 devices, drones, and other airborne sensors for SIF detection [**Section 6**].

1095 So far, retrieval accuracy has been evaluated mainly through numerical experiments in which RT
1096 simulations – ones that consider comprehensive variability of reflectance, fluorescence and
1097 atmospheric conditions – are performed according to specific instrument characteristics
1098 (sampling interval, FWHM, SNR, etc.). But the reliability of accuracy statistics obtained in this
1099 way depends on the overall assumptions included in the canopy and atmospheric RT models and
1100 how accurately the models are coupled. Most numerical simulations are based on homogenous
1101 1D surfaces and Lambertian assumption (e.g., Damm et al., 2011; Liu et al., 2015; Meroni et al.,
1102 2010; Zhao et al., 2014), and in only a few cases has a full bidirectional reflectance distribution
1103 function (BRDF) scenario been included in the forward model (Cogliati et al., 2015b; Liu and
1104 Liu, 2018; Mazzoni et al., 2010; Verhoef et al., 2018). More recently, full 3D RT models
1105 incorporating fluorescence (e.g., FluorWPS, FluorFLIGHT, and DART) [**Section 4**] were

1106 developed, offering more complex strategies to calculate retrieval accuracy in heterogenous
1107 canopies and landscapes.

1108 A more direct evaluation of SIF retrieval accuracies from airborne and satellite sensors is
1109 possible using direct comparisons with ground-based data. These data can provide more reliable
1110 estimations of fluorescence because surface irradiance is measured, and atmospheric effects may
1111 be neglected. This has been used successfully for airborne observations from the *HyPlant* sensor,
1112 operating at spatial resolution of one meter (Rascher et al., 2015; Rossini et al., 2015). However,
1113 since ground-based methods (e.g., from towers) sample a footprint of only a few square meters,
1114 it presents difficulties for validation of medium and coarse-spatial-resolution data. Validation of
1115 SIF retrievals from medium-resolution satellite missions such as FLEX (300 x 300 m²) could be
1116 feasible by combining data from field spectroscopy instruments – to get continuous temporal
1117 data – with less frequent acquisitions over larger spatial areas using robotic systems, UAVs, or
1118 other airborne sensors in selected sites.

1119 **5.6. Challenges and future directions in SIF retrieval**

1120 Main novelties in retrieval strategies include protocols for satellites using FLs and derivation of
1121 the full SIF spectrum. A recent shift from the use of terrestrial oxygen absorption bands – nearly
1122 all papers reviewed by Meroni et al. (2009) – to FLs alone, or in parallel with O₂ bands, is seen
1123 also in applications using atmospheric satellite sensors. Development of FL procedures was
1124 prompted by the convenient availability of atmospheric chemistry satellites, which allowed
1125 researchers to capitalize on the simplified modelling of atmospheric effects in the solar
1126 absorption bands to quantify SIF at coarse spatial resolution [**Section 7**]. However, such results

1127 have suffered from the fact that the sensors employed were not specifically designed for SIF.
1128 Therefore, the instantaneous retrievals are aggregated to improve their quality at the cost of
1129 spatio-temporal resolution. However, improved observational capabilities and better SNR are
1130 offered by new atmospheric sensors (e.g., TROPOMI aboard the S-5P satellite) (Guanter et al.,
1131 2015).

1132 Retrieval methods that use O₂ absorption features have their pros and cons. On the one hand,
1133 they have access to features where the fluorescence contribution is more prominent, but on the
1134 other hand they require much more complex modelling to correct for atmospheric absorption and
1135 scattering inside the O₂ bands. The particular design of the tandem FLEX/S-3 mission concept,
1136 aimed at SIF retrieval using the O₂ bands, was developed specifically to address requirements for
1137 an accurate atmospheric correction and SIF detection. The broad spectral coverage (from blue
1138 bands to IR wavelengths), the high-spectral resolution in the red and far-red region, and the dual-
1139 view (nadir and oblique) offered by the tandem mission provide the spectral and directional
1140 information for an accurate atmospheric characterization (Drusch et al., 2017; ESA, 2015;
1141 Sabater et al., 2017).

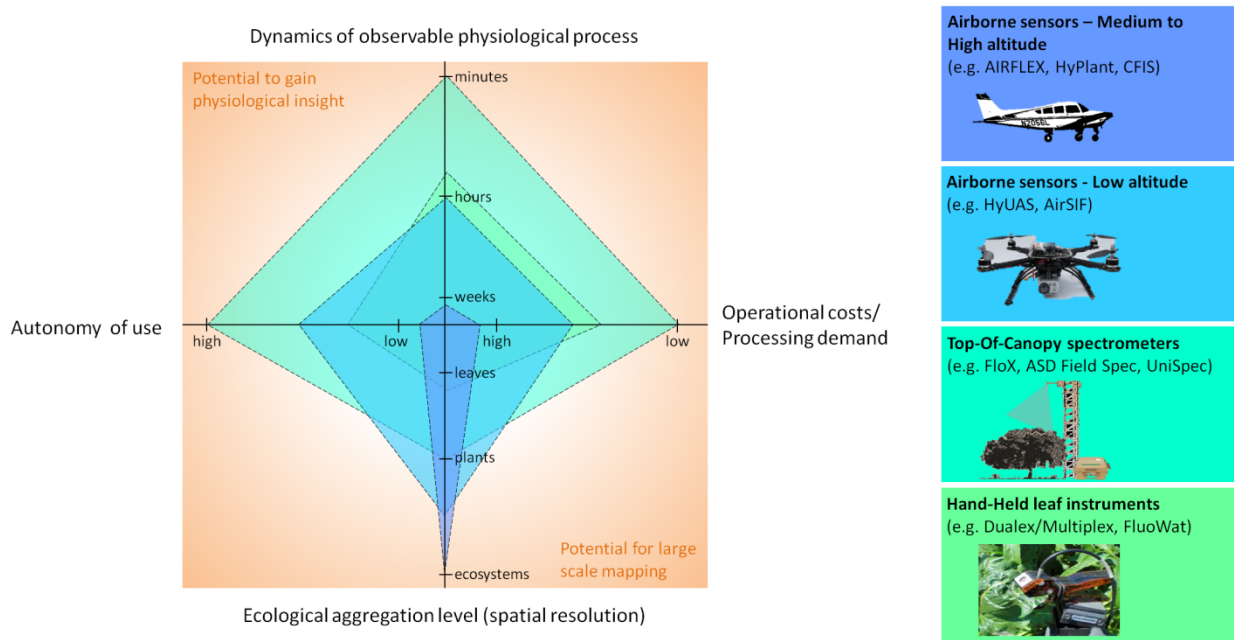
1142 Most methods emphasize selected absorption bands at both O₂ and FLs to provide independent
1143 fluorescence values, neglecting the possible functional relationship between red and far-red
1144 fluorescence emission peaks. Only the new generation of methods – full SIF spectrum and
1145 model-based inversion – offers a broader spectral characterization of SIF, and makes consistent
1146 use of the spectral detail available from the two fluorescence emission regions. The perspective
1147 of exploiting the full SIF spectrum is relevant for future work on fluorescence in relation to
1148 different canopy species, chemical/physical variables, and physiology. Knowledge of the entire

1149 fluorescence spectrum may be helpful to better quantify canopy re-absorption, as well as for
1150 deriving the respective PSI/PSII contributions and the fluorescence quantum efficiency.
1151 However, the full SIF spectrum is influenced at leaf and canopy levels by diverse factors which
1152 are not necessarily related directly to the photosynthetic activity of the plants [**Section 2**]. To
1153 further help understanding of all these combined effects, model inversion methods have the
1154 additional advantage of offering physiologically consistent estimates of canopy parameters that
1155 are essential to better interpretation of fluorescence. Nonetheless, in the model inversion
1156 approach VNIR information is needed for adjusting the canopy reflectance model parameters.
1157 Given that two spectrometers will likely be needed to acquire such data, accurate co-registration
1158 and intercalibration methods will be critical.

1159 **6. SIF measurement technologies – Field and airborne systems**

1160 **6.1. Technological overview**

1161 A range of field sensors have been developed over the years, from hand-held and clip-on devices
1162 to TOC sensors deployable from stationary or mobile ground-based platforms, unmanned aerial
1163 vehicles (UAVs), and traditional aircraft. These technologies provide complementary capacity
1164 for measuring and interpreting fluorescence in the context of physiological processes. Airborne
1165 imaging allows mapping of fluorescence over plant canopies and derivation of indicators of
1166 photosynthetic functionality and pre-visual stress at ecological and management-relevant scales.
1167 Field and airborne systems also support satellite-based measurements through validation,
1168 interpretation, and provision of data inputs to models. The types of field systems are compared in
1169 **Figure 9**, indicating relative merits with respect to operational and biological considerations.



1170
 1171 **Figure 9.** Comparison and complementarity of hand-held, top-of-canopy, and airborne
 1172 instrumentation to gain insight into the information content of fluorescence and facilitate
 1173 mapping. (Colours on the left panel correspond to those on the right.)

1174 **6.2. Hand-held leaf instrumentation**

1175 Portability is a priority for passive SIF field devices. But unlike the availability of active
 1176 fluorometers that detect steady-state fluorescence in leaves – for which there are multiple
 1177 commercial devices – instruments designed specifically for SIF are still rare. One such device is
 1178 FluoWat, a hand-held leaf clip designed for use in natural sunlight. When coupled to a field-
 1179 portable spectrometer, the device allows quantification of the full SIF emission and also
 1180 reflectance and transmittance. FluoWat uses a short-pass filter (<650 nm) to control incoming
 1181 light, so only the fluorescence emission is measured when the filter is in place. Its fiber-optic
 1182 probe may be positioned to measure upward- or downward-directed fluorescence (typically from
 1183 adaxial or abaxial leaf surfaces, respectively), thereby allowing study of the interplay among
 1184 vertical pigment gradients, re-absorption, scattering properties, and leaf fluorescence emission.

1185 The instrument has been used to facilitate linking canopy and leaf-level SIF data, and for stress
1186 detection (Cendrero-Mateo et al., 2016; Van Wittenberghe et al., 2015, 2014, 2013). 6.3. Top-of-
1187 canopy spectrometers

1188 Early work in passive detection of TOC fluorescence was inspired by the development of the
1189 MKII Fraunhofer line discriminator, an airborne instrument for remote sensing of solar-induced
1190 ‘luminescence’ (Hemphill et al., 1977; Plascyk, 1975). Used with leaves and canopies to reveal
1191 subtle changes at the H α FL (656.3 nm), was applied successfully by McFarlane et al. (1980) to
1192 identify water stress in citrus crops, and by Carter et al. (1990) to relate SIF to carbon
1193 assimilation in field vegetation. But limitations to using the H α band were its distance from the
1194 fluorescence peaks and its narrow width (\sim 0.1 nm FWHM) which necessitated very high SNR.

1195 Detection of SIF in the O₂ bands has been researched intensively in the last twenty years
1196 [**Section 5**], and assorted instruments have emerged (Meroni et al., 2009). Kebabian et al. (1999)
1197 introduced a plant fluorescence sensor to detect photons re-emitted after absorption of
1198 fluorescence by oxygen contained in a low-pressure cell. Carter et al. (1996) used a Fraunhofer
1199 Line Radiometer measuring in the O₂-B band to study herbicide effects on leaf fluorescence.
1200 Moya et al. (2004) invented an instrument using narrow-band interference filters to derive
1201 fluorescence in the O₂-A band. And Evain et al. (2001) introduced a Passive Multi-wavelength
1202 Fluorescence Detector (PMFD) to measure fluorescence and reflectance at 760 nm and at 687
1203 nm. Quantification of SIF in the O₂-B and O₂-A bands also was done by Fournier et al. (2012)
1204 using their SpectroFLEX canopy instrument, able to perform continuous and automatic
1205 measurements over several weeks. Finally, Pérez-Priego et al. (2005) illustrated the sensitivity of
1206 fluorescence (in-filling) at the O₂-A band to water stress by using a high-resolution spectrometer

1207 housed in a temperature-controlled box and connected to a 15-m-long fiber-optic cable for
1208 acquisition of reflectance from single tree crowns.

1209 Developments in sensor technologies have sought to harness the combined information of
1210 reflectance and fluorescence (Burkart et al., 2015; Cheng et al., 2013; Migliavacca et al., 2017a;
1211 Panigada et al., 2014; Pérez-Priego et al., 2015, 2005; Yang et al., 2015). Well-calibrated ASD
1212 FieldSpec devices, for example, which have high SNR (even though the O₂ absorption bands are
1213 not well resolved), have been used to capture diurnal courses of canopy SIF and reflectance
1214 (Damm et al., 2014, 2010; Liu et al., 2005), an approach also tested with some success from low-
1215 flying research aircraft (Damm et al., 2014; Schickling et al., 2016).

1216 Sophisticated apparatus have emerged to better resolve absorption features and leverage the
1217 availability of low-cost miniaturized spectrometers. A fully automatic system, consisting of three
1218 miniature high-resolution HR2000+ spectrometers (Ocean Optics, Florida, USA) enclosed in a
1219 temperature-stabilized box and connected to collimated optic fibers, was installed atop a crane to
1220 continuously monitor SIF and reflectance spectra at a high repetition rate (1 Hz) (Daumard et al.,
1221 2012, 2010; Goulas et al., 2017). Two inter-calibrated spectrometers allowed almost
1222 simultaneous determinations of incoming and reflected radiation, with an automated routine
1223 continuously adjusting integration time to the intensity of incoming radiation in order to optimize
1224 SNR.

1225 New instrument architectures introduced by researchers at the University of Milano and their
1226 colleagues combined high-resolution spectrometers in a temperature-stabilized box, with optical
1227 multiplexers and a dedicated intercalibration routine, creating a stable TOC measurement system
1228 (Cogliati et al., 2015a). In ecosystem studies, this apparatus provided the first concise

1229 comparison of fluorescence emissions across different plant functional types (Rossini et al.,
1230 2016). The Milano system, known commercially under the name ‘FloX’ (Julitta et al., 2017),
1231 houses two spectrometers (one broadband, one high-resolution) with bifurcated fibers to allow
1232 almost simultaneous measurements of incoming and reflected irradiance. Precise calibration of
1233 the integrated system and automated data retrieval algorithms permit estimation of red and far-
1234 red fluorescence. The systems have been installed on about a dozen observation towers
1235 internationally to date.

1236 An automated, tower-based canopy system called FUSION, developed by NASA-GSFC,
1237 integrates multi-directional spectral, thermal, and SIF observations (Middleton et al., 2018). Its
1238 two dual-channel systems (upward- and downward-looking spectrometers) simultaneously
1239 collect high-spectral-resolution data of reflected light and fluorescence and can operate
1240 continuously during daylight hours to capture diurnal and seasonal dynamics. Data products
1241 include VNIR surface reflectance spectra from ~350-1100 nm, red and far-red SIF, and surface
1242 temperature.

1243 Other tower-based examples include FluoSpec, PhotoSpec, and AutoSIF. FluoSpec (Yang et al.,
1244 2018c, 2015) is an automated system that provides high SR (~0.13 nm FWHM) between 680 and
1245 775 nm for red and far-red SIF; it has been used since 2012 in a site network called FluoNet.
1246 PhotoSpec assesses the red (670-732 nm) and far-red (729-784 nm) wavelength ranges and also
1247 canopy reflectance (400-900 nm); it has a high SNR and SR to allow FL retrievals and has been
1248 used successfully for continuous daytime monitoring of SIF (Grossmann et al., 2018). AutoSIF
1249 (Zhou et al., 2016; Xu et al., 2018) uses a single spectrometer to capture a spectral range of

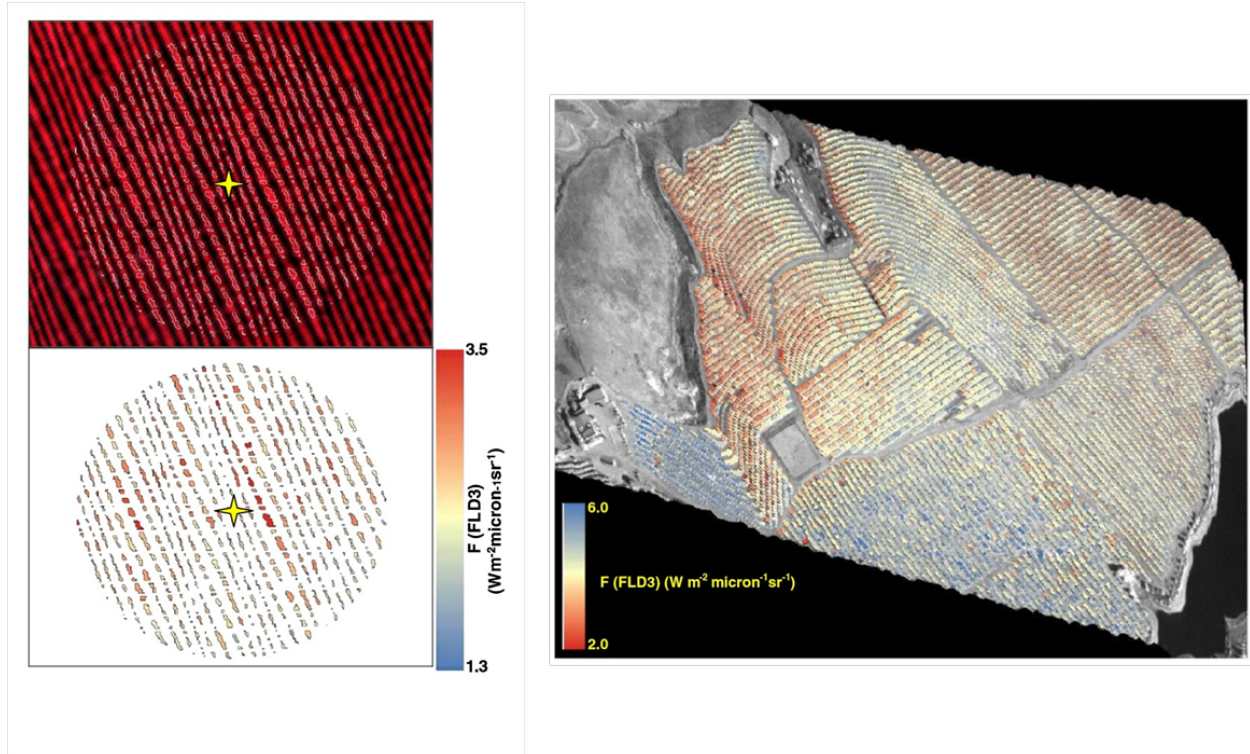
1250 ~480-850 nm, with a spectral resolution of 0.9 nm, SNR of 1000:1, and spectral sampling
1251 interval of 0.4 nm; it has been used to quantify red and far-red SIF (Xu et al., 2018).

1252 **6.4. Airborne systems**

1253 **6.4.1. Low-altitude systems – Unmanned aerial vehicles**

1254 Unmanned aerial vehicles (UAVs) (also called unmanned aircraft systems, UAS) provide
1255 observations of vegetation optical properties at the intermediate scales between ground-based
1256 and higher-altitude airborne systems. The appeal of this approach is the flexibility to provide on-
1257 demand hyperspectral imagery at high spatial and temporal resolutions (Berni et al., 2009;
1258 Garzonio et al., 2017; Lucieer et al., 2014; Malenovský et al., 2017; Zarco-Tejada et al., 2012,
1259 2009). UAV deployments over vegetation is a fairly recent undertaking, with first prototypes
1260 developed in the early 2000s used in agricultural applications (e.g., Herwitz et al., 2004; Johnson
1261 et al., 2003). Subsequent trials were restricted primarily to multispectral and broad-band thermal
1262 imagery acquisition (e.g., Turner et al., 2014) – but in the last decade UAV systems suitable for
1263 SIF retrieval have emerged.

1264 UAV capability to retrieve SIF has been demonstrated in several investigations. Some early
1265 experiments used a fixed-wing type of unmanned aircraft equipped with a micro-hyperspectral
1266 imager and thermal camera (**Figure 10**) (Zarco-Tejada et al., 2013b, 2012). SIF emission (O₂-A)
1267 derived from the extracted spectral radiance of pure-crown 30-cm or 40-cm pixels showed, along
1268 with independent ground observations and models, that SIF signals from individual trees with
1269 different water stress status could be discriminated (using the 3FLD method with a 6-nm FWHM



1270
 1271 **Figure 10.** High (30- or 40-cm) resolution SIF retrievals from hyperspectral imagery acquired
 1272 from an unmanned aerial vehicle flown over an eddy covariance flux tower in an olive orchard
 1273 (left, false colour composite) (Source: Zarco-Tejada et al., 2013b), and over a citrus field
 1274 subjected to water stress treatments (right) (Source: Zarco-Tejada et al., 2012). The high
 1275 resolution imagery acquired by the micro-hyperspectral camera enabled the quantification of SIF
 1276 (O_2 -A band) on pure tree crowns, removing the large effects caused by shadows and background
 1277 in heterogeneous canopies.

1278 and 1.85 nm sampling spectra). Other systems followed, such as the HyUAS (Garzonio et al.,
 1279 2017), a non-imaging multi-rotor-platform apparatus designed to optimize optical and data
 1280 acquisition, e.g., under changing meteorological conditions (Cogliati et al., 2015a) and for
 1281 provision of a more homogenous footprint at a given flight height. Another development, the
 1282 Piccolo doppio (Mac Arthur et al., 2014), incorporates two fiber-optic-based spectrometers and
 1283 allows near-simultaneous measurements of reflectance and fluorescence in the oxygen bands.
 1284 Finally, there is AirSIF, which uses a QE PRO spectrometer (Ocean Optics) with bifurcated two-
 1285 channel optical fibers, and was designed to achieve accurate ground localization and shape

1286 reconstruction of the SIF and reflectance footprints – by considering exact UAV posture,
1287 geographic position, and detailed digital surface modelling of the vegetation canopy (Bendig et
1288 al., 2018).

1289 Technical advantages of UAVs include the capability for highly customized deployments (e.g.,
1290 low and slow flights allowing for high spatial resolutions and long integration times) and quick
1291 response and turn-around for planning and investigation. Although miniaturized and lightweight,
1292 UAV systems need to have a stable high spectral performance, with sufficient SNR and precision
1293 to provide accurate SIF retrievals. On the other hand, for some applications, the primary value
1294 might be a high spatial resolution with a more accurate geolocation rather than precise SIF
1295 estimates (Gautam et al., 2018), to allow e.g., mapping of SIF spatial variability in stressed
1296 vegetation. In controlled studies, high spatial resolution can also help to discriminate the many
1297 confounding influences on SIF magnitude (e.g., shadows, vegetated background with different
1298 structure, pigment contents, etc.), thereby complementing coarser-resolution airborne and
1299 satellite systems.

1300 **6.4.2. Medium- or high-altitude systems**

1301 **Line scanners**

1302 Over 30 years ago, it was shown that, despite the low emission of SIF in natural environments, it
1303 was detectable using airborne sensors in marine systems. Using the fluorescence line height
1304 feature, the fluorescence peak at 685 nm emitted by phytoplankton was clearly discriminated
1305 from background radiance of the sea surface (Gower and Borstad, 1990; Neville and Gower,
1306 1977). But this differential technique was not applicable to terrestrial vegetation owing to its
1307 very different spectral properties such as higher reflectance – the shape of which is controlled

1308 mainly by photosynthetic pigment content and strong re-absorption of the red fluorescence
1309 (Zarco-Tejada et al., 2000b). Instead, passive detection of vegetation SIF using airborne systems
1310 came to rely on narrow absorption features of the incident radiation. To the best of our
1311 knowledge, the first reported airborne test over vegetation was performed with the MKII
1312 Fraunhofer Line Discriminator deployed onboard a helicopter (Watson and Hemphill, 1976).
1313 Later, using the enhanced sensitivity provided by the oxygen bands, the AIRFLEX line scanner
1314 became the first dedicated airborne instrument for measuring SIF in terrestrial vegetation (Moya
1315 et al., 2006). AIRFLEX is a multichannel radiometer that uses narrowband interference filters
1316 (FWHM between 0.5 and 1 nm, depending on the channel) to sample the in-band and out-of-
1317 band radiances at 687 nm and 760 nm. Interference filters allow for the detection of a high flux,
1318 enhancing SNR (albeit at the expense of spectral resolution). AIRFLEX was first tested in
1319 campaigns of the SENtinel-2 and FLuorescence EXperiment (SEN2FLEX) program, and it
1320 demonstrated clearly the feasibility of analysis in the O₂ bands (Moya et al., 2006). These early
1321 experiments were crucial in proving the distinctive nature of the fluorescence signal compared to
1322 conventional reflectance (Rascher et al., 2009).

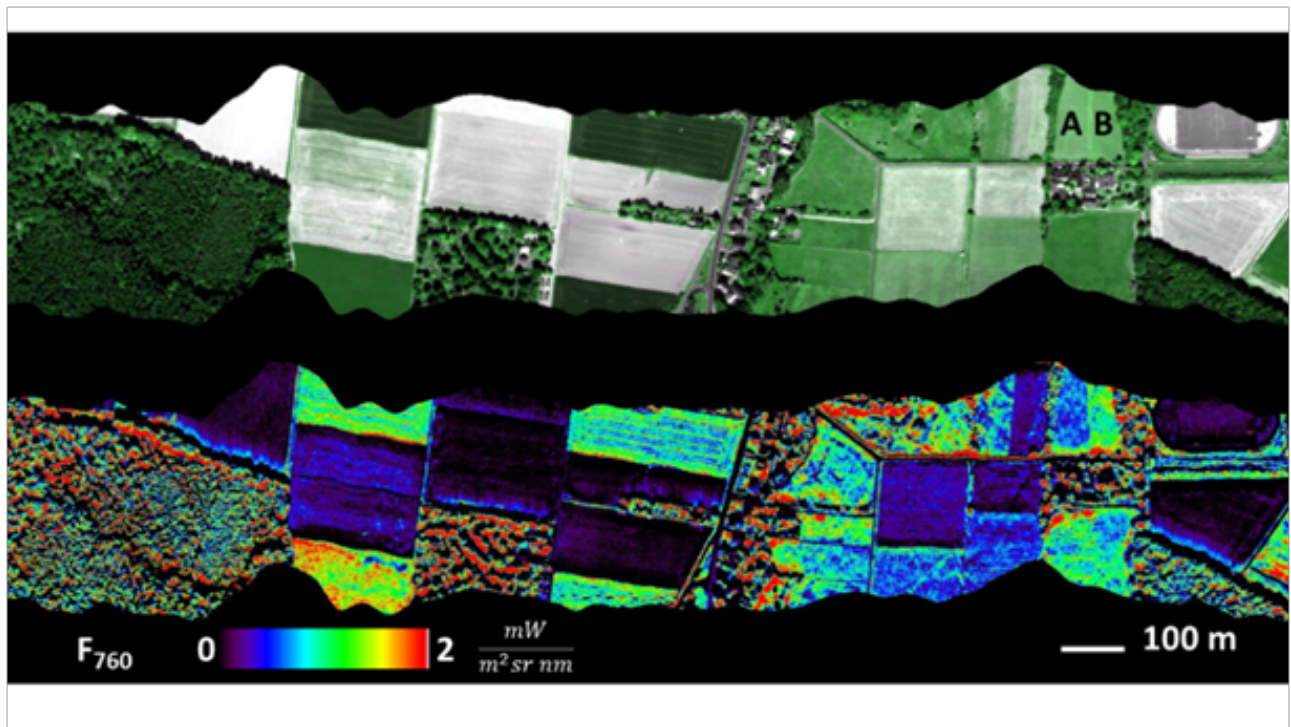
1323 **Airborne imaging spectrometers**

1324 Until airborne imaging sensors specialized for measuring SIF became available, spectrometers
1325 with lower SR were used. They included, for example, the Reflective Optics System Imaging
1326 Spectrometer (ROSIS) (Maier et al., 2003), the CASI (Zarco-Tejada et al., 2002, 2001), and the
1327 Airborne Prism Experiment (APEX) (Damm et al., 2015a) – to retrieve SIF in the wider O₂-A
1328 band. From today's perspective, such instruments are considered sub-optimal due to their low SR
1329 (e.g., 2.2 nm for CASI-1500, 5.7 nm for APEX, and 7 nm for ROSIS), which allows

1330 fluorescence maps only in relative units, but some of these imagers (e.g., APEX) benefited from
1331 a high SNR, partly compensating for the lower SR (Damm et al., 2011). These case studies
1332 propelled the entire field by providing relevant and interesting insight into the spatial and
1333 temporal variability of SIF. They demonstrated the value of the 3FLD technique (Maier et al.,
1334 2003), the feasibility of using airborne data to validate maps of SIF retrieved from satellite
1335 sensors (Guanter et al., 2007), and the possibility to derive multi-year data to study relationships
1336 between SIF and ecosystem GPP (Damm et al., 2015a).

1337 After some attempts to use existing imaging spectrometers in a reprogrammed mode (Rascher et
1338 al., 2009), the *HyPlant* airborne imaging spectrometer was developed as a cooperative endeavour
1339 between Germany's Forschungszentrum Jülich and the Finnish company SPECIM. As the core
1340 reference instrument and demonstrator for the FLEX satellite mission, *HyPlant* was the first
1341 airborne sensor optimized optically for full-spectrum SIF retrieval, taking advantage of the
1342 oxygen absorption and FLs near 685 and 760 nm. *HyPlant*'s core module operates with high SR
1343 (0.25 nm) and a spectral sampling interval of 0.11 nm to resolve the spectral window between
1344 670 and 780 nm (Rascher et al., 2015). Initial testing starting in 2012 confirmed that SIF could be
1345 retrieved successfully in the O₂-A band from such an airborne platform to provide information
1346 not discernible from reflectance (**Figure 11**) (Rascher et al., 2015; Rossini et al., 2015; Simmer
1347 et al., 2015). While the first version of the instrument had an imperfect point-spread function and
1348 limited SNR, subsequent improvements have increased SNR and pointing accuracy. The optical
1349 path of the fluorescence module has been redesigned and upgraded to achieve a stable optical
1350 performance of the detector, also helping retrieval of both fluorescence peaks using the O₂-A and
1351 Gerhards et al. 2018, Liu et al. 2018, von Hebel et al. 2018, Yang et al. in press).

1352 Two airborne imaging spectrometers were developed recently in the US. One is the NASA/JPL
 1353 CFIS, an imaging system developed for validation of OCO-2 SIF retrievals. CFIS has a high SR
 1354 (<0.1 nm) and spectral coverage between 737-772 nm for estimation of far-red SIF (Frankenberg
 1355 et al., 2018; Sun et al., 2017). It has been used in airborne campaigns to under-fly orbital tracks
 1356 of the OCO-2 satellite, revealing strong agreement between SIF retrieved from OCO-2 and CFIS
 1357 along latitudinal gradients (Sun et al., 2017). A second imager, the Hyperspec High Resolution
 1358 Chlorophyll Fluorescence Sensor, is a lightweight sensor developed by Headwall Photonics, Inc.
 1359 (Bolton, Massachusetts) in partnership with NASA/Goddard to capture the spectral range



1360

1361 **Figure 11.** Reflectance (upper panel) and canopy SIF (lower panel) maps obtained with the
 1362 *HyPlant* airborne sensor over an agricultural research site in Klein Altendorf, Germany. Lower
 1363 SIF is evident in forests (left in lower panel) and higher SIF in dense agricultural fields (middle
 1364 and right in lower panel). Fluorescence emission reveals information on vegetation status which
 1365 is not visible in the reflectance domain. For example, the two fields denoted as A and B display
 1366 almost identical reflectance (upper panel), whereas their fluorescence emission is very different
 1367 (lower panel). (Source: U. Rascher/Forschungszentrum Jülich)

1368 of 670-780 nm (~0.2 nm SR), allowing retrieval of both red and far-red SIF. This sensor has
1369 been integrated into NASA/Goddard's G-LiHT airborne package which also collects lidar,
1370 thermal, and hyperspectral visible-NIR optical data (Middleton et al., 2017).

1371 **6.5. Adapting theory to the 'real world'**

1372 The study of fluorescence in natural field conditions and at different biological and spatial scales
1373 requires consideration of multiple factors to acquire coherent measurements, to avoid retrieval
1374 artefacts, and to correctly interpret results. Sensor technologies, retrieval strategies, and the
1375 specific influential factors in a given situation can all affect robustness and reliability of
1376 fluorescence results. Aspects that change between proximal and remote sensing with
1377 implications for fluorescence retrievals include (i) non-uniformities and instabilities of the
1378 detectors, (ii) spatial footprint of the instrumentation, and (iii) impact of atmospheric effects.
1379 Also important is the appropriate use and the relative height placement of canopy versus
1380 reference sensors for accurate SIF measurements (Sabater et al., 2018).

1381 With field spectrometers positioned within a short distance of the surface target, information on
1382 atmospheric functions (including atmospheric transmittances, path scattered radiance, and
1383 spherical albedo) can be provided by measuring reference panels. But with increasing distances
1384 (i.e., using tower, airborne or satellite sensors), a combination of measured and modelled
1385 atmospheric functions is required, necessitating accurate dynamic calibration status of the
1386 sensors during operation (i.e., SR, center wavelength position, stray light, etc.). It is common for
1387 spectrometers to change their spectral and radiometric performance due to pressure or
1388 temperature variations during operations. As a result, spectral non-uniformities associated with

1389 changing center wavelength position or SR during operations eventually impact the point spread
1390 function of the spectral detector element. Radiometric non-uniformities are associated with, for
1391 instance, temperature-dependent changes in dark noise (D’Odorico et al., 2010; Schlapfer et al.,
1392 2007). In situations where sensors deviate during operations from their nominal lab performance,
1393 or where they were imperfectly calibrated, the combination of modelled atmospheric functions
1394 with measured radiances is prone to error and even substantial uncertainties in retrieved
1395 fluorescence (Damm et al., 2011; Moreno et al., 2014).

1396 The spatial footprint measured by instrumentation can have implications for the validity of
1397 assumptions used in atmospheric correction [**Section 5**]. For example, SIF retrievals using tower-
1398 based or airborne instrumentation with very small pixels (e.g., < 2 m) may be subject to artefacts
1399 due to greater dominance of geometric optical scattering by canopy components and higher
1400 likelihood of measuring (partly) shaded surfaces (i.e., a reduced fraction of direct irradiance)
1401 (Damm et al., 2015b). This could violate atmospheric correction tools that assume fully
1402 illuminated, homogeneous, and Lambertian reflecting surfaces, with isotropic and volumetric
1403 scattering being the dominant scattering processes.

1404 While the emphasis here is on passive sensing of SIF, the broader context of fluorescence
1405 evaluation includes active sensors and other spectral technologies helpful for studying
1406 fluorescence characteristics and the influence of multiple factors [**Section 2**]. Active
1407 technologies tend to allow better control of excitation conditions and are well suited to
1408 measurement of parameters such as fluorescence yield (the metric often associated to plant
1409 physiology). They can be an important complement to passive devices for proximal field work.

1410 **6.6. Challenges and future directions in field and airborne sensing of SIF**

1411 Substantial progress has been achieved in measuring SIF in field settings using ground-based and
1412 airborne systems, with noteworthy prospects for applications [Section 8]. Airborne SIF sensors,
1413 for example, have been used to reveal pre-visual stress effects from a bacterial pathogen (*Xylella*
1414 *fastidiosa*) currently infecting economically vital crops worldwide (Zarco-Tejada et al., 2018) or
1415 were applied to early signs of photosynthetic down regulation during drought stress in various
1416 crop species (Yang et al., in press). Such applications will be supported by an expanding choice
1417 of available instruments which allows analysis of SIF across spatial scales. We expect that UAV-
1418 based sensors will become more available in the near future and that a next generation of
1419 *HyPlant*-like instruments will be developed. In light of the recommendations from Section 5 –
1420 for improved spatio-temporal capacity; flexibility to measure both red and far-red fluorescence
1421 (including the full emission spectrum of SIF); sufficiently high SR and SNR to allow accurate
1422 SIF retrieval; and the provision of surface reflectance VNIR spectra to support model inversion –
1423 it is evident that modern options are well the way to realizing those objectives.

1424 Some of the required techniques and corrections are well established for high-performance
1425 airborne systems, and they are being refined for miniaturized or lightweight sensors so as to
1426 avoid instrument and retrieval artefacts. Priorities for improvements include the correction of
1427 sensor stray light, non-linearity, and point-spread-function artefacts. [Straylight aspects have
1428 been covered by Coppo et al. (2017) in their discussion of the FLEX sensors, and it is instructive
1429 for sensors in general.] Overcoming the problem of illumination artefacts originating from
1430 geometric optical scattering in high-spatial-resolution data (i.e., individual scattering elements
1431 dominate the sensor's field-of-view; Kückenbrink et al., in press) is still an open issue. With

1432 controlled field observations, it appears to be of smaller impact, but when airborne spectrometers
1433 with high spatial resolution are used, retrieval artefacts are possible and new retrieval concepts
1434 accounting for varying fractions of direct and diffuse irradiance components must be developed
1435 (Damm et al., 2015b). We expect that technical advances in ground-, tractor-, UAV-, and
1436 aircraft-based instruments will facilitate realization of the full potential of SIF techniques for
1437 applications in vegetation and crop management, and in validation and interpretation of SIF
1438 retrievals from satellite spectrometers. In this context, these sensors will complement satellite
1439 based measurements and will provide SIF data at higher spatial and temporal scales, necessary
1440 for local mapping of natural ecosystems and in agriculture. .

1441 **7. SIF measurement technologies – Satellite systems**

1442 **7.1. Technological overview**

1443 Breakthroughs in understanding the effects of fluorescence on apparent reflectance, coupled with
1444 advances in modelling, SIF retrieval approaches, and sensor capabilities, have contributed to the
1445 realization of satellite-based SIF detection. In 1999, Marc-Philippe Stoll and colleagues proposed
1446 to the European Space Agency that a satellite mission, FLEX, be developed to measure SIF from
1447 terrestrial vegetation to support science and applications in agriculture, forestry and global
1448 change issues (Stoll et al., 1999). This concept was developed, evaluated, and refined over the
1449 ensuing years (ESA, 2015; Moreno et al., 2006; Rascher et al., 2008), and in 2015 FLEX was
1450 approved to be ESA's 8th Earth Explorer, with a projected launch date of 2022 (Drusch et al.,
1451 2017). During the preparatory activities, ESA commissioned scientific studies, field and airborne
1452 campaigns with prototype sensors, and modelling developments foundational to satellite-based

1453 SIF science (e.g., Ač et al., 2015; Magnani et al., 2009; Miller et al., 2005; Mohammed et al.,
1454 2016, 2014; Moreno et al., 2014; Pedrós et al., 2010; Rascher et al., 2015, 2009; Van der Tol et
1455 al., 2014, 2009b; Verhoef et al., 2018; Verrelst et al., 2016, 2015a; Zarco-Tejada et al., 2006).

1456 Meanwhile, researchers independently working with the atmospheric chemistry satellite GOSAT
1457 reported that chlorophyll fluorescence could indeed be retrieved in the very narrow far-red
1458 wavelengths adjacent to the O₂-A band, albeit at very coarse spatial resolution ($\geq 0.5^\circ$), from
1459 which global maps could be produced (Frankenberg et al., 2011a, 2011b; Joiner et al., 2011).
1460 This exciting finding affirmed the earlier work of Guanter et al. (2007) who had shown that far-
1461 red SIF could be discriminated in terrestrial vegetation using the MERIS satellite sensor onboard
1462 EnviSat. Several satellite sensors designed primarily for measurement of atmospheric trace gases
1463 (e.g., CO₂, methane, and cloud parameters) have since been used to quantify SIF regionally and
1464 globally at coarse spatial scales. Retrievals from almost all of these missions have been of far-red
1465 SIF.

1466 **7.2. The FLuorescence EXplorer (FLEX): A tandem mission with Sentinel-3**

1467 FLEX is the first satellite mission designed specifically for SIF measurement. It will obtain the
1468 suite of SIF features and ancillary data types considered necessary for quantification and
1469 interpretation of vegetation parameters related to photosynthetic function (Drusch et al., 2017).
1470 The overarching scientific objective of FLEX is to achieve an improved understanding of global
1471 seasonally variable photosynthetic functioning and efficiency of vegetation, including
1472 physiological indicators of plant stress. The five-year global mission will cover terrestrial
1473 vegetation and coastal regions, including land areas between 75°N and 56°S, islands > 100 km²,

1474 and coastal zones within 370 km of coastlines. FLEX will produce imagery and maps at $300 \times$
1475 300 m^2 spatial resolution, intended for the monitoring of vegetation at scales of local to
1476 landscape-scale management units and ecosystems (Drusch et al., 2017).

1477 FLEX will be deployed in a tandem mission with Sentinel-3 (**Figure 12**), a European operational
1478 satellite carrying the Ocean and Land Colour Imager (OLCI) and the Sea and Land Surface
1479 Temperature Radiometer (SLSTR) sensors. The FLEX mission will carry a single payload,
1480 FLORIS, which is a dual-spectrometer imaging system consisting of narrow-band (high SR) and
1481 wide-band (low SR) sensors, measuring the spectral range of 500-780 nm to capture the full SIF
1482 emission as well as reflectance for vegetation indices. Instruments from S-3 will provide
1483 atmospheric and thermal data, geolocation information, and other ancillary data (ESA, 2018).

1484 Unique products from the FLEX/S-3 tandem mission include: (i) total fluorescence emission
1485 (F_{tot} , 650-780 nm); (ii) red and far-red fluorescence at the peaks (F_{685} , F_{740}) and at the O₂-B and
1486 O₂-A features (F_{687} , F_{760}); (iii) photosynthetic activity estimates; and (iv) biophysical variables
1487 and indices derived from reflectance (e.g., surface fractional vegetation cover; canopy
1488 chlorophyll content; LAI; the fraction of photosynthetically active radiation absorbed by
1489 chlorophyll, $f\text{APAR}_{\text{chl}}$; and PRI) (ESA, 2018). These products will be derived from harmonized
1490 TOA Synergy data products using FLORIS, OLCI, and SLSTR radiances cross-calibrated,
1491 geometrically co-registered, and ortho-rectified to a common $300 \times 300 \text{ m}^2$ grid. Higher-level
1492 products include physiological response variables derived from temporal composites and spatial
1493 mosaics (e.g., activation/deactivation of photosynthesis; fluorescence quantum efficiency; and
1494 PSII and PSI contributions). These data are expected to improve estimation of GPP and surface
1495 fluxes at the local scale and to provide indicators of plant stresses that could reduce or

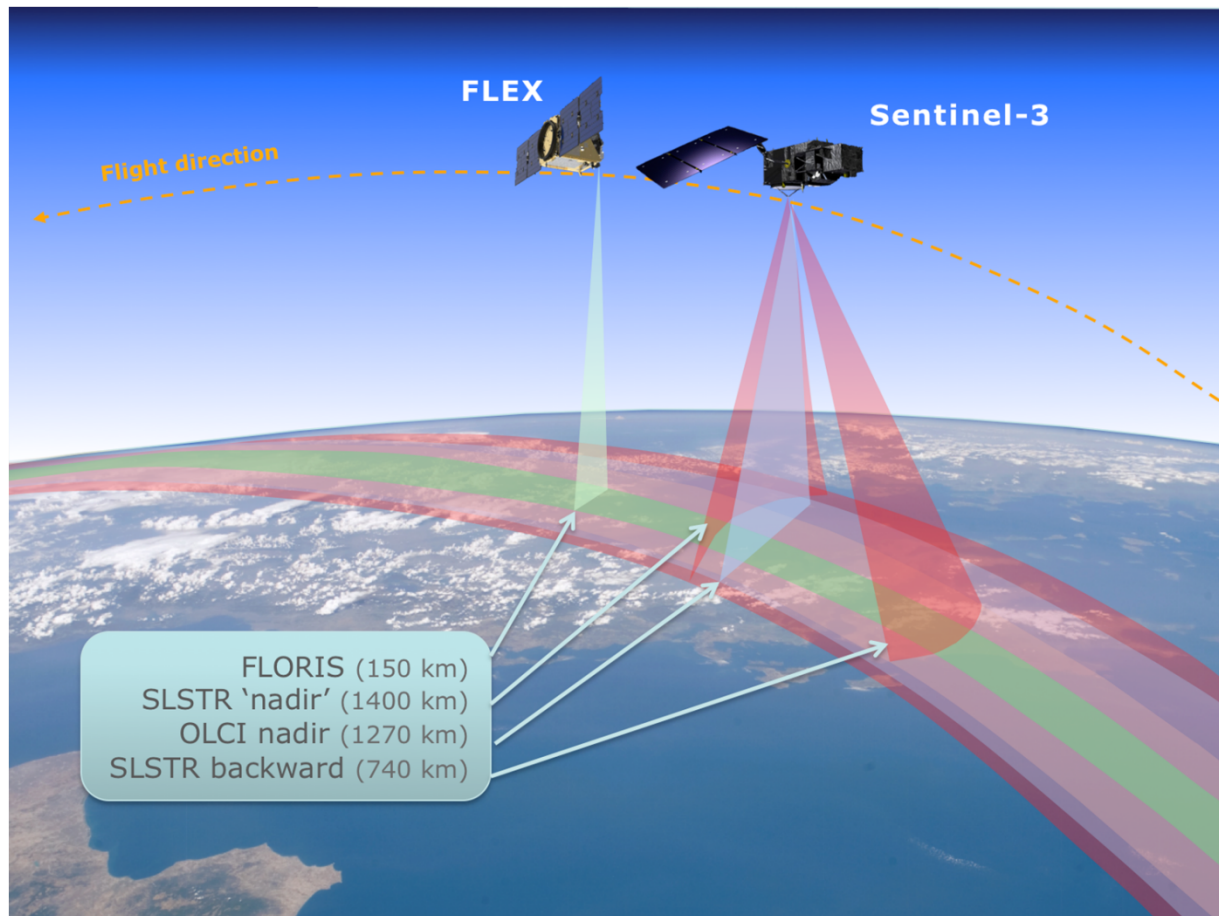
1496 compromise productivity and functional resilience. While the spatial resolution of FLEX exceeds
1497 existing satellite missions being used for SIF, it is not of the very high spatio-temporal
1498 granularity suited to precision agriculture. Also, the monthly repeat cycle (i.e., nadir view of the
1499 same area) at low latitude is not geared to applications requiring very frequent sampling – but at
1500 high latitudes, FLEX revisits (i.e., off-nadir view) will be more frequent, for example, 1-2 weeks
1501 in boreal areas, owing to orbital overlap, but also subject to viewing angle effects (Middleton et
1502 al., 2018; Wei et al., 2018). Studies currently underway for FLEX are investigating error
1503 analytics for mission products, and refinement of Cal/Val strategies, with fine-tuning of
1504 algorithms as required. The FLEX mission design and a conceptual framework for SIF
1505 applications have been described in detail elsewhere (e.g., Coppo et al., 2017; Drusch et al.,
1506 2017; ESA, 2018, 2015; Mohammed et al., 2014).

1507 **7.3. Atmospheric chemistry satellites used for SIF retrieval**

1508 Several global SIF datasets have been produced in the last years using spaceborne spectrometers
1509 that were originally designed for atmospheric chemistry applications (**Table 3**). In all cases,
1510 retrieval has been based on the utilization of FLs [**Section 5.2.2**].

1511 The FL in-filling approach was pursued independently by Joiner et al. (2011), Frankenberg et al.
1512 (2011a, 2001b), and Guanter et al. (2012), with global application to the Thermal And Near-
1513 infrared Sensor for carbon Observation Fourier Transform Spectrometer (TANSO-FTS) on the
1514 Japanese satellite, GOSAT. This high-spectral-resolution instrument has a channel covering the
1515 O₂-A band. The original purpose of the O₂-A band channel was to quantify the effects of
1516 aerosols and clouds on carbon dioxide (CO₂) and methane (CH₄) estimation. Several isolated FLs

1517



1518

1519 **Figure 12.** Schematic of the FLEX two-satellite tandem mission combining the FLORIS free-
1520 flyer with an operational Sentinel-3 satellite having a 10:00 am equatorial overpass time. FLEX's
1521 150 km nadir swath (green track) lies within the wider swath of the nadir OLCI camera (blue
1522 track, 1270 km). The SLSTR (red tracks) has a back-looking swath (740 km, 500 x 500 m²
1523 pixels) and a nadir swath (1400 km, 1000 x 1000 m² pixels). (Source: European Space Agency.)

1524 can be observed within this channel on either side of the O₂-A band, enabling retrieval of SIF.

1525 While the first global maps of SIF were generated from TANSO-FTS, its low SNR and relatively

1526 low sampling necessitated averaging the data over larger footprints (~2° latitude by 2° longitude)

1527 to obtain reliable contiguous coverage.

1528 A similar channel in NASA's OCO-2 includes a high SR grating spectrometer designed to
1529 measure CO₂. Observations of SIF from OCO-2 (Frankenberg et al., 2014; Sun et al., 2018,
1530 2017), have been compared with SIF results from the airborne CFIS instrument (Frankenberg et
1531 al., 2018; Sun et al., 2017). The OCO-2 ground footprint is much smaller than that of TANSO-
1532 FTS and it has denser sampling that enables more precise gridded measurements. But the higher
1533 spatial resolution of OCO-2 comes with a trade-off in that it does not provide contiguous orbital
1534 collections nor complete global coverage with its 10 km-wide swath.

1535 The higher repeat cycle (on the order of days) afforded by wide-swath satellite sensors designed
1536 for global analyses of atmospheric trace gases prompted Joiner et al. (2013) to examine whether
1537 those moderate-spectral-resolution sensors could be used reliably to quantify SIF. These include
1538 GOME-2 and similar sensors such as SCIAMACHY (which operated onboard the EnviSat
1539 satellite until contact was lost in 2012). They do have spectral coverage throughout the SIF
1540 emission range, but their ground footprints tend to be large. For example, SCIAMACHY's native
1541 footprint is approximately 30 km by 60 km for the nominal nadir mode that applies to red SIF,
1542 but due to onboard spectral averaging to reduce data volumes, the resolution is degraded to 30
1543 km by 240 km for far-red SIF observations. GOME-2 spatial footprints are 40 km by 80 km in
1544 the nominal wide swath mode, or 40 km by 40 km in a reduced swath mode. There are currently
1545 two GOME-2 instruments in orbit: the GOME-2A (on the MetOp-A satellite), which operated in
1546 the nominal mode from January 2007 through mid-July 2013 and since then is operating in the
1547 small-swath mode; and GOME-2B (on MetOp-B) which has operated in the nominal mode since
1548 mid-2013.

1549

1550 **Table 3.** Current and future satellite missions. Instruments in space or planned for launch that
 1551 have SIF measurement capability (red SIF wavelengths ~680-690 nm, and far-red ~730-780 nm).
 1552 A few of these also capture PRI wavelengths (between 520 and 580 nm). This list is not
 1553 exhaustive; e.g., follow-on missions such as OCO-3 and GOSAT-2 are not included. Pixel
 1554 quality refers to the combined utility of data products for uses based on influences of sensor
 1555 specifications (spectral range and parameters retrieved, FWHM, SNR), spatial resolution,
 1556 temporal collections, and Level 2-4 mission product support.

Mission / Sensor	Status / Launch	Coverage	Footprint (km)	Equatorial Overpass Time	Repeat Cycle	Spectral Range (nm)	FWHM (nm) (SIF)	SIF & PRI meas.	SNR	SIF Pixel Quality	Adequate Support meas.
FLEX / FLORIS	Selected/ ~2022	56°S-75°N	0.3 x 0.3	10:00	27 day	500-780	0.3-2.0	FR, R, full, PRI			
Sentinel-5P/ TROPOMI	In Orbit	Global	7 x 7	13:30	16 day	270-500 675-775 2305-2385	0.5	FR, full, (R)			
MetOp / GOME-2	In Orbit	Global	40 x 40 40 x 80	09:30	29 day	270-790	0.5	FR, full, (R), PRI			
TEMPO	Selected/ ~2019	CONUS	4 x 5	GEO	1 hour	290-490 540-740	0.6	(FR), PRI			
OCO-2	In Orbit	Global**	1.3 x 2.25	13:30	16 day	757-775	0.04	FR			
GOSAT / TANSO-FTS	In Orbit	Global**	10 x 10	13:00	3 day	758-775 1560-1720 1920-2080 5550-14300	0.025	FR			
MTG-S / Sentinel-4	Selected/ 2019	Europe	8 x 8	GEO	1 hour	290-500 750-775	0.12	FR			
GeoCARB	Selected/ 2021	N & S America	~3 x 3	GEO	8 hour	757-772 1591-1621 2045-2085 2300-2345	0.05	FR	N/A	N/A	N/A
TanSat / ACGS	In Orbit	Global**	2 x 2	13:30	16 day	758-778 1594-1624 2042-2082	0.04	FR			

References:

FLEX: Drusch et al. (2017)
 TROPOMI: Guanter et al. (2015)
 GOME-2: Joiner et al. (2016, 2013)
 TEMPO: Zoogman et al. (2016)
 OCO-2: Frankenberg et al. (2014)
 GOSAT: Joiner et al. (2011); Frankenberg et al. (2011b)
 Sentinel-4: Meijer et al. (2014)
 GeoCARB: O'Brien et al. (2016)
 TanSat: Du et al. (2018)

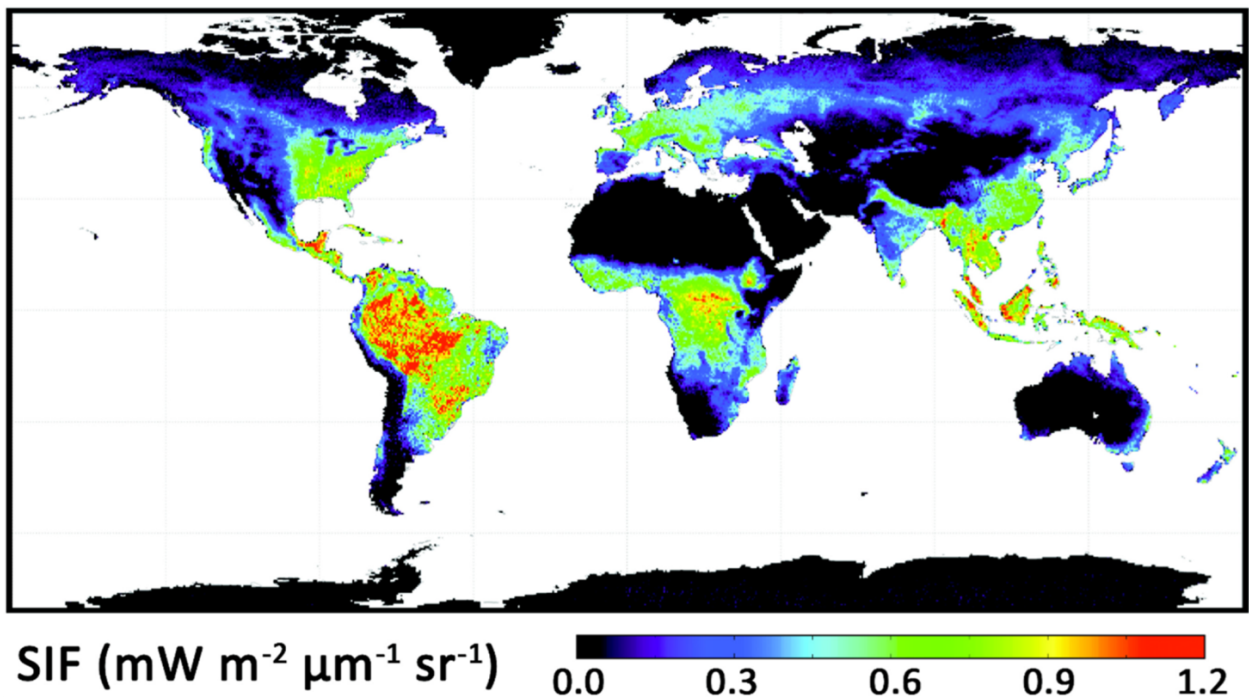
Excellent Very Good Good Fair Poor

** = Global coverage, discontinuous
 GEO = Geo-Synchronous Orbit
 FR = Far-Red SIF
 R = Red SIF
 Full = 650-780 nm
 (FR), (R) = retrieval possible
 PRI = Reflectance @ 530nm, and reference wavelength (usually 570nm)

1557

1558 Joiner et al. (2013) showed that GOME-2 data could be used for discrimination of far-red SIF
 1559 and that they produced higher fidelity global monthly maps of the far-red SIF emission as
 1560 compared with GOSAT. A sample global map for annually integrated far-red SIF is shown in
 1561 **Figure 13.** Such retrieval is possible with GOME-2 due to its SR of ~0.5 nm in the SIF emission
 1562 region, a high SNR (> ~1000), and a wider spectral coverage interval that surrounds the far-red

1563 peak (at 740 nm) and enables a fitting window between 712 to 775 nm. Monthly maps of far-red
1564 SIF have been produced at higher spatial resolution than was possible with GOSAT (typically
1565 $\sim 0.5^\circ$ latitude by 0.5° longitude); somewhat noisier maps could be made with similar spatial
1566 resolution at weekly time scales. [Note also that retrievals of the red SIF have been reported
1567 using GOME-2 and SCIAMACHY (Joiner et al., 2016; Wolanin et al., 2015; see also
1568 Section 5).]



1570 **Figure 13.** Global map showing the 2009 annual average of observations for far-red SIF derived
1571 from the GOME-2 satellite, utilizing observations acquired throughout 2009. (Source: Joiner et
1572 al., 2013.)

1573 Europe's S-5P satellite, carrying the TROPOMI, was launched in late 2017 and flies in formation
1574 with NASA's Suomi National Polar Partnership satellite timed for an early afternoon overpass. It
1575 provides daily SIF observations of similar or better quality as compared to those from GOME-2
1576 and SCIAMACHY but at a much higher spatial resolution of $7 \text{ km} \times 7 \text{ km}$ (Köhler et al., 2018a;

1577 Guanter et al., 2015) and up to 7 km x 3.5 km in the VNIR (ESA, undated). Preliminary
1578 TROPOMI far-red SIF retrievals show that its mapping capabilities far surpass those of its
1579 predecessors, offering intriguing opportunities to map SIF at biome scales (Köhler et al., 2018a;
1580 Guanter et al., 2015).

1581 Another advance will be from geostationary Earth orbit (GEO) spectrometers. Several planned
1582 GEO missions should provide a significant upgrade in temporal resolution of satellite-derived
1583 SIF as compared to currently available information, although at variable coarse spatial
1584 resolutions. The Tropospheric Emissions Monitoring of Pollution (TEMPO) mission will provide
1585 hourly scans over much of North America (Zoogman et al., 2016). Spectral coverage from the
1586 ultraviolet up to the near infrared (~740 nm) – with only one gap near 500 nm – should allow for
1587 determination of red and possibly far-red SIF as well as other vegetation indices. The Sentinel-4
1588 GEO spectrometer on the Meteosat Third Generation-Sounder (MTG-S) satellite and the planned
1589 Geostationary Carbon Cycle Observatory (GeoCarb) instrument, like GOSAT and OCO-2, will
1590 have spectral coverage of the O₂-A band and its shoulders (Meijer et al., 2014; Moore and
1591 Crowell, 2018; O’Brien et al., 2016) for Europe and the Americas, respectively. Their SRs of
1592 0.05-0.12 nm are sufficient to retrieve far-red SIF using FL methodology, several times per day.

1593 **7.4. Factors affecting SIF retrieval accuracy of satellite data**

1594 There are several issues that complicate current satellite SIF retrievals. Large-footprint
1595 instruments in particular are affected by clouds and aerosols that contaminate the vast majority of
1596 observations. Since the atmosphere modifies the depth of atmospheric absorption features such
1597 as O₂ bands that are used in SIF detection, one benefit of using FLs as opposed to O₂ bands for

1598 satellite SIF retrieval is that atmospheric effects do not modify the relative depth of the FLs
1599 (although the absolute depths are still attenuated by aerosol scattering). The impact of clouds
1600 when using far-red FLs has been studied by several research groups (Frankenberg et al., 2012;
1601 Köhler et al., 2015; Guanter et al., 2015) who have concluded that a sufficient amount of SIF
1602 emitted by the canopy is seen by the satellite even in the presence of optically thin or moderate
1603 amounts of broken clouds (optical thicknesses $< \sim 5$). However, this is an open topic that requires
1604 more study (W. Verhoef, personal communication). Compared to SIF, clouds and aerosols have
1605 a greater impact on reflectance-based indices such as the Normalized Difference Vegetation
1606 Index (NDVI), as demonstrated with radiative transfer simulations by Guanter et al. (2015).

1607 Another issue that affects all current coarse-spatial-scale sensors is systematic instrument errors.
1608 This was first found in GOSAT data, where it was coined ‘zero-level offset’. The general
1609 problem is that non-zero values for SIF often get retrieved when zero values are expected (such
1610 as over the Sahara). These biases – which may have complex dependences on radiance levels and
1611 may vary over time – must be accounted for in order to obtain accurate SIF estimates. [The
1612 causes of zero-level offset for different types of instrumentation and their mitigation strategies
1613 are discussed by Frankenberg et al. (2011b), Guanter et al. (2012), Köhler et al. (2015), Khosravi
1614 et al. (2015), and Joiner et al. (2016, 2012).]

1615 Finally, overall sensor degradation occurs at greater or lesser rates in all satellite-based
1616 instruments and should be tracked and quantified. Degradation – which might be sudden or
1617 discontinuous – can be due to temperature changes, high radiation exposure, mechanical wear
1618 and tear, particles adhering to lenses, jolts from space debris, etc. This issue is particularly
1619 evident in data acquired by the very high-SR instruments used for atmospheric chemistry. Koren

1620 et al. (2018) and Zhang et al. (2018c) have identified possible artefacts in GOME-2 SIF results
1621 that may have been due to sensor degradation. This underscores the need for consideration of
1622 such effects when using long-term records for analysis of SIF trends over time.

1623 **7.5. Challenges and future directions in satellite sensing of SIF**

1624 Earth observation from space provides a powerful way to assess and monitor the status of the
1625 biosphere. The potential of satellite-based SIF as an indicator of large-scale photosynthetic
1626 activity is evident from the growing body of literature on the use of satellite-retrieved SIF to
1627 examine global SIF patterns and dynamics (Frankenberg and Berry, 2018) [**Section 8**].

1628 Although retrieval of SIF using space-based sensors offers an exciting new tool for studying
1629 vegetation dynamics, there are a number of challenges to basic understanding of carbon and
1630 water cycles at macroscales. The greatest challenge is to develop measurement and modelling
1631 approaches that bridge the SIF emission's vertical pathway and profile through the atmosphere,
1632 from vegetation at the surface to the observing satellite sensor above the Earth – in other words,
1633 we need reliable upscaling and downscaling capabilities in both temporal and spatial dimensions
1634 for SIF and carbon/water/energy processes. From basic science, it is known that chlorophyll
1635 fluorescence is influenced directly or indirectly by environmental and biological factors and this
1636 is not considered in a comprehensive way in the current satellite-based approaches [**Section 8**].
1637 These factors often are manifested at the local scale, but tend to be overlooked or averaged out in
1638 large footprints and/or monthly aggregates (Magnani et al., 2014; Verrelst et al., 2016).
1639 Consequently, it is also essential that calibration and validation methods be developed and
1640 demonstrated that (i) prove conclusively whether satellite-retrieved SIF measures the same

1641 biological processes as ground-based instruments, and (ii) provide reliable quantitative results at
1642 local as well as global scales. The atmospheric chemistry satellites all have wide swaths to
1643 facilitate global coverage. Thus far, no corrections have been applied to account for the
1644 directional effects in the retrieved SIF values due to off-nadir viewing directions, and this
1645 definitely should be included in mature versions of the data processing chain for SIF. Also
1646 important will be consideration of the surface anisotropy of SIF (Middleton et al., 2018; Verhoef
1647 et al., 2018), which has received insufficient attention to date. Therefore, future retrieval schemes
1648 will likely be necessary to consider a number of factors not currently addressed, including
1649 surface anisotropy, surface reflectance, and aerosol type/amount.

1650 While the atmospheric chemistry missions have provided novel and compelling large-scale
1651 information about SIF, the pressing societal applications in agriculture, food security, and forest
1652 ecology and management require high spatial resolution (≤ 0.5 km) as well as frequent
1653 observations, as prescribed by the application. With atmospheric chemistry missions, the
1654 observations are frequent but the footprints can be large. Future geostationary missions will
1655 provide moderate but variable spatial scale (e.g., 2-5 km²) observations at several times of day
1656 (i.e., diurnally) for specific regions of the world. With FLEX, a higher spatial resolution will be
1657 possible globally, but observations will be less frequent. There is an obvious synergy between
1658 these different satellite SIF capabilities for achieving global mapping of vegetation health across
1659 the Earth's land surfaces. For future operational monitoring of the health of our ecosystems and
1660 food sources, we will want to have both aspects: frequent SIF measurements, at local scales.

1661 **8. Applications of remotely sensed SIF**

1662 **8.1. Overview of research and application areas**

1663 Remotely detected SIF in terrestrial vegetation has been investigated for use in stress detection,
1664 estimation of photosynthesis and GPP, and tracking of temporal and phenological changes in
1665 terrestrial vegetation types (**Table 4**) (Ač et al., 2015; Frankenberg and Berry, 2018; Malenovský
1666 et al., 2009; Meroni et al., 2009; Middleton et al., 2018). These efforts have been encouraged
1667 significantly by advances in measurement technologies, retrieval methods, and modelling.

1668 Airborne and satellite-based technological developments have stirred considerable interest in SIF
1669 usage for research and operational applications. They have also nudged the scientific community
1670 back to the basics, including consideration of fundamental drivers and influential factors for SIF
1671 to better understand and interpret remote observations. Field and airborne studies are proving
1672 essential to interpretation, valuable for ground-truthing of satellite-derived SIF, and helpful for
1673 local-to-landscape scale research. Thus, there is a confluence of investigative and developmental
1674 efforts that are synergistic and complementary, and which should expedite further progress.

1675 **Table 4.** Studies investigating remotely detected SIF in terrestrial vegetation for photosynthesis and stress detection. Tc: canopy
 1676 temperature; Ta: air temperature. **Vegetation:** C: cropland; F: forest; G: grassland; O: orchard; V: various biomes. **Scale:** G: ground-
 1677 based; A: airborne-based; S: satellite-based. **SIF:** R: red; FR: far-red; PR: fluorescence peak ratio; F-SIF: full SIF emission.

1678

Objective	Vegetation	Scale	SIF	Publication examples
Photosynthesis and its estimation				
absorbed PAR	C, F, O	G	FR	Cui et al., 2017a; Miao et al., 2018; Wagle et al., 2016; Yang et al., 2015; Zhang et al., 2016a
diurnal dynamics	C, F	G, A	R, FR	Cogliati et al., 2015a; Damm et al., 2010; Middleton et al., 2017; Schickling et al., 2016; Sobrino et al., 2011
GPP (empirical)	C, F, G, V	G, A, S	R, FR	Alden et al., 2016; Berkelhammer et al., 2017; Chang et al., 2016; Gentine and Alemohammad, 2018; Goulas et al., 2017; Guan et al., 2015; Hu et al., 2018a; Guanter et al., 2014; Köhler et al., 2018b; Li et al., 2018a; Sun et al., 2018, 2017; Wieneke et al., 2016
GPP (modelled)	V	S	FR	Luus et al., 2017; MacBean et al., 2018; Parazoo et al., 2014; Qiu et al., 2018; Thum et al., 2017; Verma et al., 2017; Wagle et al., 2016; Yoshida et al., 2015
light use efficiency	C, F, G, V	G, S	R, FR	Cheng et al., 2013; Miao et al., 2018; Song et al., 2018; Walther et al., 2018; Verma et al., 2017; Yang et al., 2015
NPP	C	S	FR	Patel et al., 2018
phenological stage	C	G	R, FR	Daumard et al., 2012; Miao et al., 2018
seasonal dynamics	C, F, G, O, V	G, A, S	R, FR	Koffi et al., 2015; Joiner et al., 2014; Meroni et al., 2011; Parazoo et al., 2013; Rascher et al., 2015; Rossini et al., 2010; Smith et al., 2018; Wang et al., 2018; Wieneke et al., 2018; Wyber et al., 2017; Zarco-Tejada et al., 2013b
vegetation type	C, F, G, V	G, A, S	R, FR	Damm et al., 2015a; Guan et al., 2016; Guanter et al., 2012; Li et al., 2018b; Liu et al., 2017; Madani et al., 2017; Rascher et al., 2009; Rossini et al., 2016; Sun et al., 2018
Stress detection				
bacterial infection	O	A	FR	Zarco-Tejada et al., 2018
fungal infection	C, F	A	FR	Calderón et al. 2015; Hernández-Clemente et al., 2017
heat	C	S	FR	Guan et al., 2016; Song et al., 2018
herbicide	C, G	G, A	R, FR	Pinto et al., 2016; Rossini et al., 2015
nitrogen deficit	F	G	PR	Freedman et al., 2002
transpiration	F	G	F-SIF	Lu et al., 2018b
water deficit, drought	C, F, O, V	G, A, S	R, FR, PR	Daumard et al., 2010; Koren et al., 2018; Lee et al., 2013; Ma et al., 2016; Sanders et al., 2016; Sun et al., 2015; Wang et al., 2016; Wieneke et al., 2018, 2016; Xu et al., 2018; Zarco-Tejada et al., 2012; Zuromski et al., 2018
Ancillary indices				
chlorophyll content	C, O	G, A, S	R, FR	Panigada et al., 2014; Zhou et al., 2016; Zarco-Tejada et al., 2018, 2013b; Zhang et al., 2014
EVI	V	S	FR	Ma et al., 2016
MTCI	C	S	FR	Zhang et al., 2014
NDVI	C, F, G	G, A	R, FR	Garzonio et al., 2017; Rascher et al., 2009
PRI	C, G	G, A, S	FR, PR	Middleton et al., 2018; Paul-Limoges et al., 2018; Schickling et al., 2016; Verma et al., 2017
Tc-Ta; or Tc	C, F, O	A	FR	Calderón et al. 2015; Middleton et al., 2017; Zarco-Tejada et al., 2018, 2012

1679 **8.2. Studies performed and lessons learned**

1680 **8.2.1. Ground-based canopy studies**

1681 Ground-based canopy studies have produced encouraging findings for using SIF to help quantify
1682 photosynthesis (Goulas et al., 2017; Pérez-Priego et al., 2015; Rascher et al., 2009; Rossini et al.,
1683 2010; Yang et al., 2015), transpiration (Lu et al., 2018b), and stress effects (Daumard et al.,
1684 2010; Xu et al., 2018). They have also demonstrated SIF responsiveness to vegetation
1685 phenological changes (Daumard et al., 2012; Middleton et al., 2018), diurnal patterns (Rascher et
1686 al., 2009), and seasonal adjustments (Meroni et al., 2011; Hu et al., 2018b; Wyber et al., 2017).

1687 Ground-based investigations have afforded insights relevant to the findings of satellite-based
1688 studies showing a relationship (even linear) between far-red SIF and GPP. Links to GPP are
1689 recognized now to be based in a strong relationship of far-red SIF to APAR (**Section 4.6**) (Cui et
1690 al., 2017a; Miao et al., 2018; Rossini et al., 2010; Wieneke et al., 2018; Yang et al., 2015; Zhang
1691 et al., 2016a). (Note: Fluorescence data often are normalized by incident PAR, APAR, or APAR
1692 of photosynthetic components of the vegetation, to obtain quantum yield; Damm et al., 2010;
1693 Rascher et al., 2009; Rossini et al., 2010.) There are also reports of SIF being associated with
1694 LUE – which is another important variable in GPP estimation (Yang et al., 2015; Zhang et al.,
1695 2016a) – especially when APAR is constant (Cheng et al., 2013). However, Wohlfahrt et al.
1696 (2018) showed that even with constant APAR, the red or far-red SIF accounted for less than 35%
1697 of the variability in GPP, whereas air temperature explained 77%. Empirical studies also report a
1698 stronger association of far-red SIF to environmental conditions such as high light, vapour

1699 pressure deficit, and nitrogen availability than to GPP (Paul-Limoges et al., 2018; Pérez-Priego
1700 et al., 2015).

1701 The form of SIF-GPP relationships found can vary, becoming linear with spatio-temporal scaling
1702 or aggregation of SIF data (e.g., Damm et al., 2015a, 2015b; Zhang et al., 2016a). Goulas et al.
1703 (2017) further showed for wheat that a simple linear SIF-GPP relationship may apply only under
1704 some circumstances, such as when using far-red SIF and in the presence of a high dynamic range
1705 of green biomass and a low range of LUE variation. For crops and mixed forests, Paul-Limoges
1706 et al. (2018) found that SIF-GPP association was hyperbolic on stress-free days, and linear on
1707 days when conditions were stressful, and was attributed to reduced midday SIF values under
1708 stress. Liu et al. (2017) emphasized the importance of considering also the photosynthetic
1709 pathway (e.g., C₃, C₄) when analyzing far-red SIF-GPP correlations and diurnal patterns.

1710 Improvement in the correlation between SIF with daily GPP has been achieved by upscaling
1711 instantaneous far-red SIF to a daily value. Hu et al. (2018a) suggest that a PAR-based correction
1712 factor may be more effective than that based on the ratio of instantaneous cos(SZA) to daily
1713 integrated cos(SZA) (e.g., Zhang et al., 2018d), as the latter does not account for cloud cover.

1714 Remotely detected SIF has been shown to be responsive to stress effects and to transpiration. The
1715 meta-analysis of Ač et al. (2015) concluded that canopy red or far-red SIF declines with water
1716 stress, while the ratio of red to far-red fluorescence increases with nitrogen deficit. Red and far-
1717 red SIF can also be early indicators of water stress and of recovery, but red SIF signals tend to be
1718 ‘noisier’ under stress (Daumard et al., 2010; Xu et al., 2018). Far-red SIF has been used to
1719 estimate transpiration during the growing season, but this works only in unstressed vegetation
1720 and where leaf area is not high (affects scattering and reabsorption of SIF) (Lu et al., 2018b).

1721 Ground-based studies confirm the influence of chlorophyll content, canopy structure and
1722 heterogeneity on SIF, factors which can influence re-absorption and scattering within canopies.
1723 Scaling from the leaf to the canopy, the ratio of red to far-red SIF (e.g. F687/F760) has been seen
1724 to decrease (Daumard et al., 2012; Fournier et al., 2012), likely because of stronger re-absorption
1725 of red fluorescence within the canopy (Louis et al., 2005). The ratio also decreases with
1726 increasing leaf chlorophyll content (Daumard et al., 2012) and under high light (Fournier et al.,
1727 2012). Another factor is leaf inclination in canopies, which can affect light absorption and also
1728 detectability of the SIF signal by the remote sensor. A lower far-red SIF signal has been
1729 observed with erectophile as compared to either planophile or spherical leaf orientation
1730 (Migliavacca et al., 2017b; Pinto et al., 2017). Such factors contribute to differences in SIF
1731 emissions among plant functional types or species, resulting in, for example, higher TOC
1732 emissions from some crop species than from broadleaf and needleleaf ones (Rossini et al., 2010).

1733 Studies of diurnal behaviour in SIF have shown that far-red SIF measured across days (inter-day)
1734 was affected mainly by chlorophyll content, whereas intra-day changes were influenced by
1735 photosynthetic activity (Cogliati et al., 2015a; Pinto et al., 2016). Also, when Paul-Limoges et al.
1736 (2018) measured far-red SIF in mixed forest or crop canopies during sunny days, they found SIF
1737 varied with vegetation type and the presence or absence of stress; midday depression in SIF was
1738 evident in a forest canopy and a barley crop, and was associated with increased NPQ (quantified
1739 with PRI). Rascher et al. (2009) found a modest reduction in far-red SIF during early afternoon
1740 in winter wheat, coincident with maximal light intensity, but red SIF closely followed PPFD.
1741 Louis et al. (2005) saw a decline in fluorescence at leaf level but not in the canopy of a pine

1742 forest, and suggested the cause was perhaps a canopy structural effect that moderated the
1743 intensity of light penetrating into deeper canopy layers, thereby reducing the need for NPQ.

1744 Understanding possible NPQ effects is important for interpretation of SIF (Cheng et al., 2013;
1745 Daumard et al., 2010; Xu et al., 2018). Using PRI (and modified formulations) to estimate NPQ
1746 activity has been helpful in short-term assessments (i.e., over hours or a few days) if chlorophyll
1747 and structural traits are stable. Combining SIF with PRI also has helped to improve estimation of
1748 gross productivity (e.g., Pérez-Priego et al., 2015; Rossini et al., 2010). The caveat is always that
1749 PRI is subject to structural, anisotropic, and illumination effects that can confound links to NPQ
1750 behaviour (Schickling et al., 2016). Over longer timeframes, boreal evergreen conifers for
1751 instance had PRI better affiliated with seasonally changing carotenoid-to-chlorophyll pigment
1752 ratios and shifting leaf albedo during periods of deep cold than with NPQ (Wong and Gamon,
1753 2015). Wyber et al. (2017) observed that at seasonal scales, SIF appears principally correlated
1754 with increased *constitutive* (rather than *regulated*) heat dissipation along with changes in leaf
1755 irradiance and electron transport rate. Measurements of environmental conditions (e.g., incident
1756 light intensity, relative humidity and vapour pressure deficit, air temperature, etc.), additional
1757 reflectance-based data, and illumination geometry can be helpful for disentangling some of these
1758 temporal effects (Goulas et al., 2017; Middleton et al., 2018; Paul-Limoges et al., 2018).

1759 Regarding phenologically associated SIF responses, Daumard et al. (2012) found that during
1760 early growth in sorghum, the red SIF (687 nm) increased rapidly then became saturated, even as
1761 far-red SIF (760 nm) continued to increase. During growth, they found that the ratio of red to far-
1762 red SIF was lower in the canopy than in leaves and decreased with increasing leaf chlorophyll
1763 content (likely increasing re-absorption of red SIF). Meroni et al. (2011) found that for grassland,

1764 far-red SIF increased in spring, peaked in summer, then declined in late summer, responding
1765 primarily to the amount of chlorophyll in the canopy and the intensity of PPFD. Middleton et
1766 al.'s (2018) review of their studies on corn point to the combined effects of water stress,
1767 phenological state, and anisotropy on red and far-red SIF.

1768 The relative merits of red and far-red SIF have been examined. Ač et al. (2018) and the review of
1769 Middleton et al. (2018) indicate the value of the ratio of red to far-red SIF for identifying nutrient
1770 deficiency (notably nitrogen). Modelling exercises using SCOPE (Verrelst et al., 2016, 2015b)
1771 also identify benefits to retrieving both emissions, especially in heterogenous canopies. In
1772 comparison, Goulas et al. (2017) found far-red SIF to be more informative for GPP in wheat.
1773 The complicating factor for red SIF is its susceptibility to re-absorption which can cause
1774 substantive reduction in signal strength at the top of the canopy (Rascher et al., 2009).

1775 Overall, ground-based canopy studies offer good prospects for SIF in research and extended
1776 applications, but the influence of extraneous factors must be taken into consideration.

1777 **8.2.2. Airborne-based studies**

1778 Airborne-based deployments for SIF have demonstrated the added value of imaging and
1779 mapping of spatial distribution or spatio-temporal trends for stress detection (Rascher et al.,
1780 2015; Zarco-Tejada et al., 2013b). Some have served as pilot studies for early identification of
1781 plant disease (Zarco-Tejada et al., 2018), and in validation of satellite-based SIF retrievals (Sun
1782 et al., 2017). They have indicated the utility of having both red and far-red SIF (Middleton et al.,
1783 2018; Rossini et al., 2015; Wieneke et al., 2016), established natural quantitative ranges in SIF
1784 values in different vegetation types (Garzonio et al., 2017), and helped to clarify diurnal as well

1785 as canopy functional versus structural influences on SIF (Middleton et al., 2017; Rascher et al.,
1786 2015, 2009; Schickling et al., 2016; Sobrino et al., 2011). Hyperspectral imagery of
1787 heterogeneous canopies has revealed vegetation age effects, ecosystem type effects, spatio-
1788 temporal scaling on SIF-GPP relationships, and surface anisotropic effects (Colombo et al.,
1789 2018; Damm et al., 2015a, 2015b; Zarco-Tejada et al., 2013b).

1790 In stress detection, SIF has been used to detect plant diseases (Calderón et al., 2015, 2013;
1791 Hernández-Clemente et al., 2017; Zarco-Tejada et al., 2018), water stress (Panigada et al., 2014;
1792 Wieneke et al., 2016; Zarco-Tejada et al., 2012), and herbicide stress (Rossini et al., 2015).
1793 Zarco-Tejada et al. (2018) were able to identify incipient infection in olive trees by the pathogen
1794 *Xylella fastidiosa*, with prediction accuracies exceeding 80%. Their approach combined
1795 fluorescence, thermography, and spectral indicators of chlorophyll content and of vegetation
1796 structural changes. They suggested the importance of relying on a spectral bandset combination
1797 that enables retrieval of the most sensitive host-plant traits linked with a specific disease. For
1798 detection of *Phytophthora* infection, advanced modelling strategies have helped to decipher
1799 aggregated heterogeneous pixels of complex vegetation systems (Hernández-Clemente et al.,
1800 2017).

1801 With herbicide stress, the red and far-red SIF were able to track variations in photosynthetic
1802 efficiency caused by a chemical known to inhibit photosynthesis and selectively intensify
1803 fluorescence, whereas surface reflectance was almost unaffected (Rossini et al., 2015). This trial
1804 demonstrated the capability of SIF to detect herbicide damage before visual symptoms.

1805 For water stress, it has been shown that a helpful index to support interpretation of SIF changes
1806 is the temperature difference between the plant canopy and the surrounding air (Calderón et al.

1807 2015; Panigada et al., 2014; Zarco-Tejada et al., 2012). When stress induces stomatal closure,
1808 such as in the cases of water deficit or high vapour pressure deficit, evaporative cooling is
1809 restricted and foliage can warm to above air temperature, with a concomitant increase in NPQ
1810 and decrease in SIF. The temperature differential is a good alternative or complementary index
1811 to PRI (Panigada et al., 2014; Schickling et al., 2016).

1812 SIF retrieved from airborne sensors has also been applied for estimation of GPP, although
1813 ground-based canopy approaches and satellite-based methods are perhaps the more obvious
1814 choices for this purpose owing to the need for continuous or routine monitoring. Zarco-Tejada et
1815 al. (2013b) used UAVs to investigate spatio-temporal trends of far-red SIF (and other narrow-
1816 band physiological and structural indices, and found canopy SIF and indices related to
1817 chlorophyll content and LUE (i.e., PRI) had similar seasonal trend as GPP assessed from EC
1818 towers at the time of the flights. Wieneke et al. (2016) used a semi-mechanistic approach with
1819 far-red SIF to improve forward modelling of GPP, as did Damm et al. (2015a) using SCOPE for
1820 mechanistic understanding and scaling, whereby they revealed a linearization of SIF-GPP
1821 relationships with leaf-to-canopy and temporal scaling.

1822 To support future operational applications, Garzonio et al. (2017) studied far-red SIF in different
1823 vegetation types (crops, meadow, broadleaf species) using the HyUAS system, and found diverse
1824 average SIF values, which could have resulted from strong species-related canopy directional
1825 effects. They emphasize the existence of potentially complex overlaps and cross-effects among
1826 vegetation types and anticipate valuable developments using integrative methods based on
1827 combined analysis of reflectance and SIF.

1828 In applications of SIF, age effects should be considered. In different even-aged stands of loblolly
1829 pine forest, young stands had a nearly two-fold higher red SIF yield than plantations older than
1830 10-15 years, but the far-red SIF was constant (Colombo et al., 2018). This effect was interpreted
1831 as arising mainly from stomatal limitation in the older vegetation, with possible residual
1832 influences from canopy structure with aging and higher re-absorption of the red SIF. Middleton
1833 et al. (2017) assessed the same sites and found that temperature difference between the forest
1834 canopy and the surrounding air had stronger daily amplitude change for young versus older
1835 stands. It was recommended to combine SIF, reflectance, and canopy structural information to
1836 help distinguish such functional and structural effects.

1837 **8.2.3. Satellite-based studies**

1838 Over the short lifetime of the global satellite SIF data era, a number of papers have reported that
1839 far-red SIF from current satellites have the potential to indicate large-scale photosynthetic
1840 activity. First trials with GOSAT showed a high correlation of retrieved SIF with data-driven
1841 GPP results at coarse global and annual scales (Frankenberg et al., 2011b), although a per-biome
1842 dependency in the SIF-to-GPP ratio was also identified (Guanter et al., 2012). Joiner et al. (2014)
1843 analyzed time series of SIF retrievals and compared them with GPP estimates from data-driven
1844 and process-based models and measurements from eddy covariance flux towers. Those studies
1845 found a good correspondence between the temporal trajectories of retrieved far-red SIF and GPP,
1846 which performed as well as remote sensing-based vegetation parameters. Initial indications are
1847 that far-red SIF might also contain information about LUE, in this case in tundra vegetation, and
1848 this aspects warrants further study (Walther et al., 2018).

1849 Global SIF measurements retrieved from GOSAT and GOME-2 satellites for different
1850 ecosystem-level vegetation monitoring applications have been published. Space-based far-red
1851 SIF data from GOME-2 were shown to have a higher sensitivity to crop photosynthesis than
1852 reflectance-based vegetation indices and data-driven GPP models, the latter failing to capture the
1853 high GPP levels found in some areas of the US Corn Belt (Guanter et al., 2014). This finding
1854 was applied to produce estimates of crop photosynthetic capacity from SIF (Guan et al., 2016;
1855 Zhang et al., 2018a; Zhang et al., 2014). Zhang et al. (2014) tuned the maximal carboxylation
1856 capacity (V_{cmax}) in SCOPE to match simulated-to-satellite observed SIF, and found it improved
1857 estimates of GPP compared to using an *a priori* V_{cmax} . In their approach the values of other
1858 parameters of SCOPE were obtained from ancillary satellite data. Guan et al. (2016) used a more
1859 direct empirical relation to derive the electron transport rate from observed SIF per unit of
1860 APAR. The values of GPP they obtained after multiplication of ETR by a photosynthetic-
1861 pathway-dependent electron use efficiency, were an improvement over other satellite-derived
1862 approaches considered.

1863 Several satellite-based trials have reported the potential of far-red SIF to indicate drought and
1864 temperature stress at ecosystem scales (Berkelhammer et al., 2017; Koren et al., 2018; Song et
1865 al., 2018; Sun et al., 2015; Wang et al., 2018, 2016; Wu et al., 2018; Yoshida et al., 2015;
1866 Zuromski et al., 2018). Other works have used far-red SIF in monitoring the dynamics of
1867 photosynthesis in the Amazon forest (e.g., Alden et al., 2016; Guan et al., 2015; Köhler et al.,
1868 2018b; Koren et al., 2018; Lee et al., 2013; Parazoo et al., 2013), high latitude forests (Jeong et
1869 al., 2017; Walther et al., 2016), tundra ecosystems (Luus et al., 2017; Walther et al., 2018),
1870 dryland ecosystems of southwestern North America (Smith et al., 2018; Zhang et al., 2016c) and

1871 across Australia (Ma et al., 2016; Sanders et al., 2016). The links between large-scale far-red SIF
1872 and GPP (e.g., He et al., 2017; Koffi et al., 2015; Zhang et al., 2018b) have resulted in the use of
1873 SIF to analyse the coupling between carbon and water fluxes at regional to global scales (e.g.,
1874 Alemohammad et al., 2017; Cui et al., 2017b; Green et al., 2017; Madani et al., 2017; Qiu et al.,
1875 2018; Wagle et al., 2016; Zhang et al., 2016b) and to benchmark GPP representations and other
1876 parameters in global models (e.g., Chang et al., 2016; Lee et al., 2015; MacBean et al., 2018;
1877 Parazoo et al., 2014; Thum et al., 2017; Walker et al., 2017).

1878 Methods to downscale SIF spatially from large-pixel instruments such as GOME-2 to smaller
1879 scales using higher-resolution imager data also have been developed (Duveiller and Cescatti,
1880 2016; Gentine and Alemohammad, 2018; Joiner et al., 2018). Lately, the advent of higher spatial
1881 resolution data from OCO-2 has enabled new possibilities (e.g., Lu et al., 2018a; Sun et al.,
1882 2018; Wei et al., 2018; Zhang et al., 2018c, 2018d), including direct comparisons between far-
1883 red SIF retrievals and tower-based GPP for the understanding of SIF-GPP relationships (Sun et
1884 al., 2017). For instance, Verma et al. (2017) looked at the effect of environmental conditions on
1885 the relationship between far-red SIF and GPP at a grassland site and concluded that the linear
1886 relationship is more robust at ecosystem scale than the theory based on leaf-level processes
1887 might suggest, but that NPQ (besides APAR and LUE) might need to be explicitly factored into
1888 GPP estimations in future analyses. Wood et al. (2017) also took advantage of direct
1889 comparisons between SIF derived from OCO-2 observations and tower-based estimates of GPP
1890 to investigate the effect of different spatial and temporal scales on SIF-GPP relationships. They
1891 found a robust linear GPP-SIF scaling that is sensitive to plant physiology but insensitive to the
1892 spatial or temporal scale. Li et al. (2018a) performed similar comparisons between OCO-2 SIF

1893 retrievals and tower-level GPP to show a linear relationship between SIF and GPP in temperate
1894 forests. It was further shown, in a study of the Indo-Gangetic Plains of India, that far-red SIF is
1895 related to net primary productivity (NPP) and that SIF values for C₄-crop-dominated areas were
1896 higher than for C₃-crop districts during summer and low during winter (Patel et al., 2018). These
1897 types of studies are expected to become more comprehensive as further OCO-2 and also
1898 TROPOMI results become available (Li et al., 2018b).

1899 **8.3. Summary of SIF drivers and influential factors**

1900 For applications, correct interpretation of SIF data is a high priority. Daumard et al. (2012)
1901 suggested that the modification of leaf level fluorescence emission by canopy structural
1902 attributes is one of the major issues that must be addressed to interpret the fluorescence signal in
1903 the context of large-scale remote sensing applications. And recently, a historical review of
1904 global-scale assessment of photosynthesis (Ryu et al., 2019) which included a perspective on the
1905 potential of SIF for large-scale estimation of GPP, noted that canopy structure effects – which
1906 influence, among other parameters, the escape of SIF to the top of the canopy (Yang and Van der
1907 Tol, 2018) – might play a more important role in the SIF-GPP relationship than LUE of canopy
1908 fluorescence. That review emphasized the need to understand sources of uncertainty in SIF-
1909 photosynthesis relationships at a range of scales, which has also been highlighted by others
1910 (Malenovský et al., 2009; Porcar-Castell et al., 2014).

1911 We can suggest a consolidated tabulation of SIF drivers and influential factors, and their relevant
1912 spatio-temporal scales (**Table 5**). These factors could influence light absorption, re-absorption,
1913 and scattering, as well as PQ, NPQ, and other photoprotective processes. This information is a

1914 synthesis of published papers, as well as our own theoretical understanding (chart updated from
1915 Mohammed et al., 2016) (see also reviews by Buschmann et al., 2000; Buschmann and
1916 Lichtenthaler, 1998; Cerovic et al., 1999; Donaldson and Williams, 2018; García-Plazaola et al.,
1917 2015; Lagorio et al., 2015; Lichtenthaler and Rinderle, 1988; Middleton et al., 2018; Moya and
1918 Cerovic, 2004; Porcar-Castell et al., 2014; Schreiber, 2004). The matrix serves as a starting point
1919 to stimulate thinking and support research planning, development of hypotheses, design of
1920 interpretative frameworks, and refinement of process-based models. Not all factors are expected
1921 to be influential or equally important in a given situation.

1922

1923 **Table 5.** Drivers of steady-state fluorescence, processes that may be affected, and ecological and
1924 temporal scales of influence. **Process:** **A:** absorption of incident light; **R:** re-absorption of
1925 fluorescence; **S:** fluorescence scattering; **PQ:** photochemical quenching; **NPQ:** non-
1926 photochemical quenching; **OP:** other photoprotection. **Ecological scale:** **L:** leaf; **C:** canopy;
1927 **E:** ecosystem; **B:** biome. **Temporal scale:** **ST** (short-term): seconds, minutes, hours, diurnal; **MT**
1928 (medium-term): days, weeks; **LT** (long-term): months, years; **SV:** seasonal variation.
1929 **Definitions of ecological scales:** Leaf: a single leaf or leaf cluster on a single plant; Canopy: a
1930 single plant or monospecific closed canopy stand; Ecosystem: a mixed-species stand with closed
1931 or open heterogeneous structure; Biome: a major habitat (e.g., tundra, grassland, tropical
1932 rainforest) with multiple ecosystems and heterogeneous structure. (Note: For photosynthetic
1933 pathway, switching between pathways occurs in some species.)

1934

Fluorescence driver	Process potentially affected						Ecological scale				Temporal scale			
	A	R	S	PQ	NPQ	OP	L	C	E	B	ST	MT	LT	SV
Vegetation traits and processes														
age														
carboxylation capacity														
chlorophyll content														
chloroplast movements														
electron transport rate														
epicuticular wax														
evapotranspiration														
fraction functional PSII reaction centres														
fraction open PSII reaction centres														
leaf area index, LAI distribution														
leaf inclination, heliotropism														
leaf internal anatomy														
leaf thickness														
light use efficiency														
mesophyll conductance														
non-chlorophyll pigments														
non-foliar photosynthesis														
phenological stage														
photodamage														
photoinhibition (reversible)														
photorespiration														
photosynthetic pathway (C ₃ , C ₄ , CAM)														
photosystem state transitions														
photosystem stoichiometry (PSII : PSI)														
PSII efficiency (quantum yield)														
species, plant functional type														
stomatal conductance														
surface albedo														
thermal dissipation – constitutive														
thermal dissipation – regulated														
water content														
vegetative competition														
Environmental, atmospheric, and stress factors														
air temperature; cold or heat stress														
atmospheric aerosols, pollutants, ozone														
carbon dioxide concentration														
cloud cover														
daylength														
herbicide stress														
incident light intensity														
incident light spectral quality														
nutrient deficiency, toxicity														
oxygen concentration														
pest stress (insect, viral, fungal, bacterial)														
relative humidity, vapour pressure deficit														
solar zenith angle														
surface (atmospheric) pressure														
water stress														
wind stress														

1936 **8.4. Challenges and future directions**

1937 Several future directions are indicated for remote sensing of SIF. First, planning in SIF satellite-
1938 based research should consider more deliberately the types of influential factors and drivers that
1939 could confound interpretation of SIF data in a given situation. This will involve consideration of
1940 vegetation, site, and environmental factors; possible ancillary data at relevant spatial scales; and
1941 application of current modelling capabilities to analyze key drivers in a given situation (Verrelst
1942 et al., 2016, 2015a). A trend in satellite-based Earth Observation has been for acquisition of
1943 ancillary and complementary data from multiple sensors and missions, which could accelerate in
1944 the future as more technologies operating at diverse spatial scales become available (Lausch et
1945 al., 2017, 2016; Scholze et al., 2017). Geostationary satellite-based systems for SIF are a further
1946 helpful development to acquire high-temporal-resolution data from space.

1947 Second, the capabilities of the remote sensor and the efficacy of retrieval algorithms must be
1948 critically appraised in light of the needs of the particular application and the drivers likely to be
1949 encountered. Whereas validation of SIF retrievals is more feasible for airborne systems, it has
1950 only begun for satellite-based detection (e.g., Sun et al., 2017). Understandably, this has been a
1951 challenge for sensors such as GOME-2, and GOSAT, but prospects are improving with the
1952 recent higher-spatial-resolution sensors (Frankenberg and Berry, 2018; Guanter et al., 2015).
1953 Acquisition of useful ground-truthing information for the satellites can incorporate data from
1954 multiple scales at least initially then in a more streamlined way as appropriate. Development of
1955 some airborne sensors as demonstrators of satellite counterparts (e.g., *HyPlant* and CFIS for the
1956 FLEX and OCO-2 missions, respectively) is a modern strategy that assists mission preparatory
1957 activities and post-launch validation and interpretation – key topics for the coming years.

1958 Accuracies of retrieved SIF and achieving satisfactory representativeness for the vegetation of
1959 interest are also of key significance, especially in heterogeneous systems with many extraneous
1960 factors, or where SIF signals are inherently low (e.g., at high latitudes) which makes those data
1961 prone to systematic errors (Thum et al., 2016). Sensor stability is essential to capture real
1962 changes in space and time.

1963 Third, routines to ingest diverse and complex data for SIF analytics and applications may be
1964 refined and also streamlined for a range of users to apply the information. SIF is already being
1965 incorporated into models addressing leaf and canopy SIF and photosynthesis (Van der Tol et al.,
1966 2016, 2014), re-absorption phenomena in leaves and canopies (Romero et al., 2018), and 3D
1967 vegetation architecture (Gastellu-Etchegorry et al., 2017). Downstream applications geared to
1968 non-expert users will eventually require expedited procedures, perhaps involving the use of
1969 model emulators (Rivera et al., 2015; Verrelst and Rivera, 2017).

1970 Finally, it is essential that future efforts continue to encompass the full suite of technological
1971 options allowing SIF measurement at different spatial and temporal scales. Hand-held devices,
1972 stationary and mobile field systems, UAVs and other airborne sensors, and satellite systems offer
1973 versatility and flexibility for SIF analysis. It is anticipated that future developments will offer
1974 further options for measurement of related photosynthetic and environmental variables. Some
1975 systems will serve the requirements of researchers for comprehensive or sophisticated data while
1976 others could be tools for non-expert users. Concomitantly, non-expert users also need to be
1977 aware of the possibility for artefacts, and so communication between researchers and
1978 downstream users is vital. It is an exciting challenge for scientists and R&D professionals to

1979 navigate this rather intricate new avenue of remote sensing with diverse users from forestry,
1980 agriculture, and environmental domains.

1981 This paper has focused on the progress in remote sensing of fluorescence in terrestrial
1982 vegetation. But chlorophyll fluorescence also has been studied remotely in marine systems for
1983 decades, with well-established applications addressing estimation of chlorophyll and productivity
1984 (Blondeau-Patissier et al., 2014; Gower, 2016). Until recently, satellite options for coastal and
1985 inland water bodies lagged behind those for open waters, according to a review by Mouw et al.
1986 (2015), who underscored the need for orbital missions sampling on the scales of high variability
1987 encountered in coastal and inland water bodies, with the finer spectral, spatial and temporal
1988 detail needed for resampling in a variety of applications. Synergies are possible across land and
1989 aquatic satellite missions suitable for analyzing these optically complex waters, such as with the
1990 Terra/Aqua (MODerate resolution Imaging Spectroradiometer, MODIS), Sentinel-5/5P
1991 (TROPOMI), and FLEX/Sentinel-3 missions.

1992 **9. Conclusion**

1993 Solar-induced chlorophyll fluorescence is a promising optical indicator of photosynthetic status
1994 and related stress effects in terrestrial vegetation. In the last few decades, remote detection of SIF
1995 has undergone advances in measurement techniques, retrieval algorithms, and modelling of
1996 fluorescence-photosynthesis and radiative transfer processes. Assessment of SIF is now possible
1997 across a range of biological, spatial, and temporal scales, with intriguing applications prospects
1998 in terrestrial vegetation science. These developments are noteworthy because SIF is not a very
1999 simple phenomenon. To fully realize its potential, developments in all subject areas considered

2000 in this review will be needed so that researchers and applied users will be able to utilize SIF with
2001 confidence. High-priority topics for the future include understanding and addressing of
2002 confounding factors, validation of SIF retrievals and related products, provision of user-friendly
2003 modelling and data processing options, and availability of technologies to meet the different
2004 needs of researchers and non-expert users. Encouraging results in satellite-based detection of SIF
2005 have been reported in the last decade which, in concert with ground-based and airborne methods,
2006 opens the door to study actual photosynthetic dynamics in canopies, ecosystems, landscapes, and
2007 biomes. In the near future, there will be tailored space-based technologies for SIF emphasizing
2008 quantifiably high accuracy, availability of multiple SIF metrics, relevant ancillary data, and high
2009 spectral, spatial and temporal resolutions. This will allow satellite-derived SIF to be used in local
2010 to landscape scale applications – a benefit already evident with field and airborne-based SIF
2011 methods. The vision of the early proposers of satellite-based SIF detection was for optimized
2012 systems that would reduce uncertainties – and that vision remains strong today. As remote
2013 sensing of SIF matures, such systems will allow a more comprehensive appraisal of the
2014 capabilities of SIF and will help to shape the trajectory of the *next* 50 years.

2015 **Acknowledgements**

2016 We are very grateful to individuals who provided helpful contributions during the preparation of
2017 this paper: Ralf Bock, Matthias Drusch, and Pedro José Jurado Lozano (European Space
2018 Agency), for providing information and the schematic Figure 12 of the FLEX/S-3 tandem
2019 mission; David R. Landis (NASA/GSFC), for assistance with Table 3 on the satellite missions;
2020 and Dan Pernokis (P&M Technologies), for assistance in proofreading and editing the
2021 manuscript. In addition, we recognize the following funding: Zbyněk Malenovský was supported

2022 by the Australian Research Council Future Fellowship *Bridging Scales in Remote Sensing of*
2023 *Vegetation Stress* (FT160100477). Uwe Rascher acknowledges the SEN2Exp project funded by
2024 the European Space Agency in supporting part of this work.

2025

2026 **Acronyms and abbreviations**

ACGS	Atmospheric Carbon dioxide Grating Spectroradiometer
APEX	Airborne Prism EXperiment
BEPS	Boreal Ecosystems Productivity Simulator
BESS	Breathing Earth System Simulator
BOA	Bottom of atmosphere
BRDF	Bidirectional reflectance distribution function
CAM	Crassulacean acid metabolism
CASI	Compact Airborne Spectrographic Imager
CF	Chlorophyll fluorescence
CFIS	Chlorophyll Fluorescence Imaging Spectrometer
CLM	Community Land Model
DART	Discrete Anisotropic Radiative Transfer
DOAS	Differential optical absorption spectroscopy
EnviSat	Environmental Satellite
ESA	European Space Agency
EVI	Enhanced Vegetation Index
fAPAR	Fraction of photosynthetically active radiation absorbed
fAPAR _{chl}	Fraction of photosynthetically active radiation absorbed by chlorophyll
FIPAM	Frequency Induced Pulse Amplitude Modulation
FL	Fraunhofer line
FLD	Fluorescence line depth
FLEX	FLuorescence EXplorer
FLORIS	FLuORescence Imaging Spectrometer
FSR	Fluorescence Spectrum Reconstruction
FluorWPS	Fluorescence model with Weighted Photon Spread
FRT	Fluorescence–Reflectance–Transmittance
F-SFM	Full-spectrum spectral fitting method
FWHM	Full width at half maximum
GEO	Geostationary Earth orbit
GeoCARB	Geostationary Carbon Cycle Observatory
GEP	Gross ecosystem productivity
GOSAT	Greenhouse gases Observing SATellite
GOME-2	Global Ozone Monitoring Experiment-2
GPP	Gross primary productivity
KMF	Kubelka-Munk Fluorescence
LEAF-NL	Laser Environmental Active Fluorosensor
LIF	Laser-induced fluorescence
LIFT	Laser-Induced (<i>or</i> Light-Induced) Fluorescence Transient
LSM	Land surface model
MERIS	MEDium Resolution Imaging Spectrometer
MetOp-A, -B	Meteorological Operational satellite-A or -B
MODIS	MODerate resolution Imaging Spectroradiometer
MODTRAN	MODerate resolution atmospheric TRANsmission
MTCI	MERIS Terrestrial Chlorophyll Index
MTG-S	Meteosat Third Generation-Sounder
NDVI	Normalized Difference Vegetation Index

NPP	Net primary productivity
NPQ	Non-photochemical quenching
OCO	Orbiting Carbon Observatory
OLCI	Ocean and Land Colour Imager
ORCHIDEE	Organising Carbon and Hydrology In Dynamic Ecosystems
PAM	Pulse-amplitude modulation
PCA	Principal Component Analysis
PMFD	Passive Multi-wavelength Fluorescence Detector
PQ	Photochemical quenching
PRI	Photochemical Reflectance Index
PROSPECT	<u>PRO</u> priétés <u>SPECT</u> rales
PSII, PSI	Photosystem II or I
RC	Reaction center
ROSI	Reflective Optics System Imaging Spectrometer
RTM	Radiative transfer model
SAIL	Scattering of Arbitrarily Inclined Leaves
S-3	Sentinel-3
SCIAMACHY	SCanning Imaging Absorption spectroMeter for Atmospheric CHartography
SCOPE	Soil-Canopy-Observation of Photosynthesis and Energy fluxes
SEN2FLEX	SENTinel-2 and FLuorescence EXperiment
S-5P	Sentinel-5 Precursor
SiB2	Simple Biosphere Model (2)
SVAT	Soil-Vegetation-Atmosphere-Transfer
SVD	Singular Value Decomposition
SFM	Spectral fitting methods
SLSTR	Sea and Land Surface Temperature Radiometer
SNR	Signal-to-noise ratio
SR	Spectral resolution
TanSat	Carbon Dioxide Observation Satellite
TANSO-FTS	Thermal And Near-infrared Sensor for carbon Observation – Fourier Transform Spectrometer
TEMPO	Tropospheric Emissions: Monitoring of Pollution
TOA	Top of atmosphere
TOC	Top of canopy
TROPOMI	TROPOspheric Monitoring Instrument
UAS	Unmanned aircraft system
UAV	Unmanned aerial vehicle
VIRAF	Visible Infrared Reflectance Absorbance Fluorescence
VNIR	Visible and near-infrared

2027

2028

2029

2030 **References**

- 2031 Ač, A., Malenovský, Z., Olejníčková, J., Gallé, A., Rascher, U., Mohammed, G., 2015. Meta-analysis
2032 assessing potential of steady-state chlorophyll fluorescence for remote sensing detection of plant water,
2033 temperature and nitrogen stress. *Remote Sens. Environ.* 168, 420-436.
- 2034 Agati, G., Mazzinghi, P., Fusi, F., Ambrosini, I., 1995. The F685/F730 chlorophyll fluorescence ratio as a
2035 tool in plant physiology: Response to physiological and environmental factors. *J. Plant Physiol.* 145,
2036 228-238.
- 2037 Aldea, M., Frank, T.D., DeLucia, E.H., 2006. A method for quantitative analysis of spatially variable
2038 physiological processes across leaf surfaces. *Photosynth. Res.* 90, 161-172.
- 2039 Alden, C.B., Miller, J.B., Gatti, L.V., Gloor, M.M., Guan, K., Michalak, A.M., Van der Laan-Luijckx, I.T.,
2040 Touma, D., Andrews, A., Basso, L.S., Correia, C.S.C., Domingues, L.G., Joiner, J., Krol, M.C.,
2041 Lyapustin, A.I., Peters, W., Shiga, Y.P., Thoning, K., Van der Velde, I., Van Leeuwen, T.T., Yadav, V.,
2042 and Diffenbaugh, N.S., 2016. Regional atmospheric CO₂ inversion reveals seasonal and geographic
2043 differences in Amazon net biome exchange. *Glob. Change Biol.* 22, 3427-3443.
- 2044 Alemohammad, S.H., Fang, B., Konings, A.G., Aires, F., Green, J.K., Kolassa, J., Miralles, D., Prigent,
2045 C., and Gentile, P., 2017. Water, Energy, and Carbon with Artificial Neural Networks (WECANN): A
2046 statistically based estimate of global surface turbulent fluxes and gross primary productivity using solar-
2047 induced fluorescence. *Biogeosciences* 14, 4101-4124.
- 2048 Allen, W.A., Gausman, H.W., Richardson, A.J., Thomas, J.R., 1969. Interaction of isotropic light with a
2049 compact plant leaf. *J. Opt. Soc. Am.* 59, 1376-1379.
- 2050 Allen, W.A., Gayle, T.V., Richardson, A.J., 1970. Plant-canopy irradiance specified by the Duntley
2051 equations. *J. Opt. Soc. Am.* 60, 372-376.
- 2052 Alonso, L., Gómez-Chova, L., Vila-Francés, J., Amorós-López, J., Guanter, L., Calpe, J., Moreno, J.,
2053 2008. Improved Fraunhofer line discrimination method for vegetation fluorescence quantification. *IEEE*
2054 *Geosci. Remote Sens. Lett.* 5, 620-624.
- 2055 Anderson, M.C., 1963. Studies of the woodland light climate: I. The photographic computation of light
2056 conditions. *J. Ecol.* 52, 27-41.
- 2057 Atherton, J., Nichol, C.J., Porcar-Castell, A., 2016. Using spectral chlorophyll fluorescence and the
2058 photochemical reflectance index to predict physiological dynamics. *Remote Sens. Environ.* 176, 17-30.
- 2059 Baker, N.R., Rosenqvist, E., 2004. Applications of chlorophyll fluorescence can improve crop production
2060 strategies: An examination of future possibilities. *J. Exp. Bot.* 55, 1607-1621.
- 2061 Ball, J.T., Woodrow, I.E., Berry, J.A., 1987. A model predicting stomatal conductance and its
2062 contribution to the control of photosynthesis under different environmental conditions, in: Biggins, J.
2063 (Ed.), *Progress in Photosynthesis Research*. Martinus Nijhoff, Dordrecht, pp. 221-224.
- 2064 Barón, M., Pineda, M., Pérez-Bueno, M.L., 2016. Picturing pathogen infection in plants. *Z. Naturforsch.*
2065 *C.* 71, 355-368.

- 2066 Bendig, J., Gautam, D., Malenovský, Z., Lucieer, A., 2018. Influence of cosine corrector and UAS
2067 platform dynamics on airborne spectral irradiance measurements, in: Proc. IEEE International Geoscience
2068 and Remote Sensing Symposium (IGARSS), 22-27 July 2018, Valencia, Spain, pp. 8826-8829.
- 2069 Benediktyová, Z., Nedbal, L., 2009. Imaging of multi-color fluorescence emission from leaf tissues.
2070 Photosynth. Res. 102, 169.
- 2071 Bennett, D.I.G., Fleming, G.R., Amarnath, K., 2018. Energy-dependent quenching adjusts the excitation
2072 diffusion length to regulate photosynthetic light harvesting. Proc. Natl. Acad. Sci. USA 115, E9523-
2073 E9531.
- 2074 Berk, A., Conforti, P., Kennett, R., Perkins, T., Hawes, F., Van den Bosch, J., 2014. MODTRAN6: a
2075 major upgrade of the MODTRAN radiative transfer code, in: Proc. SPIE 9088, Algorithms and
2076 Technologies for Multispectral, Hyperspectral, and Ultraspectral Imagery XX, 90880H, 13 June 2014.
- 2077 Berkelhammer, M., Stefanescu, I.C., Joiner, J., Anderson, L., 2017. High sensitivity of gross primary
2078 production in the Rocky Mountains to summer rain. Geophys. Res. Lett. 44, 3643-3652.
- 2079 Berni, J.A.J., Zarco-Tejada, P.J., Suárez, L., Fereres, E., 2009. Thermal and narrowband multispectral
2080 remote sensing for vegetation monitoring from an unmanned aerial vehicle. IEEE Trans. Geosci. Remote
2081 Sens. 47, 722-738.
- 2082 Bilger, W., Björkman, O., 1990. Role of the xanthophyll cycle in photoprotection elucidated by
2083 measurements of light-induced absorbance changes, fluorescence and photosynthesis in leaves of *Hedera*
2084 *canariensis*. Photosynth. Res. 25, 173-185.
- 2085 Blondeau-Patissier, D., Gower, J.F.R., Dekker, A.G., Phinn, S.R., Brando, V.E., 2014. A review of ocean
2086 color remote sensing methods and statistical techniques for the detection, mapping and analysis of
2087 phytoplankton blooms in coastal and open oceans. Prog. Oceanogr. 123, 123-144.
- 2088 Boardman, N.K., Thorne, S.W., Anderson, J.M., 1966. Fluorescence properties of particles obtained by
2089 digitonin fragmentation of spinach chloroplasts. Proc. Natl. Acad. Sci. USA 56, 586-593.
- 2090 Bolhår-Nordenkampf, H.R., Long, S.P., Baker, N.R., Oquist, G., Schreiber, U., Lechner, E.G., 1989.
2091 Chlorophyll fluorescence as a probe of the photosynthetic competence of leaves in the field: A review of
2092 current instrumentation. Funct. Ecol. 3, 497-514.
- 2093 Bonan, G.B., 1996. A land surface model (LSM version 1.0) for ecological, hydrological, and
2094 atmospheric studies: Technical description and user's guide. NCAR Technical Note NCAR/TN-417-STR.
2095 National Center for Atmospheric Research, Boulder, CO (United States). Climate and Global Dynamics
2096 Div., doi:10.5065/D6DF6P5X.
- 2097 Bonan, G.B., Lawrence, P.J., Oleson, K.W., Levis, S., Jung, M., Reichstein, M., Lawrence, D.M.,
2098 Swenson, S.C., 2011. Improving canopy processes in the Community Land Model version 4 (CLM4)
2099 using global flux fields empirically inferred from FLUXNET data, J. Geophys. Res. Biogeosci. 116,
2100 G02014, doi: 10.1029/2010JG001593.
- 2101 Bornman, J.F., Vogelmann, T.C., Martin, G., 1991. Measurement of chlorophyll fluorescence within
2102 leaves using a fiberoptic microprobe. Plant Cell Environ. 14, 719-725.

- 2103 Bradbury, M., Baker, N.R., 1981. Analysis of the slow phases of the *in vivo* chlorophyll fluorescence
2104 induction curve. Changes in redox state of Photosystem II electron acceptors and fluorescence emission
2105 from Photosystem I and II. *Biochim. Biophys. Acta* 635, 542-551.
- 2106 Brewster, D., 1834. On the colours of natural bodies. *Trans. R. Soc. Edinburgh* 12, 538-545.
- 2107 Brugnoli, E., Björkman, O., 1992. Chloroplast movements in leaves: Influence on chlorophyll
2108 fluorescence and measurements of light-induced absorbance changes related to ΔpH and zeaxanthin
2109 formation. *Photosynth. Res.* 32, 23-35.
- 2110 Burkart, A., Schickling, A., Cendrero Mateo, M.P., Wrobel, T.J., Rossini, M., Cogliati, S., Julitta, T.,
2111 Rascher, U., 2015. A method for uncertainty assessment of passive sun-induced chlorophyll fluorescence
2112 retrieval using an infrared reference light. *IEEE Sens. J.* 15, 4603-4611.
- 2113 Buschmann, C., 2007. Variability and application of the chlorophyll fluorescence emission ratio red/far-
2114 red of leaves. *Photosynth. Res.* 92, 261-271.
- 2115 Buschmann, C., Lichtenthaler, H.K., 1988. Reflectance and chlorophyll fluorescence signatures in leaves,
2116 in: Lichtenthaler, H.K. (Ed.), *Applications of Chlorophyll Fluorescence in Photosynthesis Research,*
2117 *Stress Physiology, Hydrobiology and Remote Sensing.* Springer, Dordrecht, pp. 325-332.
- 2118 Buschmann, C., Lichtenthaler, H.K., 1998. Principles and characteristics of multi-colour fluorescence
2119 imaging of plants. *J. Plant Physiol.* 152, 297-314.
- 2120 Buschmann, C., Langsdorf, G., Lichtenthaler, H.K., 2000. Imaging of the blue, green, and red
2121 fluorescence emission of plants: An overview. *Photosynthetica* 38, 483-491.
- 2122 Buschmann, C., Langsdorf, G., Lichtenthaler, H.K., 2009. Blue, green, red, and far-red fluorescence
2123 signatures of plant tissues, their multicolor fluorescence imaging, and application for agrofood
2124 assessment, in: Zude, M. (Ed.), *Optical Monitoring of Fresh and Processed Agricultural Crops.* Taylor &
2125 Francis / CRC Press, Boca Raton, pp. 272-319.
- 2126 Buurman, E.P., Sanders, R., Draaijer, A., Gerritsen, H.C., Van Veen, J.J.F., Houpt, P.M., Levine, Y.K.,
2127 1992. Fluorescence lifetime imaging using a confocal laser scanning microscope. *Scanning* 14, 155-159.
- 2128 Calatayud, A., Roca, D., Martinez, P.F., 2006. Spatio-temporal variations in rose leaves under water
2129 stress conditions studied by chlorophyll fluorescence imaging. *Plant Physiol. Biochem.* 44, 564-573.
- 2130 Calderón, R., Navas-Cortés, J.A., Lucena, C., Zarco-Tejada, P.J., 2013. High-resolution airborne
2131 hyperspectral and thermal imagery for early detection of *Verticillium* wilt of olive using fluorescence,
2132 temperature and narrow-band spectral indices. *Remote Sens. Environ.* 139, 231-245.
- 2133 Calderón, R., Navas-Cortés, J.A., Zarco-Tejada, P.J., 2015. Early detection and quantification of
2134 *Verticillium* wilt in olive using hyperspectral and thermal imagery over large areas. *Remote Sens.* 7,
2135 5584-5610.
- 2136 Campbell, P.K.E., Middleton, E.M., McMurtrey, J.E., Corp, L.A., Chappelle, E.W., 2007. Assessment of
2137 vegetation stress using reflectance or fluorescence measurements. *J. Environ. Qual.* 36, 832-845.
- 2138 Campbell, P.K.E., Middleton, E.M., Corp, L.A., Kim, M.S., 2008. Contribution of chlorophyll
2139 fluorescence to the apparent vegetation reflectance. *Sci. Total Environ.* 404, 433-439.

- 2140 Carter, G.A., Jones, J.H., Mitchell, R.J., Brewer, C.H., 1996. Detection of solar-excited chlorophyll *a*
2141 fluorescence and leaf photosynthetic capacity using a Fraunhofer line radiometer. *Remote Sens. Environ.*
2142 55, 89-92.
- 2143 Carter, G.A., Theisen, A.F., Mitchell, R.J., 1990. Chlorophyll fluorescence measured using the
2144 Fraunhofer line-depth principle and relationship to photosynthetic rate in the field. *Plant Cell Environ.* 13,
2145 79-83.
- 2146 Cazzaniga, S., Dall'Osto, L., Kong, S.-G., Wada, M., Bassi, R., 2013. Interaction between avoidance of
2147 photon absorption, excess energy dissipation and zeaxanthin synthesis against photooxidative stress in
2148 *Arabidopsis*. *Plant J.* 76, 568-579.
- 2149 Cecchi, G., Mazzinghi, P., Pantani, L., Valentini, R., Tirelli, D., De Angelis, P., 1994. Remote sensing of
2150 chlorophyll *a* fluorescence of vegetation canopies. 1. Near and far field measurement techniques. *Remote*
2151 *Sens. Environ.* 47, 18-28.
- 2152 Celesti, M., Van der Tol, C., Cogliati, S., Panigada, C., Yang, P., Pinto, F., Rascher, U., Miglietta, F.,
2153 Colombo, R., Rossini, M., 2018. Exploring the physiological information of sun-induced chlorophyll
2154 fluorescence through radiative transfer model inversion. *Remote Sens. Environ.* 215, 97-108.
- 2155 Cendrero-Mateo, M.P., Moran, M.S., Papuga, S.A., Thorp, K.R., Alonso, L., Moreno, J., Ponce-Campos,
2156 G., Rascher, U., Wang, G., 2016. Plant chlorophyll fluorescence: Active and passive measurements at
2157 canopy and leaf scales with different nitrogen treatments. *J. Exp. Bot.* 67, 275-286.
- 2158 Cerovic, Z.G., Goulas, Y., Gorbunov, M., Briantais, J.-M., Camenen, L., Moya, I., 1996. Fluoresensing of
2159 water stress in plants: Diurnal changes of the mean lifetime and yield of chlorophyll fluorescence,
2160 measured simultaneously and at a distance with a τ -LIDAR and a modified PAM-fluorimeter, in maize,
2161 sugar beet, and kalanchoë. *Remote Sens. Environ.* 58, 311-321.
- 2162 Cerovic, Z.G., Samson, G., Morales, F., Tremblay, N., Moya, I., 1999. Ultraviolet-induced fluorescence
2163 for plant monitoring: Present state and prospects. *Agronomie* 19, 543-578.
- 2164 Chaerle, L., Leinonen, I., Jones, H.G., Van der Straeten, D., 2007. Monitoring and screening plant
2165 populations with combined thermal and chlorophyll fluorescence imaging. *J. Exp. Bot.* 58, 773-784.
- 2166 Chang, J., Ciais, P., Herrero, M., Havlik, P., Campioli, M., Zhang, X., Bai, Y., Viovy, N., Joiner, J.,
2167 Wang, X., Peng, S., Yue, C., Piao, S., Wang, T., Hauglustaine, D.A., Soussana, J.-F., Pregon, A.,
2168 Kosykh, N., Mironycheva-Tokareva, N., 2016. Combining livestock production information in a process-
2169 based vegetation model to reconstruct the history of grassland management. *Biogeosciences*, 13, 3757-
2170 3776.
- 2171 Chappelle, E.W., Williams, D.L., 1987. Laser-induced fluorescence (LIF) from plant foliage. *IEEE Trans.*
2172 *Geosci. Remote Sens.*, GE-25, 726-736.
- 2173 Chekalyuk, A.M., Hoge, F.E., Wright, C.W., Swift, R.N., 2000. Short-pulse pump-and-probe technique
2174 for airborne laser assessment of Photosystem II photochemical characteristics. *Photosynth. Res.* 66, 33-
2175 44.
- 2176 Chen, J.M., Liu, J., Cihlar, J., Goulden, M.L., 1999. Daily canopy photosynthesis model through temporal
2177 and spatial scaling for remote sensing applications. *Ecol. Modell.* 124, 99-119.

- 2178 Chen, J.M., Leblanc, S.G., 1997. A four-scale bidirectional reflectance model based on canopy
2179 architecture. *IEEE Trans. Geosci. Remote Sens.* 35, 1316–1337.
- 2180 Cheng, Y.-B., Middleton, E.M., Zhang, Q., Huemmrich, K.F., Campbell, P.K.E., Corp, L.A., Cook, B.D.,
2181 Kustas, W.P., Daughtry, C.S., 2013. Integrating solar induced fluorescence and the photochemical
2182 reflectance index for estimating gross primary production in a cornfield. *Remote Sens.* 5, 6857-6879.
- 2183 Cogliati, S., Colombo, R., Celesti, M., Tagliabue, G., Rascher, U., Schickling, A., Rademske, P., Alonso,
2184 L., Sabater, N., Schuettemeyer, D., Drusch, M., 2018. Red and far-red fluorescence emission retrieval
2185 from airborne high-resolution spectra collected by the Hyplant-Fluo sensor, in: *Proc. IEEE International
2186 Geoscience and Remote Sensing Symposium (IGARSS)*, 22-27 July 2018, Valencia, Spain, pp. 3935-
2187 3938.
- 2188 Cogliati, S., Rossini, M., Julitta, T., Meroni, M., Schickling, A., Burkart, A., Pinto, F., Rascher, U.,
2189 Colombo, R., 2015a. Continuous and long-term measurements of reflectance and sun-induced chlorophyll
2190 fluorescence by using novel automated field spectroscopy systems. *Remote Sens. Environ.* 164, 270-281.
- 2191 Cogliati, S., Verhoef, W., Kraft, S., Sabater, N., Alonso, L., Vicent, J., Moreno, J., Drusch, M., Colombo,
2192 R., 2015b. Retrieval of sun-induced fluorescence using advanced spectral fitting methods. *Remote Sens.*
2193 *Environ.* 169, 344-357.
- 2194 Collatz, G.J., Ball, J.T., Grivet, C., Berry, J.A., 1991. Physiological and environmental regulation of
2195 stomatal conductance, photosynthesis and transpiration: A model that includes a laminar boundary layer.
2196 *Agric. For. Meteorol.* 54, 107-136.
- 2197 Colombo, R., Celesti, M., Bianchi, R., Campbell, P.K.E., Cogliati, S., Cook, B.D., Corp, L.A., Damm, A.,
2198 Domec, J.-C., Guanter, L., Julitta, T., Middleton, E.M., Noormets, A., Panigada, C., Pinto, F., Rascher,
2199 U., Rossini, M., Schickling, A., 2018. Variability of sun-induced chlorophyll fluorescence according to
2200 stand age-related processes in a managed loblolly pine forest. *Glob. Change Biol.* 24, 2980-2996.
- 2201 Coppo, P., Taiti, A., Pettinato, L., Francois, M., Taccola, M., Drusch, M., 2017. Fluorescence Imaging
2202 Spectrometer (FLORIS) for ESA FLEX mission. *Remote Sens.* 9, 649.
- 2203 Corp, L.A., McMurtry, J.E., Middleton, E.M., Mulchi, C.L., Chappelle, E.W., Daughtry, C.S.T., 2003.
2204 Fluorescence sensing systems: In vivo detection of biophysical variations in field corn due to nitrogen
2205 supply. *Remote Sens. Environ.* 86, 470-479.
- 2206 Cui, T., Sun, R., Qiao, C., Zhang, Q., Yu, T., Liu, G., Liu, Z., 2017a. Estimating diurnal courses of gross
2207 primary production for maize: A comparison of sun-induced chlorophyll fluorescence, light-use
2208 efficiency and process-based models. *Remote Sens.* 9, 1267.
- 2209 Cui, Y., Xiao, X., Zhang, Y., Dong, J., Qin, Y., Doughty, R.B., Zhang, G., Wang, J., Wu, X., Qin, Y.,
2210 Zhou, S., Joiner, J., Moore III, B., 2017b. Temporal consistency between gross primary production and
2211 solar-induced chlorophyll fluorescence in the ten most populous megacity areas over years. *Sci. Rep.* 7,
2212 14963.
- 2213 Dai, Y., Dickinson, R.E., Wang, Y.-P., 2004. A Two-Big-Leaf Model for Canopy Temperature,
2214 Photosynthesis, and Stomatal Conductance, *Journal of Climate* 17, 2281–2299.
- 2215 Dall'Osto, L., Cassaniga, S., Wada, M., Bassi, R., 2014. On the origin of a slowly reversible fluorescence
2216 decay component in the *Arabidopsis npq4* mutant. *Phil. Trans. R. Soc. B* 369, 20130221.

- 2217 Damm, A., Elbers, J.A., Erler, A., Giolis, B., Hamdi, K., Hutjes, R.W.A., Kosvancova, M., Meroni, M.,
 2218 Miglietta, F., Moersch, A., Moreno, J., Schickling, A., Sonnenschein, R., Udelhoven, T., Van der Linden,
 2219 S., Hostert, P., Rascher, U., 2010. Remote sensing of sun-induced fluorescence to improve modeling of
 2220 diurnal courses of gross primary production (GPP). *Glob. Change Biol.* 16, 171-186.
- 2221 Damm, A., Erler, A., Hillen, W., Meroni, M., Schaepman, M.E., Verhoef, W., Rascher, U., 2011.
 2222 Modeling the impact of spectral sensor configurations on the FLD retrieval accuracy of sun-induced
 2223 chlorophyll fluorescence. *Remote Sens. Environ.* 115, 1882-1892.
- 2224 Damm, A., Guanter, L., Laurent, V. C. E., Schaepman, M. E., Schickling, A., Rascher, U., 2014. FLD-
 2225 based retrieval of sun-induced chlorophyll fluorescence from medium spectral resolution airborne
 2226 spectroscopy data. *Remote Sens. Environ.* 147, 256-266.
- 2227 Damm, A., Guanter, L., Paul-Limoges, E., Van der Tol, C., Hueni, A., Buchmann, N., Eugster, W.,
 2228 Ammann, C., Schaepman, M.E., 2015a. Far-red sun-induced chlorophyll fluorescence shows ecosystem-
 2229 specific relationships to gross primary production: An assessment based on observational and modeling
 2230 approaches. *Remote Sens. Environ.* 166, 91-105.
- 2231 Damm, A., Guanter, L., Verhoef, W., Schläpfer, D., Garbari, S., Schaepman, M.E., 2015b. Impact of
 2232 varying irradiance on vegetation indices and chlorophyll fluorescence derived from spectroscopy data.
 2233 *Remote Sens. Environ.* 156, 202-215.
- 2234 Daumard, F., Champagne, S., Fournier, A., Goulas, Y., Ounis, A., Hanocq, J.-F., Moya, I., 2010. A field
 2235 platform for continuous measurement of canopy fluorescence. *IEEE Trans. Geosci. Remote Sens.* 48,
 2236 3358-3368.
- 2237 Daumard, F., Goulas, Y., Champagne, S., Fournier, A., Ounis, A., Olioso, A., Moya, I., 2012. Continuous
 2238 monitoring of canopy level sun-induced chlorophyll fluorescence during the growth of a sorghum field.
 2239 *IEEE Trans. Geosci. Remote Sens.* 50, 4292-4300.
- 2240 DeEll, J.R., Toivonen, P.M.A. (Eds.), 2003. *Practical Applications of Chlorophyll Fluorescence in Plant*
 2241 *Biology*. Kluwer/Springer, Dordrecht.
- 2242 Demmig-Adams, B., 1990. Carotenoids and photoprotection in plants: A role for the xanthophyll
 2243 zeaxanthin. *Biochim. Biophys. Acta* 1020, 1-24.
- 2244 Demmig-Adams, B., Adams III, W.W., Heber, U., Neimanis, S., Winter, K., Krüger, A., Czygan, F.-C.,
 2245 Bilger, W., Björkman, O., 1990. Inhibition of zeaxanthin formation and of rapid changes in radiationless
 2246 energy dissipation by dithiothreitol in spinach leaves and chloroplasts. *Plant Physiol.* 92, 293-301.
- 2247 Demmig-Adams, B., Cohu, C.M., Muller, O., Adams III, W.W., 2012. Modulation of photosynthetic
 2248 energy conversion efficiency in nature: From seconds to seasons. *Photosynth. Res.* 113, 75-88.
- 2249 De Pury, D.G.G., Farquhar, G.D., 1997. Simple scaling of photosynthesis from leaves to canopies without
 2250 the errors of big-leaf models. *Plant Cell Environ.* 20, 537-557.
- 2251 De Wit, C.T., 1965. *Photosynthesis of leaf canopies*. Agricultural Research Report No. 663. PUDOC,
 2252 Wageningen.
- 2253 Disney, M., 2016. Remote sensing of vegetation: Potentials, limitations, developments and applications,
 2254 in: Hikosaka, K., Niinemets, Ü., Anten, N.P.R. (Eds.), *Canopy Photosynthesis: From Basics to*
 2255 *Applications*. Springer, Dordrecht, pp. 289-331.

- 2256 Disney, M.I., Lewis, P., North, P.R.J., 2000. Monte Carlo ray tracing in optical canopy reflectance
2257 modelling. *Remote Sensing Reviews* 18, 163-196.
- 2258 D'Odorico, P., Alberti, E., Schaepman, M.E., 2010. In-flight spectral performance monitoring of the
2259 Airborne Prism Experiment. *Appl. Opt.* 49, 3082-3091.
- 2260 Dobrowski, S.Z., Pushnik, J.C., Zarco-Tejada, P.J., Ustin, S.L., 2005. Simple reflectance indices track
2261 heat and water stress-induced changes in steady-state chlorophyll fluorescence at the canopy scale.
2262 *Remote Sens. Environ.* 97, 403-414.
- 2263 Donaldson, L., Williams, N., 2018. Imaging and spectroscopy of natural fluorophores in pine needles.
2264 *Plants* 7, 10.
- 2265 Drusch, M., Moreno, J., Del Bello, U., Franco, R., Goulas, Y., Huth, A., Kraft, S., Middleton, E.M.,
2266 Miglietta, F., Mohammed, G., Nedbal, L., Rascher, U., Schüttemeyer, D., Verhoef, W., 2017. The
2267 FLuorescence EXplorer mission concept - ESA's Earth Explorer 8. *IEEE Trans. Geosci. Remote Sens.* 55,
2268 1273-1284.
- 2269 Du, S., Liu, L., Liu, X., Zhang, X., Zhang, X., Bi, Y., Zhang, L., 2018. Retrieval of global terrestrial
2270 solar-induced chlorophyll fluorescence from TanSat satellite. *Sci. Bull.* 63, 1502-1512.
- 2271 Duveiller, G., Cescatti, A., 2016. Spatially downscaling sun-induced chlorophyll fluorescence leads to an
2272 improved temporal correlation with gross primary productivity. *Remote Sens. Environ.* 182, 72-89.
- 2273 Duysens, L.N.M., 1963. Role of two photosynthetic pigment systems in cytochrome oxidation, pyridine
2274 nucleotide reduction, and fluorescence. *Proc. R. Soc. Lond. B.* 157, 301-313.
- 2275 Duysens, L.N.M., Sweers, H.E., 1963. Mechanism of two photochemical reactions in algae as studied by
2276 means of fluorescence, in: Japanese Society of Plant Physiologists (Eds.), *Studies on Microalgae and*
2277 *Photosynthetic Bacteria. A collection of papers.* University of Tokyo Press, Tokyo, Japan, pp. 353-372.
- 2278 ESA (European Space Agency), undated. Sentinel-5P: TROPOMI.
2279 https://www.esa.int/Our_Activities/Observing_the_Earth/Copernicus/Sentinel-5P/Tropomi (accessed 03
2280 February 2019).
- 2281 ESA (European Space Agency), 2018. FLEX Earth Explorer 8 Mission Requirements Document, Version
2282 3.0, Issue date 05/06/2018, ESA Earth and Mission Science Division, Ref: ESAEOP-SM/2221/MDru-md.
- 2283 ESA (European Space Agency), 2015. Report for Mission Selection: FLEX. ESA SP-1330/2 (2 volume
2284 series), 197 pp., Noordwijk (The Netherlands).
2285 https://esamultimedia.esa.int/docs/EarthObservation/SP1330-2_FLEX.pdf
- 2286 Evain, S., Camenen, L., Moya, I., 2001. Three channels detector for remote sensing of chlorophyll
2287 fluorescence and reflectance from vegetation, in: *Proc. 8th International Symposium: Physical*
2288 *Measurements and Signatures in Remote Sensing*, 8-12 January 2001, Aussois, France, pp. 395-400.
- 2289 Evain, S., Flexas, J., Moya, I., 2004. A new instrument for passive remote sensing: 2. Measurement of
2290 leaf and canopy reflectance changes at 531 nm and their relationship with photosynthesis and chlorophyll
2291 fluorescence. *Remote Sens. Environ.* 91, 175-185.
- 2292 Farquhar, G.D., Von Caemmerer, S., Berry, J.A., 1980. A biochemical model of photosynthetic CO₂
2293 assimilation in leaves of C₃ species. *Planta* 149, 78-90.

- 2294 Fawcett, D., Verhoef, W., Schläpfer, D., Schneider, F.D., Schaepman, M.E., Damm, A., 2018. Advancing
2295 retrievals of surface reflectance and vegetation indices over forest ecosystems by combining imaging
2296 spectroscopy, digital object models, and 3D canopy modelling. *Remote Sens. Environ.* 204, 583-595.
- 2297 Fernandez-Jaramillo, A.A., Duarte-Galvan, C., Contreras-Medina, L.M., Torres-Pacheco, I.,
2298 Romero-Troncoso, R.J., Guevara-Gonzalez, R.G., Millan-Almaraz, J.R., 2012. Instrumentation in
2299 developing chlorophyll fluorescence biosensing: A review. *Sensors* 12, 11853-11869.
- 2300 Flexas, J., Escalona, J.M., Evain, S., Gulías, J., Moya, I., Osmond, C.B., Medrano, H., 2002. Steady-state
2301 chlorophyll fluorescence (Fs) measurements as a tool to follow variations of net CO₂ assimilation and
2302 stomatal conductance during water-stress in C₃ plants. *Physiol. Plant.* 114, 231-240.
- 2303 Flexas, J., Briantais, J.-M., Cerovic, Z., Medrano, H., Moya, I., 2000. Steady-state and maximum
2304 chlorophyll fluorescence responses to water stress in grapevine leaves: A new remote sensing system.
2305 *Remote Sens. Environ.* 73, 283-297.
- 2306 Fournier, A., Daumard, F., Champagne, S., Ounis, A., Goulas, Y., Moya, I., 2012. Effect of canopy
2307 structure on sun-induced chlorophyll fluorescence. *ISPRS J. Photogramm. Remote Sens.* 68, 112-120.
- 2308 Fournier, A., Daumard, F., Champagne, S., Ounis, A., Moya, I., Goulas, Y., 2014. Effects of vegetation
2309 directional reflectance on sun-induced fluorescence retrieval in the oxygen absorption bands, in: *Proc. 5th*
2310 *International Workshop on Remote Sensing of Vegetation Fluorescence*, 22-24 April 2014, Paris, France.
- 2311 Franck, F., Juneau, P., Popovic, R., 2002. Resolution of the photosystem I and photosystem II
2312 contributions to chlorophyll fluorescence of intact leaves at room temperature. *Biochim. Biophys. Acta*
2313 1556, 239-246.
- 2314 Franck, J., French, C.S., Puck, T.T., 1941. The fluorescence of chlorophyll and photosynthesis. *J. Phys.*
2315 *Chem.* 45, 1268-1300.
- 2316 Franck, J., Herzfeld, K.F., 1941. Contribution to a theory of photosynthesis. *J. Phys. Chem.* 45, 978-1025.
- 2317 Frankenberg, C., Berry, J., 2018. Solar induced chlorophyll fluorescence: Origins, relation to
2318 photosynthesis and retrieval. *Reference Module in Earth Systems and Environmental Sciences*, Vol. 3,
2319 143-162. Elsevier. DOI: 10.1016/B978-0-12-409548-9.10632-3.
- 2320 Frankenberg, C., Butz, A., Toon, G.C., 2011a. Disentangling chlorophyll fluorescence from atmospheric
2321 scattering effects in O₂ A-band spectra of reflected sun-light. *Geophys. Res. Lett.* 38, L03801.
- 2322 Frankenberg, C., Fisher, J.B., Worden, J., Badgley, G., Saatchi, S.S., Lee, J.-E., Toon, G.C., Butz, A.,
2323 Jung, M., Kuze, A., Yokota, T., 2011b. New global observations of the terrestrial carbon cycle from
2324 GOSAT: Patterns of plant fluorescence with gross primary productivity. *Geophys. Res. Lett.* 38, L17706.
- 2325 Frankenberg, C., Köhler, P., Magney, T.S., Geier, S., Lawson, P., Schwochert, M., McDuffie, J., Drewry,
2326 D.T., Pavlick, R., Kuhnert, A., 2018. The Chlorophyll Fluorescence Imaging Spectrometer (CFIS),
2327 mapping far red fluorescence from aircraft. *Remote Sens. Environ.* 217, 523-536.
- 2328 Frankenberg, C., O'Dell, C., Berry, J., Guanter, L., Joiner, J., Köhler, P., Pollack, R., Taylor, T.E., 2014.
2329 Prospects for chlorophyll fluorescence remote sensing from the Orbiting Carbon Observatory-2. *Remote*
2330 *Sens. Environ.* 147, 1-12.

- 2331 Frankenberg, C., O'Dell, C., Guanter, L., McDuffie, J., 2012. Remote sensing of near-infrared chlorophyll
2332 fluorescence from space in scattering atmospheres: Implications for its retrieval and interferences with
2333 atmospheric CO₂ retrievals. *Atmospheric Meas. Tech.* 5, 2081-2094.
- 2334 Gamon, J.A., Field, C.B., Bilger, W., Björkman, O., Fredeen, A.L., Peñuelas, J., 1990. Remote sensing of
2335 the xanthophyll cycle and chlorophyll fluorescence in sunflower leaves and canopies. *Oecol.* 85, 1-7.
- 2336 Gamon, J.A., Peñuelas, J., Field, C.B., 1992. A narrow-waveband spectral index that tracks diurnal
2337 changes in photosynthetic efficiency. *Remote Sens. Environ.* 41, 35-44.
- 2338 Gamon, J.A., Serrano, L., Surfus, J.S., 1997. The photochemical reflectance index: An optical indicator of
2339 photosynthetic radiation use efficiency across species, functional types, and nutrient levels. *Oecol.* 112,
2340 492-501.
- 2341 Gamon, J.A., Surfus, J.S., 1999. Assessing leaf pigment content and activity with a reflectometer. *New.*
2342 *Phytol.* 143, 105-117.
- 2343 Garbulsky, M.F., Filella, I., Peñuelas, J., 2014a. Recent advances in the estimation of photosynthetic
2344 stress for terrestrial ecosystem services related to carbon uptake, in: Alcaraz-Segura, D., Di Bella, C.M.,
2345 Straschnoy, J.V. (Eds.), *Earth Observation of Ecosystem Services*. CRC Press, Boca Raton, pp. 39-62.
- 2346 Garbulsky, M.F., Filella, I., Verger, A., Peñuelas, J., 2014b. Photosynthetic light use efficiency from
2347 satellite sensors: From global to Mediterranean vegetation. *Environ. Exp. Bot.* 103, 3-11.
- 2348 García-Plazaola, J.I., Fernández-Marín, B., Duke, S.O., Hernández, A., López-Arbeloa, F., Becerril, J.M.,
2349 2015. Autofluorescence: Biological functions and technical applications. *Plant Sci.* 236, 136-145.
- 2350 Garzonio, R., Di Mauro, B., Colombo, R., Cogliati, S., 2017. Surface reflectance and sun-induced
2351 fluorescence spectroscopy measurements using a small hyperspectral UAS. *Remote Sens.* 9, 472.
- 2352 Gastellu-Etchegorry, J.P., Demarez, V., Pinel, V., Zagolski, F., 1996. Modeling radiative transfer in
2353 heterogeneous 3-D vegetation canopies. *Remote Sens. Environ.* 58, 131-156.
- 2354 Gastellu-Etchegorry, J.-P., Lauret, N., Yin, T., Landier, L., Kallel, A., Malenovský, Z., Al Bitar, A., Aval,
2355 J., Benhmida, S., Qi, J., Medjdoub, G., Guilleux, J., Chavanon, E., Cook, B., Morton, D., Chrysoulakis,
2356 N., Mitraka, Z., 2017. DART: Recent advances in remote sensing data modeling with atmosphere,
2357 polarization, and chlorophyll fluorescence. *IEEE J. Sel. Top. Appl. Earth Obs. Remote Sens.* 10, 2640-
2358 2649.
- 2359 Gastellu-Etchegorry, J.-P., Yin, T., Lauret, N., Cajgfinger, T., Gregoire, T., Grau, E., Feret, J.-B., Lopes,
2360 M., Guilleux, J., Dedieu, G., Malenovský, Z., Cook, B.D., Morton, D., Rubio, J., Durrieu, S., Cazanave,
2361 G., Martin, E., Ristorcelli, T., 2015. Discrete anisotropic radiative transfer (DART 5) for modeling
2362 airborne and satellite spectroradiometer and LIDAR acquisitions of natural and urban landscapes. *Remote*
2363 *Sens.* 7, 1667-1701.
- 2364 Gautam, D., Watson, C., Lucieer, A., Malenovský, Z., 2018. Error budget for geolocation of
2365 spectroradiometer point observations from an unmanned aircraft system. *Sensors* 18, 3465.
- 2366 Gentine, P., Alemohammad, S.H., 2018. Reconstructed solar-induced fluorescence: A machine learning
2367 vegetation product based on MODIS surface reflectance to reproduce GOME-2 solar-induced
2368 fluorescence. *Geophys. Res. Lett.* 45, 3136-3146.

- 2369 Genty, B., Briantais, J.-M., Baker, N.R., 1989. The relationship between the quantum yield of
2370 photosynthetic electron transport and quenching of chlorophyll fluorescence. *Biochim. Biophys. Acta*
2371 990, 87-92.
- 2372 Genty, B., Meyer, S., 1995. Quantitative mapping of leaf photosynthesis using chlorophyll fluorescence
2373 imaging. *Aust. J. Plant Physiol.* 22, 277-284.
- 2374 Genty, B., Wonders, J., Baker, N.R., 1990. Non-photochemical quenching of F_0 in leaves is emission
2375 wavelength dependent: Consequences for quenching analysis and its interpretation. *Photosynth. Res.* 26,
2376 133-139.
- 2377 Gerhards, M., Schlerf, M., Rascher, U., Udelhoven, T., Juszczak, R., Alberti, G., Miglietta, F., Inoue, Y.,
2378 2018. Analysis of airborne optical and thermal imagery for detection of water stress symptoms. *Remote*
2379 *Sens.* 10, 1139.
- 2380 Gitelson, A.A., Buschmann, C., Lichtenthaler, H.K., 1999. The chlorophyll fluorescence ratio F_{735}/F_{700} as
2381 an accurate measure of the chlorophyll content in plants. *Remote Sens. Environ.* 69, 296-302.
- 2382 Gitelson, A.A., Buschmann, C., Lichtenthaler, H.K., 1998. Leaf chlorophyll fluorescence corrected for
2383 re-absorption by means of absorption and reflectance measurements. *J. Plant Physiology* 152, 283-296.
- 2384 Gómez-Chova, L., Alonso-Chorda, L., Amoros-Lopez, J., Vila-Frances, J., Del Valle-Tascon, S., Calpe,
2385 J., Moreno, J., 2006. Solar induced fluorescence measurements using a field spectroradiometer. *AIP*
2386 *Conference Proceedings* 852, 274-281.
- 2387 Gorbe, E., Calatayud, A., 2012. Applications of chlorophyll fluorescence imaging technique in
2388 horticultural research: A review. *Sci. Hort.* 138, 24-35.
- 2389 Goss, R., Lepetit, B., 2015. Biodiversity of NPQ. *J. Plant Physiol.* 172, 13-32.
- 2390 Goudriaan, J., 1977. Crop micrometeorology: A simulation study. *Simulation Monograph*. PUDOC,
2391 Wageningen.
- 2392 Goulas, Y., Fournier, A., Daumard, F., Champagne, S., Ounis, A., Marloie, O., Moya, I., 2017. Gross
2393 primary production of a wheat canopy relates stronger to far red than to red solar-induced chlorophyll
2394 fluorescence. *Remote Sens.* 9, 97.
- 2395 Govindjee, 1995. Sixty-three years since Kautsky: Chlorophyll *a* fluorescence. *Aust. J. Plant Physiol.* 22,
2396 131-160.
- 2397 Govindjee, 2004. Chlorophyll *a* fluorescence: A bit of basics and history, in: Papageorgiou, G.C.,
2398 Govindjee (Eds.), *Chlorophyll Fluorescence: A Signature of Photosynthesis*. Kluwer, Dordrecht, pp. 1-41.
- 2399 Gower, J., 2016. On the use of satellite-measured chlorophyll fluorescence for monitoring coastal waters.
2400 *Int. J. Remote Sens.* 37, 2077-2086.
- 2401 Gower, J.F.R. and Borstad, G.A., 1990. Mapping of phytoplankton by solar-stimulated fluorescence using
2402 an imaging spectrometer. *Int. J. Remote Sens.* 11, 313-320.
- 2403 Green, J.K., Konings, A.G., Alemohammad, S.H., Berry, J., Entekhabi, D., Kolassa, J., Lee, J.-E.,
2404 Gentine, P., 2017. Regionally strong feedbacks between the atmosphere and terrestrial biosphere. *Nat.*
2405 *Geosci.* 10, 410-414.

- 2406 Grossmann, K., Frankenberg, C., Magney, T.S., Hurlock, S.C., Seibt, U., Stutz, J., 2018. PhotoSpec: A
 2407 new instrument to measure spatially distributed red and far-red solar-induced chlorophyll fluorescence.
 2408 *Remote Sens. Environ.* 216, 311-327.
- 2409 Guan, K., Berry, J.A., Zhang, Y., Joiner, J., Guanter, L., Badgley, G., Lobell, D.B., 2016. Improving the
 2410 monitoring of crop productivity using spaceborne solar-induced fluorescence. *Glob. Change Biol.* 22,
 2411 716-726.
- 2412 Guan, K., Pan, M., Li, H., Wolf, A., Wu, J., Medvigy, D., Caylor, K.K., Sheffield, J., Wood, E.F., Malhi,
 2413 Y., Liang, M., Kimball, J.S., Saleska, S.R., Berry, J., Joiner, J., Lyapustin, A.I., 2015. Photosynthetic
 2414 seasonality of global tropical forests constrained by hydroclimate. *Nat. Geosci.* 8, 284-289.
- 2415 Guanter, L., Aben, I., Tol, P., Krijger, J.M., Hollstein, A., Köhler, P., Damm, A., Joiner, J., Frankenberg,
 2416 C., Landgraf, J., 2015. Potential of the TROPOspheric Monitoring Instrument (TROPOMI) onboard the
 2417 Sentinel-5 Precursor for the monitoring of terrestrial chlorophyll fluorescence. *Atmospheric Meas. Tech.*
 2418 8, 1337-1352.
- 2419 Guanter, L., Alonso, L., Gómez-Chova, L., Amorós-López, J., Vila, J., Moreno, J., 2007. Estimation of
 2420 solar-induced vegetation fluorescence from space measurements. *Geophys. Res. Lett.* 34, L08401.
- 2421 Guanter, L., Alonso, L., Gómez-Chova, L., Meroni, M., Preusker, R., Fischer, J., Moreno, J., 2010.
 2422 Developments for vegetation fluorescence retrieval from spaceborne high-resolution spectrometry in the
 2423 O₂-A and O₂-B absorption bands. *J. Geophys. Res. Atmos.* 115(D19), 303,
 2424 D19303. <https://doi.org/10.1029/2009JD013716>.
- 2425 Guanter, L., Frankenberg, C., Dudhia, A., Lewis, P.E., Gómez-Dans, J., Kuze, A., Suto, H., Grainger,
 2426 R.G., 2012. Retrieval and global assessment of terrestrial chlorophyll fluorescence from GOSAT space
 2427 measurements. *Remote Sens. Environ.* 121, 236-251.
- 2428 Guanter, L., Zhang, Y., Jung, M., Joiner, J., Voigt, M., Berry, J.A., Frankenberg, C., Huete, A.R., Zarco-
 2429 Tejada, P., Lee, J.-E., Moran, M.S., Ponce-Campos, G., Beer, C., Camps-Valls, G., Buchmann, N.,
 2430 Dianelle, D., Klumpp, K., Cescatti, A., Baker, J.M., Griffis, T.J., 2014. Global and time-resolved
 2431 monitoring of crop photosynthesis with chlorophyll fluorescence. *Proc. Natl. Acad. Sci. USA* 111,
 2432 E1327-E1333.
- 2433 He, L., Chen, J.M., Liu, J., Mo, G., Joiner, J., 2017. Angular normalization of GOME-2 sun-induced
 2434 chlorophyll fluorescence observation as a better proxy of vegetation productivity. *Geophys. Res. Lett.* 44,
 2435 5691-5699.
- 2436 Hemphill, W.R., Watson, R.D., Bigelow, R.C., Hessen, T.D., 1977. Measurement of luminescence of
 2437 geochemically stressed trees and other materials. U.S. Geological Survey Professional Paper 1015, 93-
 2438 112.
- 2439 Hendrickson, L., Chow W.S., Furbank, R.T., 2004. A simple alternative approach to assessing the fate of
 2440 absorbed light energy using chlorophyll fluorescence. *Photosynth. Res.* 82, 73-81.
- 2441 Hernández-Clemente, R., North, P.R.J., Hornero, A., Zarco-Tejada, P.J., 2017. Assessing the effects of
 2442 forest health on sun-induced chlorophyll fluorescence using the FluorFLIGHT 3-D radiative transfer
 2443 model to account for forest structure. *Remote Sens. Environ.* 193, 165-179.

- 2444 Herwitz, S.R., Johnson, L.F., Dunagan, S.E., Higgins, R.G., Sullivan, D.V., Zheng, J., Lobitz, B.M.,
2445 Leung, J.G., Gallmeyer, B.A., Aoyagi, M., Slye, R.E., Brass, J.A., 2004. Imaging from an unmanned
2446 aerial vehicle: Agricultural surveillance and decision support. *Comput. Electron. Agr.* 44, 49-61.
- 2447 Hoge, F.E., Swift, R.N., 1981. Airborne simultaneous spectroscopic detection of laser-induced water
2448 Raman backscatter and fluorescence from chlorophyll *a* and other naturally-occurring pigments. *Appl.*
2449 *Opt.* 20, 3197-3205.
- 2450 Hu, J., Liu, L., Guo, J., Du, S., Liu, X., 2018a. Upscaling solar-induced chlorophyll fluorescence from an
2451 instantaneous to daily scale gives an improved estimation of the gross primary productivity. *Remote Sens.*
2452 10, 1663.
- 2453 Hu, J., Liu, X., Liu, L., Guan, L., 2018b. Evaluating the performance of the SCOPE model in simulating
2454 canopy solar-induced chlorophyll fluorescence. *Remote Sens.* 10, 250.
- 2455 Ireland, C.R., Long, S.P., Baker, N.R., 1984. The relationship between carbon dioxide fixation and
2456 chlorophyll *a* fluorescence during induction of photosynthesis in maize leaves at different temperatures
2457 and carbon dioxide concentrations. *Planta* 160, 550-558.
- 2458 Jacquemoud, S., 1993. Inversion of the PROSPECT + SAIL canopy reflectance model from AVIRIS
2459 equivalent spectra: Theoretical study. *Remote Sens. Environ.* 44, 281-292.
- 2460 Jacquemoud, S., Baret, F., 1990. PROSPECT: A model of leaf optical properties spectra. *Remote Sens.*
2461 *Environ.* 34, 75-91.
- 2462 Jacquemoud, S., Verhoef, W., Baret, F., Bacour, C., Zarco-Tejada, P.J., Asner, G.P., François, C., Ustin,
2463 S.L., 2009. PROSPECT + SAIL models: A review of use for vegetation characterization. *Remote Sens.*
2464 *Environ.* 113, Suppl. 1, S56-S66.
- 2465 Jeong, S.-J., Schimel, D., Frankenberg, C., Drewry, D.T., Fisher, J.B., Verma, M., Berry, J.A., Lee, J.-E.,
2466 Joiner, J., 2017. Application of satellite solar-induced chlorophyll fluorescence to understanding large-
2467 scale variations in vegetation phenology and function over northern high latitude forests. *Remote Sens.*
2468 *Environ.* 190, 178-187.
- 2469 Johnson, L.F., Herwitz, S., Dunagan, S., Lobitz, B., Sullivan, D., Slye, R., 2003. Collection of ultra high
2470 spatial and spectral resolution image data over California vineyards with a small UAV, in: *Proc. 30th*
2471 *International Symposium on Remote Sensing of Environment*, 10-14 November 2003, Honolulu (HI),
2472 USA, pp. 663-665.
- 2473 Joiner, J., Guanter, L., Lindstrot, R., Voigt, M., Vasilkov, A.P., Middleton, E.M., Huemmrich, K.F.,
2474 Yoshida, Y., Frankenberg, C., 2013. Global monitoring of terrestrial chlorophyll fluorescence from
2475 moderate spectral resolution near-Infrared satellite measurements: Methodology, simulations, and
2476 application to GOME-2. *Atmospheric Meas. Tech.*, 6, 2803-2823.
- 2477 Joiner, J., Yoshida, Y., Guanter, L., Middleton, E.M., 2016. New methods for retrieval of chlorophyll red
2478 fluorescence from hyperspectral satellite instruments: Simulations and application to GOME-2 and
2479 SCIAMACHY. *Atmospheric Meas. Tech.* 9, 3939-3967.
- 2480 Joiner, J., Yoshida, Y., Vasilkov, A.P., Middleton, E.M., Campbell, P.K.E., Yoshida, Y., Kuze, A., Corp,
2481 L.A., 2012. Filling-in of near-infrared solar lines by terrestrial fluorescence and other geophysical effects:
2482 Simulations and space-based observations from SCIAMACHY and GOSAT. *Atmospheric Meas. Tech.* 5,
2483 809-829.

- 2484 Joiner, J., Yoshida, Y., Vasilkov, A.P., Schaefer, K., Jung, M., Guanter, L., Zhang, Y., Garrity, S.,
 2485 Middleton, E.M., Huemmrich, K.F., Gu, L., Belelli Marchesini, L., 2014. The seasonal cycle of satellite
 2486 chlorophyll fluorescence observations and its relationship to vegetation phenology and ecosystem
 2487 atmosphere carbon exchange. *Remote Sens. Environ.* 152, 375-391.
- 2488 Joiner, J., Yoshida, Y., Vasilkov, A.P., Yoshida, Y., Corp, L.A., Middleton, E.M., 2011. First
 2489 observations of global and seasonal terrestrial chlorophyll fluorescence from space. *Biogeosciences* 8,
 2490 637-651.
- 2491 Joiner, J., Yoshida, Y., Zhang, Y., Duveiller, G., Jung, M., Lyapustin, A., Wang, Y., Tucker, C.J., 2018.
 2492 Estimation of terrestrial global gross primary production (GPP) with satellite data-driven models and
 2493 eddy covariance flux data. *Remote Sens.* 10, 1346.
- 2494 Julitta, T., Burkart, A., Colombo, R., Rossini, M., Schickling, A., Migliavacca, M., Cogliati, S., Wutzler,
 2495 T., Rascher, U., 2017. Accurate measurements of fluorescence in the O₂A and O₂B band using the FloX
 2496 spectroscopy system - Results and prospects, in: Proc. Potsdam GHG Flux Workshop: From
 2497 Photosystems to Ecosystems, 24-26 October 2017, Potsdam, Germany. <https://www.potsdam-flux-workshop.eu/>
 2498
- 2499 Julitta, T., Corp, L.A., Rossini, M., Burkart, A., Cogliati, S., Davies, N., Hom, M., Mac Arthur, A.,
 2500 Middleton, E.M., Rascher, U., Schickling, A., Colombo, R., 2016. Comparison of sun-induced
 2501 chlorophyll fluorescence estimates obtained from four portable field spectroradiometers. *Remote Sens.* 8,
 2502 122.
- 2503 Kalaji, H.M., Goltsev, V., Bosa, K., Allakhverdiev, S.I., Strasser, R.J., Govindjee, 2012. Experimental *in*
 2504 *vivo* measurements of light emission in plants: A perspective dedicated to David Walker. *Photosynth.*
 2505 *Res.* 114, 69-96.
- 2506 Kalaji, H.M., Schansker, G., Ladle, R.J., Goltsev, V., Bosa, K., Allakhverdiev, S.I., Brestic, M., Bussotti,
 2507 F., Calatayud, A., Dabrowski, P., Elsheery, N.I., Ferroni, L., Guidi, L., Hogewoning, S.W., Jajoo, A.,
 2508 Misra, A.N., Nebauer, S.G., Pancaldi, S., Penella, C., Poli, D., Pollastrini, M., Romanowska-Duda, Z.B.,
 2509 Rutkowska, B., Serôdio, J., Suresh, K., Szulc, W., Tambussi, E., Yanniccari, M., Zivcak, M., 2014.
 2510 Frequently asked questions about *in vivo* chlorophyll fluorescence: Practical issues. *Photosynth. Res.* 122,
 2511 121-158.
- 2512 Kalma, J.D., McVicar, T.R., McCabe, M.F., 2008. Estimating land surface evaporation: A review of
 2513 methods using remotely sensed surface temperature data. *Surv. Geophys.* 29, 421-469.
- 2514 Kancheva, R., Borisova, D., Iliev, I., Yonova, P., 2007. Chlorophyll fluorescence as a quantitative
 2515 measure of plant stress, in: Bochenek, Z. (Ed.), *New Developments and Challenges in Remote Sensing*.
 2516 Millpress, Rotterdam, pp. 37-43.
- 2517 Kautsky, H., Hirsch, A., 1931. Neue versuche zur kohlenäureassimilation. *Die Naturwissenschaften* 19,
 2518 964-964.
- 2519 Kebabian, P.L., Theisen, A.F., Kallelis, S., Freedman, A., 1999. A passive two-band sensor of
 2520 sunlight-excited plant fluorescence. *Rev. Sci. Instrum.* 70, 4386-4393.
- 2521 Keller, B., Vass, I., Matsubara, S., Paul, K., Jedmowski, C., Pieruschka, R., Nedbal, L., Rascher, U.,
 2522 Muller, O., 2018. Maximum fluorescence and electron transport kinetics determined by light induced
 2523 fluorescence transients (LIFT) for photosynthesis phenotyping. *Photosynth. Res.*, doi: 10.1007/s11120-
 2524 018-0594-9.

- 2525 Khosravi, N., Vountas, M., Rozanov, V.V., Bracher, A., Wolanin, A., Burrows, J.P., 2015. Retrieval of
2526 terrestrial plant fluorescence based on the in-filling of far-red Fraunhofer lines using SCIAMACHY
2527 observations. *Front. Environ. Sci.* 3, doi: 10.3389/fenvs.2015.00078.
- 2528 Kim, H.H., 1973. New algae mapping technique by the use of an airborne laser fluorosensor. *Appl. Opt.*
2529 12, 1454-1459.
- 2530 Kitajima, M., Butler, W.L., 1975. Quenching of chlorophyll fluorescence and primary photochemistry in
2531 chloroplasts by dibromothymoquinone. *Biochim. Biophys. Acta* 376, 105-115.
- 2532 Koffi, E.N., Rayner, P.J., Norton, A.J., Frankenberg, C., Scholze, M., 2015. Investigating the usefulness
2533 of satellite-derived fluorescence data in inferring gross primary productivity within the carbon cycle data
2534 assimilation system. *Biogeosciences* 12, 4067-4084.
- 2535 Köhler, P., Guanter, L., Joiner, J., 2015. A linear method for the retrieval of sun-induced chlorophyll
2536 fluorescence from GOME-2 and SCIAMACHY data. *Atmospheric Meas. Tech.* 8, 2589-2608.
- 2537 Köhler, P., Frankenberg, C., Magney, T.S., Guanter, L., Joiner, J., Landgraf, J., 2018a. Global retrievals
2538 of solar-induced chlorophyll fluorescence with TROPOMI: First results and intersensor comparison to
2539 OCO-2. *Geophys. Res. Lett.*, <https://doi.org/10.1029/2018GL079031>.
- 2540 Köhler, P., Guanter, L., Kobayashi, H., Walther, S., Yang, W., 2018b. Assessing the potential of
2541 sun-induced fluorescence and the canopy scattering coefficient to track large-scale vegetation dynamics in
2542 Amazon forests. *Remote Sens. Environ.* 204, 769-785.
- 2543 Kolber, Z., Falkowski, P.G., 1993. Use of active fluorescence to estimate phytoplankton photosynthesis *in*
2544 *situ*. *Limnol. Oceanogr.* 38, 1646-1665.
- 2545 Kolber, Z., Klimov, D., Ananyev, G., Rascher, U., Berry, J., Osmond, B., 2005. Measuring
2546 photosynthetic parameters at a distance: Laser induced fluorescence transient (LIFT) method for remote
2547 measurements of photosynthesis in terrestrial vegetation. *Photosynth. Res.* 84, 121-129.
- 2548 Kolber, Z.S., Prášil, O., Falkowski, P.G., 1998. Measurements of variable chlorophyll fluorescence using
2549 fast repetition rate techniques: Defining methodology and experimental protocols. *Biochim. Biophys.*
2550 *Acta* 1367, 88-106.
- 2551 Koren, G., Van Schaik, E., Araújo, A.C., Boersma, K.F., Gärtner, A., Killaars, L., Kooreman, M.L.,
2552 Kruijt, B., Van der Laan-Luijkx, I.T., Von Randow, C., Smith, N.E., Peters, W., 2018. Widespread
2553 reduction in sun-induced fluorescence from the Amazon during the 2015/2016 El Niño. *Phil. Trans. R.*
2554 *Soc. B.* 373, 20170408.
- 2555 Kotchenova, S.Y., Vermote, E.F., Levy, R., Lyapustin, A., 2008. Radiative transfer codes for atmospheric
2556 correction and aerosol retrieval: Intercomparison study. *Appl. Opt.* 47, 2215-2226.
- 2557 Krause, G.H., Weis, E., 1991. Chlorophyll fluorescence and photosynthesis: The basics. *Annu. Rev. Plant*
2558 *Physiol. Plant Mol. Biol.* 42, 313-349.
- 2559 Krause, G.H., Weis, E., 1984. Chlorophyll fluorescence as a tool in plant physiology. II. Interpretation of
2560 fluorescence signals. *Photosynth. Res.* 5, 139-157.

- 2561 Krinner, G., Viovy, N., De Noblet-Ducoudré, N., Ogée, J., Polcher, J., Friedlingstein, P., Ciais, P., Sitch,
2562 S., Prentice, I.C., 2005. A dynamic global vegetation model for studies of the coupled atmosphere-
2563 biosphere system. *Global Biogeochem. Cycles* 19, GB1015.
- 2564 Kubelka, P., Munk, F., 1931. An article on optics of paint layers. *Z. Tech. Phys* 12, 593-601.
- 2565 Kuckenber, J., Tartachnyk, I., Noga, G., 2009. Detection and differentiation of nitrogen-deficiency,
2566 powdery mildew and leaf rust at wheat leaf and canopy level by laser-induced chlorophyll fluorescence.
2567 *Biosyst. Eng.* 103, 121-128.
- 2568 Kückenbrink, D., Hueni, A., Schneider, F., Damm, A., Gastellu-Etcheberry, J.P., Schaepman, M.E.,
2569 Morsdorf, F., (in press). Mapping the irradiance field of a single tree: Quantifying vegetation induced
2570 adjacency effects. *IEEE Trans. Geosci. Remote Sens.*
- 2571 Lagorio, M.G., Cordon, G.B., Iriel, A., 2015. Reviewing the relevance of fluorescence in biological
2572 systems. *Photochem. Photobiol. Sci.* 14, 1538-1559.
- 2573 Lang, M., Lichtenthaler, H.K., Sowinska, M., Heisel, F., Miehe, J.A., 1996. Fluorescence imaging of
2574 water and temperature stress in plant leaves. *J. Plant Physiol.* 148, 613-621.
- 2575 Lausch, A., Bannehr, L., Beckmann, M., Boehm, C., Feilhauer, H., Hacker, J.M., Heurich, M., Jung, A.,
2576 Klenke, R., Neumann, C., Pause, M., Rocchini, D., Schaepman, M.E., Schmidtlein, S., Schulz, K.,
2577 Selsam, P., Settele, J., Skidmore, A.K., Cord, A.F., 2016. Linking Earth Observation and taxonomic,
2578 structural and functional biodiversity: Local to ecosystem perspectives. *Ecol. Indic.* 70, 317-339.
- 2579 Lausch, A., Erasmi, S., King, D.J., Magdon, P., Heurich, M., 2017. Understanding forest health with
2580 remote sensing-Part II--A review of approaches and data models. *Remote Sens.* 9, 129.
- 2581 Lawson, T., 2009. Guard cell photosynthesis and stomatal function. *New Phytol.* 181, 13-34.
- 2582 Lee, J.-E., Berry, J.A., Van der Tol, C., Yang, X., Guanter, L., Damm, A., Baker, I., Frankenberg, C.,
2583 2015. Simulations of chlorophyll fluorescence incorporated into the Community Land Model version 4.
2584 *Glob. Chang. Biol.* 21, 3469-3477.
- 2585 Lee, J.-E., Frankenberg, C., Van der Tol, C., Berry, J.A., Guanter, L., Boyce, C.K., Fisher, J.B., Morrow,
2586 E., Worden, J.R., Asefi, S., Badgley, G., Saatchi, S., 2013. Forest productivity and water stress in
2587 Amazonia: Observations from GOSAT chlorophyll fluorescence. *Proc. R. Soc. London B Biol. Sci.* 280,
2588 20130171.
- 2589 Leuning, R., 1995. A critical appraisal of a combined stomatal-photosynthesis model for C₃ plants. *Plant*
2590 *Cell Environ.* 18, 339-355.
- 2591 Li, X., Xiao, J., He, B., 2018a. Chlorophyll fluorescence observed by OCO-2 is strongly related to gross
2592 primary productivity estimated from flux towers in temperate forests. *Remote Sens. Environ.* 204, 659-
2593 671.
- 2594 Li, X., Xiao, J., He, B., Arain, M.A., Beringer, J., Desai, A.R., Emmel, C., Hollinger, D.Y., Krasnova, A.,
2595 Mammarella, I., Noe, S.M., Ortiz, P.S., Rey-Sanchez, A.C., Rocha, A.V., Varlagin, A., 2018b. Solar-
2596 induced chlorophyll fluorescence is strongly correlated with terrestrial photosynthesis for a wide variety
2597 of biomes: First global analysis based on OCO-2 and flux tower observations. *Glob. Change Biol.* 24,
2598 3990-4008.

- 2599 Lichtenthaler, H.K. (Ed.), 1989. Applications of Chlorophyll Fluorescence in Photosynthesis Research,
2600 Stress Physiology, Hydrobiology and Remote Sensing. Kluwer, Dordrecht.
- 2601 Lichtenthaler, H.K., Rinderle, U., 1988. The role of chlorophyll fluorescence in the detection of stress
2602 conditions in plants. *Crit. Rev. Anal. Chem.* 19, Suppl. 1, S29-S85.
- 2603 Liu, J., Chen, J.M., Cihlar, J., Park, W.M., 1997. A process-based boreal ecosystem productivity
2604 simulator using remote sensing inputs. *Remote Sens. Environ.* 62, 158–175.
- 2605 Liu, L., Guan, L., Liu, X., 2017. Directly estimating diurnal changes in GPP for C3 and C4 crops using
2606 far-red sun-induced chlorophyll fluorescence. *Agric. For. Meteorol.* 232, 1-9.
- 2607 Liu, L., Zhang, Y., Wang, J., Zhao, C., 2005. Detecting solar-induced chlorophyll fluorescence from field
2608 radiance spectra based on the Fraunhofer line principle. *IEEE Trans. Geosci. Remote Sens.* 43, 827-832.
- 2609 Liu, X., Guanter, L., Liu, L., Damm, A., Malenovský, Z., Rascher, U., Peng, D., Du, S., Gastellu-
2610 Etchegorry, J.-P., (in press). Downscaling of solar-induced chlorophyll fluorescence from canopy level to
2611 photosystem level using a random forest model. *Remote Sens. Environ.*
2612 <https://doi.org/10.1016/j.rse.2018.05.035>.
- 2613 Liu, X., Liu, L., 2018. Influence of the canopy BRDF characteristics and illumination conditions on the
2614 retrieval of solar-induced chlorophyll fluorescence. *Int. J. Remote Sens.* 39, 1782-1799.
- 2615 Liu, X., Liu, L., Zhang, S., Zhou, X., 2015. New spectral fitting method for full-spectrum solar-induced
2616 chlorophyll fluorescence retrieval based on principal components analysis. *Remote Sens.* 7, 10626-10645.
- 2617 Louis, J., Cerovic, Z.G., Moya, I., 2006. Quantitative study of fluorescence excitation and emission
2618 spectra of bean leaves. *J. Photochem. Photobiol.* 85, 65-71.
- 2619 Louis, J., Ounis, A., Ducruet, J.-M., Evain, S., Laurila, T., Thum, T., Aurela, M., Wingsle, G., Alonso, L.,
2620 Pedros, R., Moya I., 2005. Remote sensing of sunlight-induced chlorophyll fluorescence and reflectance
2621 of Scots pine in the boreal forest during spring recovery. *Remote Sens. Environ.* 96, 37-48.
- 2622 Lu, X., Cheng, X., Li, X., Tang, J., 2018a. Opportunities and challenges of applications of satellite-
2623 derived sun-induced fluorescence at relatively high spatial resolution. *Sci. Total Environ.* 619-620, 649-
2624 653.
- 2625 Lu, X., Liu, Z., An, S., Miralles, D.G., Maes, W., Liu, Y., Tang, J., 2018b. Potential of solar-induced
2626 chlorophyll fluorescence to estimate transpiration in a temperate forest. *Agric. For. Meteorol.* 252, 75-87.
- 2627 Lucieer, A., Malenovský, Z., Veness, T., Wallace, L., 2014. HyperUAS—Imaging spectroscopy from a
2628 multirotor unmanned aircraft system. *J. Field Robot.* 31, 571-590.
- 2629 Luus, K.A., Commane, R., Parazoo, N.C., Benmergui, J., Euskirchen, E.S., Frankenberg, C., Joiner, J.,
2630 Lindaas, J., Miller, C.E., Oechel, W.C., Zona, D., Wofsy, S., Lin, J.C., 2017. Tundra photosynthesis
2631 captured by satellite-observed solar-induced chlorophyll fluorescence. *Geophys. Res. Lett.* 44, 1564-
2632 1573.
- 2633 Ma, X., Huete, A., Cleverly, J., Eamus, D., Chevallier, F., Joiner, J., Poulter, B., Zhang, Y., Guanter, L.,
2634 Meyer, W., Xie, Z., Ponce-Campos, G., 2016. Drought rapidly diminishes the large net CO₂ uptake in
2635 2011 over semi-arid Australia. *Sci. Rep.* 6, 37747.

- 2636 Mac Arthur, A., Robinson, I., Rossini, M., Davies, N., McDonald, K., 2014. A dual-field-of-view
2637 spectrometer system for reflectance and fluorescence measurements (Piccolo Doppio) and correction of
2638 etaloning, in: Proc. 5th International Workshop on Remote Sensing of Vegetation Fluorescence, 22-24
2639 April 2014, Paris, France.
- 2640 MacBean, N., Maignan, F., Bacour, C., Lewis, P., Peylin, P., Guanter, L., Köhler, P., Gomez-Dans, J.,
2641 Disney, M., 2018. Strong constraint on modelled global carbon uptake using solar-induced chlorophyll
2642 fluorescence data. *Sci. Rep.* 8, 1973.
- 2643 Madani, N., Kimball, J.S., Jones, L.A., Parazoo, N.C., Guan, K., 2017. Global analysis of bioclimatic
2644 controls on ecosystem productivity using satellite observations of solar-induced chlorophyll fluorescence.
2645 *Remote Sens.* 9, 530.
- 2646 Magnani, F., Olioso, A., Demarty, J., Germain, V., Verhoef, W., Moya, I., Goulas, Y., Cecchi, G., Agati,
2647 G., Zarco-Tejada, P., Mohammed, G., Van der Tol, C., 2009. Assessment of Vegetation Photosynthesis
2648 Through Observation of Solar Induced Fluorescence From Space, Final Report. ESA/ESTEC Contract
2649 No. 20678/07/NL/HE. 256 p.
- 2650 Magnani, F., Raddi, S., Mohammed, G., Middleton, E.M., 2014. Let's exploit available knowledge on
2651 vegetation fluorescence. *Proc. Natl. Acad. Sci. USA* 111, E2510.
- 2652 Magney, T.S., Frankenberg, C., Fisher, J.B., Sun, Y., North, G.B., Davis, T.S., Kornfeld, A., Siebke, K.,
2653 2017. Connecting active to passive fluorescence with photosynthesis: A method for evaluating remote
2654 sensing measurements of Chl fluorescence. *New Phytol.* 215, 1594-1608.
- 2655 Maier, S.W., 2002. Remote sensing and modelling of solar induced fluorescence, in: Proc. FLEX
2656 Workshop, 19-20 June 2002, Noordwijk, Netherlands. European Space Agency, (Special Publication)
2657 ESA SP, Issue 527.
- 2658 Maier, S.W., Günther, K.P., Stellmes, M., 2003. Sun-induced fluorescence: A new tool for precision
2659 farming, in: Schepers, J., VanToai, T. (Eds.), *Digital Imaging and Spectral Techniques: Applications to*
2660 *Precision Agriculture and Crop Physiology*. ASA Spec. Publ. 66. ASA, CSSA, and SSSA; Madison
2661 (Wisconsin), USA, pp. 209-222.
- 2662 Malenovský, Z., Lucieer, A., King, D.H., Turnbull, J.D., Robinson, S.A., 2017. Unmanned aircraft
2663 system advances health mapping of fragile polar vegetation. *Methods Ecol. Evol.* 8, 1842-1857.
- 2664 Malenovský, Z., Mishra, K.B., Zemek, F., Rascher, U., Nedbal, L., 2009. Scientific and technical
2665 challenges in remote sensing of plant canopy reflectance and fluorescence. *J. Exp. Bot.* 60, 2987-3004.
- 2666 Matsubara, S., Morosinotto, T., Osmond, C.B., Bassi, R., 2007. Short- and long-term operation of the
2667 lutein-epoxide cycle in light-harvesting antenna complexes. *Plant Physiol.* 144, 926-941.
- 2668 Maxwell, K., Johnson, G.N., 2000. Chlorophyll fluorescence -- a practical guide. *J. Exp. Bot.* 51,
2669 659-668.
- 2670 Mazzoni, M., Falorni, P., Del Bianco, S., 2008. Sun-induced leaf fluorescence retrieval in the O₂-B
2671 atmospheric absorption band. *Opt. Express* 16, 7014-7022.
- 2672 Mazzoni, M., Falorni, P., Verhoef, W., 2010. High-resolution methods for fluorescence retrieval from
2673 space. *Opt. Express* 18, 15649-15643.

- 2674 Mazzoni, M., Meroni, M., Fortunato, C., Colombo, R., Verhoef, W., 2012. Retrieval of maize canopy
2675 fluorescence and reflectance by spectral fitting in the O₂-A absorption band. *Remote Sens. Environ.* 124,
2676 72-82.
- 2677 McAlister, E.D., Myers, J., 1940. Time course of photosynthesis and fluorescence. *Science* 92, 241-243.
- 2678 McFarlane, J.C., Watson, R.D., Theisen, A.F., Jackson, R.D., Ehler, W.L., Pinter, P.J., Idso, S.B.,
2679 Reginato, R.J., 1980. Plant stress detection by remote measurement of fluorescence. *Appl. Opt.* 19, 3287-
2680 3289.
- 2681 Meijer, Y., Ingmann, P., Langen, J., Veihelmann, B., Zehner, C., 2014. Potential of current and future
2682 Copernicus satellite missions for low spatial resolution fluorescence monitoring, in: *Proceedings 5th*
2683 *International Workshop on Remote Sensing of Vegetation Fluorescence*, 22-24 April 2014, Paris, France,
2684 <http://www.congrexprojects.com/2014-events/14c04/proceedings>.
- 2685 Meroni, M., Barducci, A., Cogliati, S., Castagnoli, F., Rossini, M., Busetto, L., Migliavacca, M.,
2686 Cremonese, E., Galvagno, M., Colombo, R., Morra di Cella, U., 2011. The hyperspectral irradiometer, a
2687 new instrument for long-term and unattended field spectroscopy measurements. *Rev. Sci. Instrum.* 82,
2688 043106.
- 2689 Meroni, M., Busetto, L., Colombo, R., Guanter, L., Moreno, J., Verhoef, W., 2010. Performance of
2690 Spectral Fitting Methods for vegetation fluorescence quantification. *Remote Sens. Environ.* 114, 363-374.
- 2691 Meroni, M., Colombo, R., 2006. Leaf level detection of solar induced chlorophyll fluorescence by means
2692 of a subnanometer resolution spectroradiometer. *Remote Sens. Environ.* 103, 438-448.
- 2693 Meroni, M., Colombo, R., 2009. 3S: A novel program for field spectroscopy. *Comput. Geosci.* 35, 1491-
2694 1496.
- 2695 Meroni, M., Rossini, M., Guanter, L., Alonso, L., Rascher, U., Colombo, R., Moreno, J., 2009. Remote
2696 sensing of solar-induced chlorophyll fluorescence: Review of methods and applications. *Remote Sens.*
2697 *Environ.* 113, 2037-2051.
- 2698 Meroni, M., Rossini, M., Picchi, V., Panigada, C., Cogliati, S., Nali, C., Colombo, R., 2008. Assessing
2699 steady-state fluorescence and PRI from hyperspectral proximal sensing as early indicators of plant stress:
2700 The case of ozone exposure. *Sensors* 8, 1740-1754.
- 2701 Miao, G., Guan, K., Yang, X., Bernacchi, C.J., Berry, J.A., DeLucia, E.H., Wu, J., Moore, C.E.,
2702 Meacham, K., Cai, Y., Peng, B., Kimm, H., Masters, M.D., 2018. Sun-induced chlorophyll fluorescence,
2703 photosynthesis, and light use efficiency of a soybean field from seasonally continuous measurements. *J.*
2704 *Geophys. Res. Biogeosci.* 123, 610-623.
- 2705 Middleton, E.M., Chappelle, E.W., Cannon, T.A., Adamse, P., Britz, S.J., 1996. Initial assessment of
2706 physiological response to UV-B irradiation using fluorescence measurements. *J. Plant Physiol.* 148, 69-
2707 77.
- 2708 Middleton, E.M., Corp, L.A., Campbell, P.K.E., 2008. Comparison of measurements and FluorMOD
2709 simulations for solar-induced chlorophyll fluorescence and reflectance of a corn crop under nitrogen
2710 treatments. *Int. J. Remote Sens.* 29, 5193-5213.
- 2711 Middleton, E.M., Huemmrich, K.F., Zhang, Q., Campbell, P.K.E., Landis, D.R., 2018. Spectral bio-
2712 indicators of photosynthetic efficiency and vegetation stress, Chap. 5 in: Thenkabail, P.S., Lyon, J.G.,

- 2713 Huete, A. (Eds.), *Hyperspectral Remote Sensing of Vegetation (2nd Edition)*, Vol. III: Biophysical and
2714 Biochemical Characterization and Plant Species Studies. Taylor & Francis, New York, 133-179
- 2715 Middleton, E.M., Kim, M.S., Krizek, D.T., Bajwa, R.K., 2005. Evaluating UV-B effects and EDU
2716 protection in soybean leaves using fluorescence. *Photochem. Photobiol.* 81, 1075-1085.
- 2717 Middleton, E.M., Rascher, U., Corp, L.A., Huemmrich, K.F., Cook, B.D., Noormets, A., Schickling, A.,
2718 Pinto, F., Alonso, L., Damm, A., Guanter, L., Colombo, R., Campbell, P.K.E., Landis, D.R., Zhang, Q.,
2719 Rossini, M., Schuettemeyer, D., Bianchi, R., 2017. The 2013 FLEX–US airborne campaign at the Parker
2720 Tract loblolly pine plantation in North Carolina, USA. *Remote Sens.* 9, 612.
- 2721 Migliavacca, M., El Madany, T., Perez-Priego, O., Carrara, A., Hammer, T., Henkel, K., Kolle, O., Luo,
2722 Y., Moreno, G., Morris, K., Nair, R., Schruppf, M., Wutzler, T., Reichstein, M., 2017a. Effects of a large
2723 scale nitrogen and phosphorus fertilization on the ecosystem functioning of a Mediterranean tree-grass
2724 ecosystem, in: *Proc. 19th EGU General Assembly, EGU2017*, 23-28 April 2017, Vienna, Austria, p.
2725 11586.
- 2726 Migliavacca, M., Perez-Priego, O., Rossini, M., El-Madany, T.S., Moreno, G., Van der Tol, C., Rascher,
2727 U., Berninger, A., Bessenbacher, V., Burkart, A., Carrara, A., Fava, F., Guan, J.-H., Hammer, T.W.,
2728 Henkel, K., Juarez-Alcalde, E., Julitta, T., Kolle, O., Martín, M.P., Musavi, T., Pacheco-Labrador, J.,
2729 Pérez-Burgueño, A., Wutzler, T., Zaehle, S., Reichstein, M., 2017b. Plant functional traits and canopy
2730 structure control the relationship between photosynthetic CO₂ uptake and far-red sun-induced
2731 fluorescence in a Mediterranean grassland under different nutrient availability. *New Phytol.* 214, 1078-
2732 1091.
- 2733 Miller, J., Berger, M., Goulas, Y., Jacquemoud, S., Louis, J., Mohammed, G., Noise, N., Moreno, J.,
2734 Moya, I., Pédro, R., Verhoef, W., Zarco-Tejada, P., 2005. Development of a Vegetation Fluorescence
2735 Canopy Model, Final Report. ESA/ESTEC Contract No. 16365/02/NL/FF. 138 p.
- 2736 Mohammed, G.H., Binder, W.D., Gillies, S.L., 1995. Chlorophyll fluorescence: A review of its practical
2737 forestry applications and instrumentation. *Scandinavian Journal of Forest Research* 10, 383-410.
- 2738 Mohammed, G.H., Colombo, R., Moreno, J., Van der Tol, C., Rascher, U., Ač, A., Alonso, L., Celesti,
2739 M., Cogliati, S., Damm, A., Fawcett, D., Gomez-Dans, J., Henry, C., Lewis, P., MacBean, N., Magnani,
2740 F., Malaprada, J., Matveeva, M., Olejníčková, J., Pernokis, D., Pinto, F., Raddi, S., Rajh Vilfan, N.,
2741 Rivera, J.P., Rossini, M., Sabater, N., Schickling, A., Tenjo, C., Verhoef, W., Verrelst, J., Vicent Servera,
2742 J., Drusch, M., 2016. FLEX Bridge Study, Final Report. ESA/ESTEC Contract No.
2743 4000112341/14/NL/FF/gp. 187 p.
- 2744 Mohammed, G.H., Goulas, Y., Magnani, F., Moreno, J., Olejníčková, J., Rascher, U., Van der Tol, C.,
2745 Verhoef, W., Ač, A., Daumard, F., Gallé, A., Malenovský, Z., Pernokis, D., Rivera, J.P., Verrelst, J.,
2746 Drusch, M., 2014. FLEX/Sentinel-3 Tandem Mission Photosynthesis Study, Final Report. ESA/ESTEC
2747 Contract No. 4000106396/12/NL/AF. 159 p.
- 2748 Mohammed, G.H., Zarco-Tejada, P., Miller, J.R., 2003. Applications of chlorophyll fluorescence in
2749 forestry and ecophysiology, in: DeEll, J.R., Toivonen, P.M.A. (Eds.), *Practical Applications of*
2750 *Chlorophyll Fluorescence in Plant Biology*. Kluwer/Springer, Dordrecht, pp. 79-124.
- 2751 Mohanty, P., Braun, B.Z., Govindjee, Thornber, J.P., 1972. Chlorophyll fluorescence characteristics of
2752 system I chlorophyll *a*-protein complex and system II particles at room and liquid nitrogen temperatures.
2753 *Plant Cell Physiol.* 13, 81-91.

- 2754 Moore III, B., Crowell, S., 2018. The GeoCarb mission, in: Proc. 98th Amer. Meteor. Soc. Annual
2755 meeting, 7-11 January 2018, Austin, TX.
- 2756 Moreno, J., Asner, G.P., Bach, H., Belenguer, T., Bell, A., Buschmann, C., Calera, A., Calpe, J.,
2757 Campbell, P., Cecchi, G., Colombo, R., Corp, L.A., Court, A., Cutter, M.A., Disney, M., Dudelzak, A.,
2758 D'Urso, G., Fernandes, R., Flexas, J., Gege, P., Gielen, B., Gitelson, A., Gloor, E.U., Gower, J., Green,
2759 R.O., Hill, J., Jacquemoud, S., Jia, L., Kneubühler, M., Laurila, T., Lewis, P., Lobb, D., Magnani, F.,
2760 Maier, S.W., Marek, M.V., Martinez, A., Martinez-Cobo, P., Mazzinghi, P., Menenti, M., Merton, R.,
2761 Middleton, E., De Miguel, E., Miller, J., Mohammed, G., Milton, E.J., Morales, F., Moya, I., Nedbal, L.,
2762 Knorr, W., Otlé, C., Oliso, A., Pace, S., Palucci, A., Pedros, R., Peltoniemi, J., Peñuelas, J., Plaza, A.,
2763 Polcher, J., Rascher, U., Reuter, R., Rosema, A., Roujean, J.-L., Saito, Y., Saugier, B., Schaepman, M.,
2764 Serrano, J.B., Settle, J.J., Sierra, M., Sobrino, J., Stoll, M.-P., Su, Z.B., Tobehn, C., Tremblay, N., Valcke,
2765 R., Verhoef, W., Veroustraete, F., Verstraete, M., Zarco-Tejada, P., 2006. FLuorescence EXplorer
2766 (FLEX): An optimised payload to map vegetation photosynthesis from space, in: Proc. 57th International
2767 Astronautical Congress, 2-6 October 2006, Valencia, Spain.
- 2768 Moreno, J., Rascher, U., Goulas, Y., Colombo, R., Verhoef, W., Damm, A., Alonso, L., Cogliati, S.,
2769 Daumard, F., Rivera, J.P., Sabater, N., Schickling, A., Tenjo, C., Timmermans, J., Verrelst, J., Drusch,
2770 M., 2014. FLEX/S3 Tandem Mission Performance Analysis and Requirements Consolidation Study
2771 (PARCS), Final Report. ESA/ESTEC Contract No. 4000105078/11/NL/AF. 141 p.
- 2772 Morris, J.M., Fleming, G.R., 2018. Quantitative modeling of energy dissipation in *Arabidopsis thaliana*.
2773 Environ. Exp. Bot. 154, 99-109.
- 2774 Mouw, C.B., Greb, S., Aurin, D., DiGiacomo, P.M., Lee, Z., Twardowski, M., Binding, C., Hu, C., Ma,
2775 R., Moore, T., Moses, W., Craig, S.E., 2015. Aquatic color radiometry remote sensing of coastal and
2776 inland waters: Challenges and recommendations for future satellite missions. Remote Sens. Environ. 160,
2777 15-30.
- 2778 Moya, I., Camenen, L., Evain, S., Goulas, Y., Cerovic, Z.G., Latouche, G., Flexas, J., Ounis, A., 2004. A
2779 new instrument for passive remote sensing. I. Measurements of sunlight-induced chlorophyll
2780 fluorescence. Remote Sens. Environ. 91, 186-197.
- 2781 Moya, I., Cerovic, Z.G., 2004. Remote sensing of chlorophyll fluorescence: Instrumentation and analysis,
2782 in: Papageorgiou, G.C., Govindjee (Eds.), Chlorophyll *a* Fluorescence: A Signature of Photosynthesis.
2783 Springer, Dordrecht, pp. 429-445.
- 2784 Moya, I., Daumard, F., Moise, N., Ounis, A., Goulas, Y., 2006. First airborne multiwavelength passive
2785 chlorophyll fluorescence measurements over La Mancha (Spain) fields, in: Proc. 2nd International
2786 Symposium on Recent Advances In Quantitative Remote Sensing, 25-29 September 2006, Torrent
2787 (Valencia), Spain, pp. 820-825.
- 2788 Moya, I., Goulas, Y., Morales, F., Camenen, L., Guyot, G., Schmuck, G., 1995. Remote sensing of
2789 time-resolved chlorophyll fluorescence and back-scattering of the laser excitation by vegetation. EARSeL
2790 Advances in Remote Sensing 3, 188-197.
- 2791 Moya, I., Guyot, G., Goulas, Y., 1992. Remotely sensed blue and red fluorescence emission for
2792 monitoring vegetation. ISPRS J. Photogram. Remote Sens. 47, 205-231.
- 2793 Müller, N.J.C., 1874. Beziehungen zwischen assimilation, absorption und fluoreszenz im chlorophyll des
2794 lebenden blattes. Jahrbücher für Wissenschaftliche Botanik 9, 42-49.

- 2795 Murata, N., Nishimura, M., Tamiya, A., 1966. Fluorescence of chlorophyll in photosynthetic systems. III.
2796 Emission and action spectra of fluorescence—Three emission bands of chlorophyll *a* and the energy
2797 transfer between two pigment systems. *Biochim. Biophys. Acta* 126, 234-243.
- 2798 Murchie, E.H., Lawson, T., 2013. Chlorophyll fluorescence analysis: A guide to good practice and
2799 understanding some new applications. *J. Exp. Bot.* 64, 3983-3998.
- 2800 Nedbal, L., Trtílek, M., Kaftan, D., 1999. Flash fluorescence induction: A novel method to study
2801 regulation of photosystem II. *J. Photochem. Photobiol. B* 48, 154-157.
- 2802 Nedbal, L., Soukupová, J., Kaftan, D., Whitmarsh, J., Trtílek, M., 2000. Kinetic imaging of chlorophyll
2803 fluorescence using modulated light. *Photosynth. Res.* 66, 3-12.
- 2804 Nedbal, L., Whitmarsh, J., 2004. Chlorophyll fluorescence imaging of leaves and fruits, in: Papageorgiou,
2805 G.C., Govindjee (Eds.), *Chlorophyll *a* Fluorescence: A Signature of Photosynthesis*. Springer, Dordrecht,
2806 pp. 389-407.
- 2807 Neville, R.A., Gower, J.F.R., 1977. Passive remote-sensing of phytoplankton via chlorophyll *a*
2808 fluorescence. *J. Geophys. Res.* 82, 3487-3493.
- 2809 Ni-Meister, W., Yang, W., Kiang, N.Y., 2010. A clumped-foliage canopy radiative transfer model for a
2810 global dynamic terrestrial ecosystem model. I: Theory. *Agric. For. Meteorol.* 150, 881-894.
- 2811 Norman, J.M., 1979. Modeling the complete crop canopy, in: Barfield, B.J. Gerber, J.F. (Eds.),
2812 *Modification of the Aerial Environment of Plants*. Am. Soc. Agric. Eng., St Joseph, MI, pp. 249-277.
- 2813 North, P.R.J., 1996. Three-dimensional forest light interaction model using a Monte Carlo method. *IEEE*
2814 *Trans. Geosci. Remote Sens.* 34, 946-956.
- 2815 Norton, A.J., Rayner, P.J., Koffi, E.N., Scholze, M., 2018. Assimilating solar-induced chlorophyll
2816 fluorescence into the terrestrial biosphere model BETHY-SCOPE v1.0: Model description and
2817 information content. *Geosci. Model Dev.* 11, 1517-1536.
- 2818 O'Brien, D.M., Polonsky, I.N., Utembe, S.R., Rayner, P.J., 2016. Potential of a geostationary geoCARB
2819 mission to estimate surface emissions of CO₂, CH₄ and CO in a polluted urban environment: Case study
2820 Shanghai. *Atmospheric Meas. Tech.* 9, 4633-4654.
- 2821 Omasa, K., Hosoi, F., Konishi, A., 2007. 3D lidar imaging for detecting and understanding plant
2822 responses and canopy structure. *J. Exp. Bot.* 58, 881-898.
- 2823 Öquist, G., Wass, R., 1988. A portable, microprocessor operated instrument for measuring chlorophyll
2824 fluorescence kinetics in stress physiology. *Physiol. Plant.* 73, 211-217.
- 2825 Osmond, B., Schwartz, O., Gunning, B., 1999. Photoinhibitory printing on leaves, visualised by
2826 chlorophyll fluorescence imaging and confocal microscopy, is due to diminished fluorescence from grana.
2827 *Aust. J. Plant Physiol.* 26, 717-724.
- 2828 Ounis, A., Bach, J., Mahjoub, A., Daumard, F., Moya, I., Goulas, Y., 2016. Combined use of LIDAR and
2829 hyperspectral measurements for remote sensing of fluorescence and vertical profile of canopies. *Revista*
2830 *de Teledetección* 45, Special Issue, 87-94.

- 2831 Ounis, A., Cerovic, Z.G., Briantais, J.M., Moya, I., 2001. Dual-excitation FLIDAR for the estimation of
2832 epidermal UV absorption in leaves and canopies. *Remote Sens. Environ.* 76, 33-48.
- 2833 Oxborough, K., 2004. Imaging of chlorophyll *a* fluorescence: Theoretical and practical aspects of an
2834 emerging technique for the monitoring of photosynthetic performance. *J. Exp. Bot.* 55, 1195-1205.
- 2835 Palombi, L., Cecchi, G., Lognoli, D., Raimondi, V., Toci, G., Agati, G., 2011. A retrieval algorithm to
2836 evaluate the Photosystem I and Photosystem II spectral contributions to leaf chlorophyll fluorescence at
2837 physiological temperatures. *Photosynth. Res.* 108, 225-239.
- 2838 Panigada, C., Rossini, M., Meroni, M., Cilia, C., Busetto, L., Amaducci, S., Boschetti, M., Cogliati, S.,
2839 Picchi, V., Pinto, F., Marchesi, A., Colombo, R., 2014. Fluorescence, PRI and canopy temperature for
2840 water stress detection in cereal crops. *Int. J. Appl. Earth Obs. Geoinf.* 30, 167-178.
- 2841 Paul-Limoges, E., Damm, A., Hueni, A., Liebische, F., Eugster, W., Schaepman, M.E., Buchmann, N.,
2842 2018. Effect of environmental conditions on sun-induced fluorescence in a mixed forest and a cropland.
2843 *Remote Sens. Environ.* 219, 310-323.
- 2844 Papageorgiou, G., 1975. Chlorophyll fluorescence: An intrinsic probe of photosynthesis, in: Govindjee
2845 (Ed.), *Bioenergetics of photosynthesis*. Academic Press, New York, pp. 319-371.
- 2846 Papageorgiou, G., Govindjee (Eds.), 2004. *Chlorophyll *a* Fluorescence: A Signature of Photosynthesis*.
2847 Springer, Dordrecht.
- 2848 Parazoo, N.C., Bowman, K., Fisher, J.B., Frankenberg, C., Jones, D.B.A., Cescatti, A., Pérez-Priego, O.,
2849 Wohlfahrt, G., Montagnani, L., 2014. Terrestrial gross primary production inferred from satellite
2850 fluorescence and vegetation models. *Glob. Change Biol.* 20, 3103-3121.
- 2851 Parazoo, N.C., Bowman, K., Frankenberg, C., Lee, J.-E., Fisher, J.B., Worden, J., Jones, D.B.A., Berry,
2852 J., Collatz, G.J., Baker, I.T., Jung, M., Liu, J., Osterman, G., O'Dell, C., Sparks, A., Butz, A., Guerlet, S.,
2853 Yoshida, Y., Chen, H., Gerbig, C., 2013. Interpreting seasonal changes in the carbon balance of southern
2854 Amazonia using measurements of XCO₂ and chlorophyll fluorescence from GOSAT. *Remote Sens.*
2855 *Environ.* 40, 2829-2833.
- 2856 Patel, N.R., Padalia, H., Devadas, R., Huete, A., Kumar, A.S., Krishna Murthy, Y.V.N., 2018. Estimating
2857 net primary productivity of croplands in Indo-Gangetic Plains using GOME-2 sun-induced fluorescence
2858 and MODIS NDVI. *Curr. Sci.* 114, 1333-1337.
- 2859 Pedrós, R., Goulas, Y., Jacquemoud, S., Louis, J., Moya, I., 2010. FluorMODleaf: A new leaf
2860 fluorescence emission model based on the PROSPECT model. *Remote Sens. Environ.* 114, 155-167.
- 2861 Pedrós, R., Moya, I., Goulas, Y., Jacquemoud, S., 2008. Chlorophyll fluorescence emission spectrum
2862 inside a leaf. *Photochem. Photobiol. Sci.* 7, 498-502.
- 2863 Peñuelas, J., Llusia, J., Piñol, J., Filella, I., 1997. Photochemical reflectance index and leaf photosynthetic
2864 radiation-use-efficiency assessment in Mediterranean trees. *Int. J. Remote Sens.* 18, 2863-2868.
- 2865 Peñuelas, J., Filella, I., Llusià, J., Siscart, D., Piñol, J., 1998. Comparative field study of spring and
2866 summer leaf gas exchange and photobiology of the Mediterranean trees *Quercus ilex* and *Phillyrea*
2867 *latifolia*. *J. Exp. Bot.* 49, 229-238.

- 2868 Pérez-Priego, O., Guan, J., Rossini, M., Fava, F., Wutzler, T., Moreno, G., Carvalhais, N., Carrara, A.,
2869 Kolle, O., Julitta, T., Schrupf, M., Reichstein, M., Migliavacca, M., 2015. Sun-induced chlorophyll
2870 fluorescence and photochemical reflectance index improve remote-sensing gross primary production
2871 estimates under varying nutrient availability in a typical Mediterranean savanna ecosystem.
2872 *Biogeosciences* 12, 6351-6367.
- 2873 Pérez-Priego, O., Zarco-Tejada, P.J., Miller, J.R., Sepulcre-Cantó, G., Fereres, E., 2005. Detection of
2874 water stress in orchard trees with a high-resolution spectrometer through chlorophyll fluorescence *in-*
2875 *filling* of the O₂-A band. *IEEE Trans. Geosci. Remote Sens.* 43, 2860-2869.
- 2876 Pfündel, E., 1998. Estimating the contribution of Photosystem I to total leaf chlorophyll fluorescence.
2877 *Photosynth. Res.* 56, 185-195.
- 2878 Pingle, V.S., 2017. Detection of change in chlorophyll fluorescence using low spectral resolution
2879 spectrometer - A study for temperature induced stress detection. MSc thesis, University of Twente,
2880 Enschede, The Netherlands.
2881 https://webapps.itc.utwente.nl/librarywww/papers_2017/msc/wrem/pingle.pdf
- 2882 Pinto, F., Damm, A., Schickling, A., Panigada, C., Cogliati, S., Müller-Linow, M., Balvora, A., Rascher,
2883 U., 2016. Sun-induced chlorophyll fluorescence from high-resolution imaging spectroscopy data to
2884 quantify spatio-temporal patterns of photosynthetic function in crop canopies. *Plant Cell Environ.* 39,
2885 1500-1512.
- 2886 Pinto, F., Müller-Linow, M., Schickling, A., Cendrero-Mateo, M.P., Ballvora, A., Rascher, U., 2017.
2887 Multiangular observation of canopy sun-induced chlorophyll fluorescence by combining imaging
2888 spectroscopy and stereoscopy. *Remote Sens.* 9, 415.
- 2889 Pitman, A.J., 2003. The evolution of, and revolution in, land surface schemes designed for climate
2890 models. *Int. J. Climatol.* 23, 479-510.
- 2891 Plascyk, J.A., 1975. The MK II Fraunhofer Line Discriminator (FLD-II) for airborne and orbital remote
2892 sensing of solar-stimulated luminescence. *Opt. Eng.* 14, 144339.
- 2893 Plascyk, J.A., Gabriel, F.C., 1975. The Fraunhofer Line Discriminator MKII – An airborne instrument for
2894 precise and standardized ecological luminescence measurement. *IEEE Trans. Instrum. Meas.* 24, 306-313.
- 2895 Porcar-Castell, A., Tyystjärvi, E., Atherton, J., Van der Tol, C., Flexas, J., Pfündel, E.E., Moreno, J.,
2896 Frankenberg, C., Berry, J.A., 2014. Linking chlorophyll *a* fluorescence to photosynthesis for remote
2897 sensing applications: Mechanisms and challenges. *J. Exp. Bot.* 65, 4065-4095.
- 2898 Qiu, B., Xue, Y., Fisher, J.B., Guo, W., Berry, J.A., Zhang, Y., 2018. Satellite chlorophyll fluorescence
2899 fluorescence and soil moisture observations lead to advances in the predictive understanding of global
2900 terrestrial coupled carbon-water cycles. *Global Biogeochem. Cycles* 32, 360-375.
- 2901 Rascher, U., Agati, G., Alonso, L., Cecchi, G., Champagne, S., Colombo, R., Damm, A., Daumard, F., De
2902 Miguel, E., Fernandez, G., Franch, B., Franke, J., Gerbig, C., Gioli, B., Gómez, J.A., Goulas, Y., Guanter,
2903 L., Gutiérrez-de-la-Cámara, Ó., Hamdi, K., Hostert, P., Jiménez, M., Kosvancova, M., Lognoli, D.,
2904 Meroni, M., Miglietta, F., Moersch, A., Moreno, J., Moya, I., Neininger, B., Okujeni, A., Ounis, A.,
2905 Palombi, L., Raimondi, V., Schickling, A., Sobrino, J.A., Stellmes, M., Toci, G., Toscano, P., Udelhoven,
2906 T., Van der Linden, S., Zaldei, A., 2009. CEFLES2: The remote sensing component to quantify
2907 photosynthetic efficiency from the leaf to the region by measuring sun-induced fluorescence in the
2908 oxygen absorption bands. *Biogeosciences* 6, 1181-1198.

- 2909 Rascher, U., Alonso, L., Burkart, A., Cilia, C., Cogliati, S., Colombo, R., Damm, A., Drusch, M.,
2910 Guanter, L., Hanus, J., Hyvärinen, T., Julitta, T., Jussila, J., Kataja, K., Kokkalis, P., Kraft, S., Kraska, T.,
2911 Matveeva, M., Moreno, J., Muller, O., Panigada, C., Píkl, M., Pinto, F., Prey, L., Pude, R., Rossini, M.,
2912 Schickling, A., Schurr, U., Schüttemeyer, D., Verrelst, J., Zemek, F., 2015. Sun-induced fluorescence - a
2913 new probe of photosynthesis: First maps from the imaging spectrometer *HyPlant*. *Glob. Change Biol.* 21,
2914 4673-4684.
- 2915 Rascher U., Gioli, B., Miglietta, F., 2008. FLEX – Fluorescence Explorer: A remote sensing approach to
2916 quantify spatio-temporal variations of photosynthetic efficiency from space, in: Allen, J.F., Gantt E.,
2917 Golbeck, J.H., Osmond, B. (Eds.), *Photosynthesis. Energy from the Sun*. Springer, Dordrecht, pp. 1387-
2918 1390.
- 2919 Rascher, U., Hütt, M.-T., Siebke, K., Osmond, B., Beck, F., Lüttge, U., 2001. Spatiotemporal variation of
2920 metabolism in a plant circadian rhythm: The biological clock as an assembly of coupled individual
2921 oscillators. *Proc. Natl. Acad. Sci. USA* 98, 11801-11805.
- 2922 Rascher, U., Lüttge, U., 2002. High-resolution chlorophyll fluorescence imaging serves as a non-invasive
2923 indicator to monitor the spatio-temporal variations of metabolism during the day-night cycle and during
2924 the endogenous rhythm in continuous light in the CAM plant *Kalanchoë daigremontiana*. *Plant Biology*
2925 4, 671-681.
- 2926 Rivera, J.P., Verrelst, J., Gómez-Dans, J., Muñoz-Marí, J., Moreno, J., Camps-Valls, G., 2015. An
2927 emulator toolbox to approximate radiative transfer models with statistical learning. *Remote Sens.* 7, 9347-
2928 9370.
- 2929 Roháček, K., Soukupová, J., Barták, M., 2008. Chlorophyll fluorescence: A wonderful tool to study plant
2930 physiology and plant stress, in: Schoefs, B. (Ed.), *Plant Cell Compartments – Selected Topics*. Kerala
2931 India, Research Signpost, pp. 41-104.
- 2932 Romero, J.M., Cordon, G.B., Lagorio, M.G., 2018. Modeling re-absorption of fluorescence from the leaf
2933 to the canopy level. *Remote Sens. Environ.* 204, 138-146.
- 2934 Rosema, A., Snel, J.F.H., Zahn, H., Buurmeijer, W.F., Van Hove, L.W.A., 1998. The relation between
2935 laser-induced chlorophyll fluorescence and photosynthesis. *Remote Sens. Environ.* 65, 143-154.
- 2936 Rosema, A., Verhoef, W., Noorbergen, H., Borgesius, J.J., 1992. A new forest light interaction model in
2937 support of forest monitoring. *Remote Sens. Environ.* 42, 23-41.
- 2938 Rosema, A., Verhoef, W., Schroote, J., Snel, J.F.H., 1991. Simulating fluorescence light-canopy
2939 interaction in support of laser-induced fluorescence measurements. *Remote Sens. Environ.* 37, 117-130.
- 2940 Rossini, M., Meroni, M., Celesti, M., Cogliati, S., Julitta, T., Panigada, C., Rascher, U., Van der Tol, C.,
2941 Colombo, R., 2016. Analysis of red and far-red sun-induced chlorophyll fluorescence and their ratio in
2942 different canopies based on observed and modeled data. *Remote Sens.* 8, 412.
- 2943 Rossini, M., Meroni, M., Migliavacca, M., Manca, G., Cogliati, S., Busetto, L., Picchi, V., Cescatti, A.,
2944 Seufert, G., Colombo, R., 2010. High resolution field spectroscopy measurements for estimating gross
2945 ecosystem production in a rice field. *Agric. For. Meteorol.* 150, 1283-1296.
- 2946 Rossini, M., Nedbal, L., Guanter, L., Ač, A., Alonso, L., Burkart, A., Cogliati, S., Colombo, R., Damm,
2947 A., Drusch, M., Hanus, J., Janoutova, R., Julitta, T., Kokkalis, P., Moreno, J., Novotny, J., Panigada, C.,

- 2948 Pinto, F., Schickling, A., Schüttemeyer, D., Zemek, F., Rascher, U., 2015. Red and far-red sun-induced
2949 chlorophyll fluorescence as a measure of plant photosynthesis. *Geophys. Res. Lett.* 42, 1632-1639.
- 2950 Ryu, Y., Baldocchi, DD, Kobayashi, H., van Ingen, C., Li, J., Black, T.A., Beringer, J., van Gorsel, E.,
2951 Knohl, A., Law, B.E., Rouspard, O., 2011. Integration of MODIS land and atmosphere products with a
2952 coupled-process model to estimate gross primary productivity and evapotranspiration from 1 km to global
2953 scales. *Global Biogeochemical Cycles* 25, doi: 10.1029/2011GB004053.
- 2954 Ryu, Y., Berry, J.A., Baldocchi, D.D., 2019. What is global photosynthesis? History, uncertainties and
2955 opportunities. *Remote Sens. Environ.* 223, 95-114.
- 2956 Sabater, N., Alonso, L., Cogliati, S., Vicent, J., Tenjo, C., Verrelst, J., Moreno, J., 2015. A sun-induced
2957 vegetation fluorescence retrieval method from top of atmosphere radiance for the FLEX/Sentinel-3
2958 tandem mission, in: *Proc. IEEE International Geoscience and Remote Sensing Symposium (IGARSS)*,
2959 26-31 July 2015, Milan, Italy, pp. 2669-2672.
- 2960 Sabater, N., Vicent, J., Alonso, L., Cogliati, S., Verrelst, J., Moreno, J., 2017. Impact of atmospheric
2961 inversion effects on solar-induced chlorophyll fluorescence: Exploitation of the apparent reflectance as a
2962 quality indicator. *Remote Sens.* 9, 622.
- 2963 Sabater N., Vicent, J., Alonso, L., Verrelst, J., Middleton, E.M., Porcar–Castell, A., Moreno, J., 2018.
2964 Compensation of oxygen transmittance effects for proximal sensing retrieval of canopy-leaving sun-
2965 induced chlorophyll fluorescence. *Remote Sens.* 10, 1551.
- 2966 Sanders, A.F.J., Verstraeten, W.W., Kooreman, M.L., Van Leth, T.C., Beringer, C., Joiner, J., 2016.
2967 Spaceborne sun-induced vegetation fluorescence time series from 2007 to 2015 evaluated with Australian
2968 flux tower measurements. *Remote Sens.* 8, 895.
- 2969 Schickling, A., Matveeva, M., Damm, A., Schween, J.H., Wahner, A., Graf, A., Crewell, S., Rascher, U.,
2970 2016. Combining sun-induced chlorophyll fluorescence and photochemical reflectance index improves
2971 diurnal modeling of gross primary productivity. *Remote Sens.* 8, 574.
- 2972 Schlapfer, D., Nieke, J., Itten, K.I., 2007. Spatial PSF nonuniformity effects in airborne pushbroom
2973 imaging spectrometry data. *IEEE Trans. Geosci. Remote Sens.* 45, 458-468.
- 2974 Schmuck, G., Moya, I., 1994. Time-resolved chlorophyll fluorescence spectra of intact leaves. *Remote
2975 Sens. Environ.* 47, 72-76.
- 2976 Scholze, M., Buchwitz, M., Dorigo, W., Guanter, L., Quegan, S., 2017. Reviews and syntheses:
2977 Systematic Earth observations for use in terrestrial carbon cycle data assimilation systems.
2978 *Biogeosciences* 14, 3401-3429.
- 2979 Schreiber, U., 2004. Pulse-amplitude-modulation (PAM) fluorometry and saturation pulse method: An
2980 overview, in: Papageorgiou, G.C., Govindjee (Eds.), *Chlorophyll a Fluorescence: A Signature of
2981 Photosynthesis*. Springer, Dordrecht, pp. 279-319.
- 2982 Schreiber, U., Bilger, W., Neubauer, C., 1995. Chlorophyll fluorescence as a nonintrusive indicator for
2983 rapid assessment of *in vivo* photosynthesis, in: Schulze, E.-D., Caldwell, M.M. (Eds.) *Ecophysiology of
2984 Photosynthesis*. Springer, Berlin/Heidelberg, pp. 49-70.

- 2985 Schreiber, U., Schliwa, U., Bilger, W., 1986. Continuous recording of photochemical and non-
 2986 photochemical chlorophyll fluorescence quenching with a new type of modulation fluorometer.
 2987 Photosynth. Res. 10, 51-62.
- 2988 Sellers, P.J., Tucker, C.J., Collatz, G.J., Los, S.O., Justice, C.O., Dazlich, D.A., Randall, D.A., 1996. A
 2989 revised land surface parameterization (SiB2) for atmospheric GCMs. Part II: The generation of global
 2990 fields of terrestrial biophysical parameters from satellite data. Journal of Climate 9, 706-737.
- 2991 Simmer, C., Thiele-Eich, I., Masbou, M., Amelung, W., Bogena, H., Crewell, S., Diekkrüger, B., Ewert,
 2992 F., Hendricks Franssen, H.-J., Huisman, J.A., Kemna, A., Klitzsch, N., Kollet, S., Langensiepen, M.,
 2993 Löhnert, U., Rahman, A.S.M.M., Rascher, U., Schneider, K., Schween, J., Shao, Y., Shrestha, P., Stiebler,
 2994 M., Sulis, M., Vanderborght, J., Vereecken, H., Van der Kruk, J., Waldhoff, G., Zerenner, T., 2015.
 2995 Monitoring and modeling the terrestrial system from pores to catchments: The Transregional
 2996 Collaborative Research Center on Patterns in the Soil–Vegetation–Atmosphere System. Bull. Am.
 2997 Meteorol. Soc. 96, 1765-1787.
- 2998 Smith, W.K., Biederman, J.A., Scott, R.L., Moore, D.J.P., He, M., Kimball, J.S., Yan, D., Hudson, A.,
 2999 Barnes, M.L., MacBean, N., Fox, A.M., Litvak, M.E., 2018. Chlorophyll fluorescence better captures
 3000 seasonal and interannual gross primary productivity dynamics across dryland ecosystems of southwestern
 3001 North America. Geophys. Res. Lett. 45, 748-757.
- 3002 Sobrino, J.A., Franch, B., Jimenez-Muñoz, J.C., Hidalgo, V., Soria, G., Julien, Y., Oltra-Carrio, R.,
 3003 Mattar, C., Ruescas, A., Daumard, F., Champagne, S., Fournier, A., Goulas, Y., Ounis, A., Moya, I.,
 3004 2011. Fluorescence estimation in the framework of the CEFLES2 campaign. Int. J. Remote Sens. 32,
 3005 5875-5889.
- 3006 Song, L., Guanter, L., Guan, K., You, L., Huete, A., Ju, W., Zhang, Y., 2018. Satellite sun-induced
 3007 chlorophyll fluorescence detects early response of winter wheat to heat stress in the Indian Indo-Gangetic
 3008 Plains. Glob. Change Biol. 2018, 1-15.
- 3009 Soukupová, J., Cséfalvay, L., Urban, O., Košvancová, M., Marek, M., Rascher, U., Nedbal, L., 2008.
 3010 Annual variation of the steady-state chlorophyll fluorescence emission of evergreen plants in temperate
 3011 zone. Funct. Plant Biol. 35, 63-76.
- 3012 Srivastava, P., Pandey, J., 2012. LICF spectrum as a fast detector of chlorophyll damage in safflower
 3013 growing under mutagenic stress. World Journal of Agricultural Sciences 8, 322-325.
- 3014 Stober, F., Lang, M., Lichtenthaler, H.K., 1994. Blue, green, and red fluorescence emission signatures of
 3015 green, etiolated, and white leaves. Remote Sens. Environ. 47, 65-71.
- 3016 Stokes, G.G., 1852. On the change of refrangibility of light. Trans. R. Soc. Lond. 142, 463-562.
- 3017 Stoll, M.-P., Laurila, T., Cunin, B., Gitelson, A.A., Lichtenthaler, H.K., Häme, T. 1999. FLEX:
 3018 Fluorescence Explorer – a space mission for screening vegetated areas in the Fraunhofer lines, in: Proc.
 3019 SPIE 3868, Remote Sensing for Earth Science, Ocean, and Sea Ice Applications, 20-24 September 1999,
 3020 Florence, Italy, pp. 108-119.
- 3021 Strand, M., Öquist, G., 1988. Effects of frost hardening, dehardening and freezing stress on *in vivo*
 3022 chlorophyll fluorescence of seedlings of Scots pine (*Pinus sylvestris* L.). Plant Cell Environ. 11, 231-238.
- 3023 Strasser, R.J., Srivastava, A., Govindjee, 1995. Polyphasic chlorophyll *a* fluorescence transient in plants
 3024 and cyanobacteria. Photochem. Photobiol. 61, 32-42.

- 3025 Subhash, N., 1995. Detection of vegetation stress from laser-induced fluorescence signatures.
3026 International Centre for Theoretical Physics (Trieste, Italy), LAMP Series Report, LAMP/95/4, June
3027 1995.
- 3028 Subhash, N., Mohanan, C.N., 1997. Curve-fit analysis of chlorophyll fluorescence spectra: Application to
3029 nutrient stress detection in sunflower. *Remote Sens. Environ.* 60, 347-356.
- 3030 Suits, G.H., 1972. The calculation of the directional reflectance of a vegetative canopy. *Remote Sens.*
3031 *Environ.* 2, 117-125.
- 3032 Sun, Y., Frankenberg, C., Jung, M., Joiner, J., Guanter, L., Köhler, P., Magney, T.S., 2018. Overview of
3033 solar-induced chlorophyll fluorescence (SIF) from the Orbiting Carbon Observatory-2: Retrieval, cross-
3034 mission comparison, and global monitoring for GPP. *Remote Sens. Environ.* 209, 808-823.
- 3035 Sun, Y., Frankenberg, C., Wood, J.D., Schimel, D.S., Jung, M., Guanter, L., Drewry, D.T., Verma, M.,
3036 Porcar-Castell, A., Griffis, T.J., Gu, L., Magney, T.S., Köhler, P., Evans, B., Yuen, K., 2017. OCO-2
3037 advances photosynthesis observation from space via solar-induced chlorophyll fluorescence. *Science* 358,
3038 eaam5747, doi: 10.1126/science.aam5747.
- 3039 Sun, Y., Fu, R., Dickinson, R., Joiner, J., Frankenberg, C., Gu, L., Xia, Y., Fernando, N., 2015. Drought
3040 onset mechanisms revealed by satellite solar-induced chlorophyll fluorescence: Insights from two
3041 contrasting extreme events. *J. Geophys. Res. Biogeosci.* 120, 2427-2440.
- 3042 Sylak-Glassman, E.J., Zaks, J., Amarnath, K., Leuenberger, M., Fleming, G.R., 2016. Characterizing non-
3043 photochemical quenching in leaves through fluorescence lifetime snapshots. *Photosynth. Res.* 127, 69-76.
- 3044 Szabó, K., Lichtenthaler, H.K., Kocsányi, L., Richter, P., 1992. A CCD-OMA device for the
3045 measurement of complete chlorophyll fluorescence emission spectra of leaves during the fluorescence
3046 induction kinetics. *Radiat. Environ. Biophys.* 31, 153-160.
- 3047 Terjung, F., 1998. Reabsorption of chlorophyll fluorescence and its effects on the spectral distribution and
3048 the picosecond decay of higher plant leaves. *Z. Naturforsch. C.* 53, 924-926.
- 3049 Thum, T., Zaehle, S., Köhler, P., Aalto, T., Aurela, M., Guanter, L., Kolari, P., Laurila, T., Lohila, A.,
3050 Magnani, F., Van Der Tol, C., Markkanen, T., 2017. Modelling sun-induced fluorescence and
3051 photosynthesis with a land surface model at local and regional scales in northern Europe. *Biogeosciences*
3052 14, 1969-1987.
- 3053 Toivonen, P., Vidaver, W., 1984. Integrating fluorometer for the measurement of chlorophyll
3054 fluorescence induction in intact plants. *Rev. Sci. Instrum.* 55, 1687-1690.
- 3055 Turner, D., Lucieer, A., Malenovsky, Z., King, D.H., Robinson, S.A., 2014. Spatial co-registration of
3056 ultra-high resolution visible, multispectral and thermal images acquired with a micro-UAV over Antarctic
3057 moss beds. *Remote Sens.* 6, 4003-4024.
- 3058 Vácha, F., Sarafis, V., Benediktyová, Z., Bumba, L., Valenta, J., Vácha, M., Sheue, Ch.-R., Nedbal, L.,
3059 2007. Identification of Photosystem I and Photosystem II enriched regions of thylakoid membrane by
3060 optical microimaging of cryo-fluorescence emission spectra and of variable fluorescence. *Micron* 38, 170-
3061 175.
- 3062 Valentini, R., Cecchi, G., Mazzinghi, P., Scarascia Mungnozza, G., Agati, G., Bazzani, M., De Angelis,
3063 P., Fusi, F., Matteucci, G., Raimondi, V., 1994. Remote sensing of chlorophyll *a* fluorescence of

- 3064 vegetation canopies: 2. Physiological significance of fluorescence signal in response to environmental
3065 stresses. *Remote Sens. Environ.* 47, 29-35.
- 3066 Van de Hulst, H.C., 1981. *Light scattering by small particles*. Dover Publications, New York.
- 3067 Van de Hulst, H.C., 1957. *Light scattering by small particles*. John Wiley & Sons, New York.
- 3068 Van der Tol, C., Berry, J.A., Campbell, P.K.E., Rascher, U., 2014. Models of fluorescence and
3069 photosynthesis for interpreting measurements of solar-induced chlorophyll fluorescence. *J. Geophys. Res.*
3070 *Biogeosci.* 119, 2312-2327.
- 3071 Van der Tol, C., Rossini, M., Cogliati, S., Verhoef, W., Colombo, R., Rascher, U., Mohammed, G., 2016.
3072 A model and measurement comparison of diurnal cycles of sun-induced chlorophyll fluorescence of
3073 crops. *Remote Sens. Environ.* 186, 663-677.
- 3074 Van der Tol, C., Verhoef, W., Rosema, A., 2009a. A model for chlorophyll fluorescence and
3075 photosynthesis at leaf scale. *Agric. For. Meteorol.* 149, 96-105.
- 3076 Van der Tol, C., Verhoef, W., Timmermans, J., Verhoef, A., Su, Z., 2009b. An integrated model of soil-
3077 canopy spectral radiances, photosynthesis, fluorescence, temperature and energy balance. *Biogeosciences*
3078 6, 3109-3129.
- 3079 Van Kooten, O., Snel, J.F.H., 1990. The use of chlorophyll fluorescence nomenclature in plant stress
3080 physiology. *Photosynth. Res.* 25, 147-150.
- 3081 Van Wittenberghe, S., Alonso, L., Verrelst, J., Hermans, I., Delegido, J., Veroustraete, F., Valcke, R.,
3082 Moreno, J., Samson, R., 2013. Upward and downward solar-induced chlorophyll fluorescence yield
3083 indices of four tree species as indicators of traffic pollution in Valencia. *Environ. Pollut.* 173, 29-37.
- 3084 Van Wittenberghe, S., Alonso, L., Verrelst, J., Hermans, I., Valcke, R., Veroustraete, F., Moreno, J.,
3085 Samson, R., 2014. A field study on solar-induced chlorophyll fluorescence and pigment parameters along
3086 a vertical canopy gradient of four tree species in an urban environment. *Sci. Total Environ.* 466-467, 185-
3087 194.
- 3088 Van Wittenberghe, S., Alonso, L., Verrelst, J., Moreno, J., Samson, R., 2015. Bidirectional sun-induced
3089 chlorophyll fluorescence emission is influenced by leaf structure and light scattering properties – A
3090 bottom-up approach. *Remote Sens. Environ.* 158, 169-179.
- 3091 Verhoef, W., 1984. Light scattering by leaf layers with application to canopy reflectance modeling: The
3092 SAIL model. *Remote Sens. Environ.* 16, 125-141.
- 3093 Verhoef, W., 1985. Earth observation modeling based on layer scattering matrices. *Remote Sens.*
3094 *Environ.* 17, 165-178.
- 3095 Verhoef, W., Van der Tol, C., Middleton, E.M., 2014. Vegetation canopy fluorescence and reflectance
3096 retrieval by model inversion using optimization, in: *Proc. 5th International Workshop on Remote Sensing*
3097 *of Vegetation Fluorescence*, 22-24 April 2014, Paris, France.
- 3098 Verhoef, W., Van der Tol, C., Middleton, E.M., 2018. Hyperspectral radiative transfer modeling to
3099 explore the combined retrieval of biophysical parameters and canopy fluorescence from FLEX –
3100 Sentinel-3 tandem mission multi-sensor data. *Remote Sens. Environ.* 204, 942-963.

- 3101 Verma, M., Schimel, D., Evans, B., Frankenberg, C., Beringer, J., Drewry, D.T., Magney, T., Marang, I.,
3102 Hutley, L., Moore, C., Eldering, A., 2017. Effect of environmental conditions on the relationship between
3103 solar-induced fluorescence and gross primary productivity at an OzFlux grassland site. *J. Geophys. Res.*
3104 *Biogeosci.* 122, 716-733.
- 3105 Verrelst, J., Camps-Valls, G., Muñoz-Marí, J., Rivera, J.P., Veroustraete, F., Clevers, J.G.P.W., Moreno,
3106 J., 2015a. Optical remote sensing and the retrieval of terrestrial vegetation bio-geophysical properties – A
3107 review. *ISPRS J. Photogramm. Remote Sens.* 108, 273-290.
- 3108 Verrelst, J., Rivera, J.P., 2017. A global sensitivity analysis toolbox to quantify drivers of vegetation
3109 radiative transfer models, in: Petropoulos, G., Srivastava, P. (Eds.) *Sensitivity Analysis in Earth*
3110 *Observation Modelling*. Elsevier, pp. 319-339.
- 3111 Verrelst, J., Van der Tol, C., Magnani, F., Sabater, N., Rivera, J.P., Mohammed, G., Moreno, J., 2016.
3112 Evaluating the predictive power of sun-induced chlorophyll fluorescence to estimate net photosynthesis of
3113 vegetation canopies: A SCOPE modeling study. *Remote Sens. Environ.* 176, 139-151.
- 3114 Verrelst, J., Rivera, J.P., Van der Tol, C., Magnani, F., Mohammed, G., Moreno, J., 2015b. Global
3115 sensitivity analysis of the SCOPE model: What drives simulated canopy-leaving sun-induced
3116 fluorescence? *Remote Sens. Environ.* 166, 8-21.
- 3117 Vicent, J., Sabater, N., Tenjo, C., Acarreta, J.R., Manzano, M., Rivera, J.P., Jurado, P., Franco, R.,
3118 Alonso, L., Verrelst, J., Moreno, J., 2016. FLEX end-to-end mission performance simulator. *IEEE Trans.*
3119 *Geosci. Remote Sens.* 54, 4215-4223.
- 3120 Vilfan, N., Van der Tol, C., Muller, O., Rascher, U., Verhoef, W., 2016. Fluspect-B: A model for leaf
3121 fluorescence, reflectance and transmittance spectra. *Remote Sens. Environ.* 186, 596-615.
- 3122 Vilfan, N., Van der Tol, C., Yang, P., Wyber, R., Malenovský, Z., Robinson, S.A., Verhoef, W., 2018.
3123 Extending Fluspect to simulate xanthophyll driven leaf reflectance dynamics. *Remote Sens. Environ.* 211,
3124 345-356.
- 3125 Vogelmann, T.C., Bornman, J.F., Yates, D.J., 1996. Focusing of light by leaf epidermal cells. *Physiol.*
3126 *Plant.* 98, 43-56.
- 3127 Vogelmann, T.C., Evans, J.R., 2002. Profiles of light absorption and chlorophyll within spinach leaves
3128 from chlorophyll fluorescence. *Plant Cell Environ.* 25, 1313-1323.
- 3129 Von Hebel, C., Matveeva, M., Verweij, E., Rademske, P., Kaufmann, M.S., Brogi, C., Vereecken, H.,
3130 Rascher, U., Van der Kruk, J., 2018. Understanding soil and plant interaction by combining ground-based
3131 quantitative electromagnetic induction and airborne hyperspectral data. *Geophys. Res. Lett.* 45, 7571-
3132 7579.
- 3133 Wagle, P., Zhang, Y., Jin, C., Xiao, X., 2016. Comparison of solar-induced chlorophyll fluorescence,
3134 light-use efficiency, and process-based GPP models in maize. *Ecol. Appl.* 26, 1211-1222.
- 3135 Walker, A.P., Quaipe, T., Van Bodegom, P.M., De Kauwe, M.G., Keenan, T.F., Joiner, J., Lomas, M.R.,
3136 MacBean, N., Xu, C., Yang, X., Woodward, F.I., 2017. The impact of alternative trait-scaling hypotheses
3137 for the maximum photosynthetic carboxylation rate (V_{cmax}) on global gross primary production. *New*
3138 *Phytol.* 215, 1370-1386.

- 3139 Walthers, S., Guanter, L., Heim, B., Jung, M., Duveiller, G., Wolanin, A., Sachs, T., 2018. Assessing the
3140 dynamics of vegetation productivity in circumpolar regions with different satellite indicators of greenness
3141 and photosynthesis. *Biogeosciences* 15, 6221-6255.
- 3142 Walthers, S., Voigt, M., Thum, T., Gonsamo, A., Zhang, Y., Köhler, P., Jung, M., Varlagin, A., Guanter,
3143 L., 2016. Satellite chlorophyll fluorescence measurements reveal large-scale decoupling of photosynthesis
3144 and greenness dynamics in boreal evergreen forests. *Glob. Change Biol.* 22, 2979-2996.
- 3145 Wang, S., Huang, C., Zhang, L., Lin, Y., Cen, Y., Wu, T., 2016. Monitoring and assessing the 2012
3146 drought in the Great Plains: Analyzing satellite-retrieved solar-induced chlorophyll fluorescence, drought
3147 indices, and gross primary production. *Remote Sens.* 8, 61.
- 3148 Watson, R.D., Hemphill, W.R., 1976. Use of an airborne Fraunhofer line discriminator for the detection
3149 of solar stimulated luminescence. U.S. Geological Survey Open-File Report 76-202, 109 p.,
3150 <https://doi.org/10.3133/ofr76202>.
- 3151 Wei, X., Wang, X., Wei, W., Wan, W., 2018. Use of sun-induced chlorophyll fluorescence obtained by
3152 OCO-2 and GOME-2 for GPP estimates of the Heihe River Basin, China. *Remote Sens.* 10, 2039.
- 3153 Weis, E., Berry, J.A., 1987. Quantum efficiency of Photosystem II in relation to ‘energy’-dependent
3154 quenching of chlorophyll fluorescence. *Biochim. Biophys. Acta* 894, 198-208.
- 3155 Wieneke, S., Burkart, A., Cendrero-Mateo, M.P., Julitta, T., Rossini, M., Schickling, A., Schmidt, M.,
3156 Rascher, U., 2018. Linking photosynthesis and sun-induced fluorescence at sub-daily to seasonal scales.
3157 *Remote Sens. Environ.* 219, 247-258.
- 3158 Wieneke, S., Ahrends, H., Damm, A., Pinto, F., Stadler, A., Rossini, M., Rascher, U., 2016. Airborne
3159 based spectroscopy of red and far-red sun-induced chlorophyll fluorescence: Implications for improved
3160 estimates of gross primary productivity. *Remote Sens. Environ.* 184, 654-667.
- 3161 Wohlfahrt, G., Gerdel, K., Migliavacca, M., Rotenberg, E., Tatarinov, F., Müller, J., Hammerle, A.,
3162 Julitta, T., Spielmann, F.M., Yakir, D. 2018. Sun-induced fluorescence and gross primary productivity
3163 during a heat wave. *Sci. Rep.* 8, 14169.
- 3164 Wolanin, A., Rozanov, V.V., Dinter, T., Noël, S., Vountas, M., Burrows, J.P., Bracher, A., 2015. Global
3165 retrieval of marine and terrestrial chlorophyll fluorescence at its red peak using hyperspectral top of
3166 atmosphere radiance measurements: Feasibility study and first results. *Remote Sens. Environ.* 166, 243-
3167 261.
- 3168 Wong, C.Y., Gamon, J.A., 2015. Three causes of variation in the photochemical reflectance index (PRI)
3169 in evergreen conifers. *New Phytol.* 206, 187-195.
- 3170 Wood, J.D., Griffis, T.J., Baker, J.M., Frankenberg, C., Verma, M., Yuen, K., 2017. Multiscale analyses
3171 of solar-induced fluorescence and gross primary production. *Geophys. Res. Lett.* 44, 533-541.
- 3172 Wu, X., Xiao, X., Zhang, Y., He, W., Wolf, S., Chen, J., He, M., Gough, C.M., Qin, Y., Zhou, Y.,
3173 Doughty, R., Blanken, P.D., 2018. Spatiotemporal consistency of four gross primary production products
3174 and solar-induced chlorophyll fluorescence in response to climate extremes across CONUS in 2012. *J.*
3175 *Geophys. Res. Biogeosci.* 123, doi.org/10.1029/2018JG004484.

- 3176 Wyber, R., Malenovsky, Z., Ashcroft, M.B., Osmond, B., Robinson, S.A., 2017. Do daily and seasonal
3177 trends in leaf solar induced fluorescence reflect changes in photosynthesis, growth or light exposure?
3178 Remote Sens. 9, 604.
- 3179 Xu, S., Liu, Z., Zhao, L., Zhao, H., Ren, S., 2018. Diurnal response of sun-induced fluorescence and PRI
3180 to water stress in maize using a near-surface remote sensing platform. Remote Sens. 10, 1510.
- 3181 Yang, J., Tian, H., Pan, S., Chen, G., Zhang, B., Dangal, S., 2018a. Amazon drought and forest response:
3182 Largely reduced forest photosynthesis but slightly increased canopy greenness during the extreme drought
3183 of 2015/2016. Glob. Change Biol. 24, 1919-1934.
- 3184 Yang, K., Ryu, Y., Dechant, B., Berry, J.A., Hwang, Y., Jiang, C., Kang, M., Kim, J., Kimm, H.,
3185 Kornfeld, A., Yang, X., 2018b. Sun-induced chlorophyll fluorescence is more strongly related to absorbed
3186 light than to photosynthesis at half-hourly resolution in a rice paddy. Remote Sens. Environ. 216, 658-
3187 673.
- 3188 Yang, P., Van der Tol, C., 2018. Linking canopy scattering of far-red sun-induced chlorophyll
3189 fluorescence with reflectance. Remote Sens. Environ. 209, 456-467.
- 3190 Yang P., Van der Tol, C., Verhoef, W., Damm, A., Schickling, A., Kraska, T., Muller, O., Rascher, U. (in
3191 press). Using reflectance to explain vegetation biochemical and structural effects on sun-induced
3192 chlorophyll fluorescence. Remote Sens. Environ., doi 10.1016/j.rse.2018.11.039.
- 3193 Yang, P., Verhoef, W., Van der Tol, C., 2017. The mSCOPE model: A simple adaptation to the SCOPE
3194 model to describe reflectance, fluorescence and photosynthesis of vertically heterogeneous canopies.
3195 Remote Sens. Environ. 201, 1-11.
- 3196 Yang, X., Tang, J., Mustard, J.F., Lee, J.-E., Rossini, M., Joiner, J., Munger, J.W., Kornfeld, A.,
3197 Richardson, A.D., 2015. Solar-induced chlorophyll fluorescence that correlates with canopy
3198 photosynthesis on diurnal and seasonal scales in a temperate deciduous forest. Geophys. Res. Lett. 42,
3199 2977-2987.
- 3200 Yang, X., Shi, H., Stovall, A., Guan, K., Miao, G., Zhang, Y., Zhang, Y., Xiao, X., Ryu, Y., Lee, J.-E.,
3201 2018c. FluoSpec 2—An automated field spectroscopy system to monitor canopy solar-induced
3202 fluorescence. Sensors 18, 2063.
- 3203 Yoshida, Y., Joiner, J., Tucker, C., Berry, J., Lee, J.-E., Walker, G., Reichle, R., Koster, R., Lyapustin,
3204 A., Wang, Y., 2015. The 2010 Russian drought impact on satellite measurements of solar-induced
3205 chlorophyll fluorescence: Insights from modeling and comparisons with parameters derived from satellite
3206 reflectances. Remote Sens. Environ. 166, 163-177.
- 3207 Zaks, J., Amarnath, K., Kramer, D.M., Niyogi, K.K., Fleming, G.R., 2012. A kinetic model of rapidly
3208 reversible nonphotochemical quenching. Proc. Natl. Acad. Sci. USA 109, 15757-15762.
- 3209 Zarco-Tejada, P.J., Camino, C., Beck, P.S.A., Calderon, R., Hornero, A., Hernández-Clemente, R.,
3210 Kattenborn, T., Montes-Borrego, M., Susca, L., Morelli, M., Gonzalez-Dugo, V., North, P.R.J., Landa,
3211 B.B., Boscia, D., Saponari, M., Navas-Cortes, J.A., 2018. Previsual symptoms of *Xylella fastidiosa*
3212 infection revealed in spectral plant-trait alterations. Nat. Plants 4, 432-439.
- 3213 Zarco-Tejada, P.J., Catalina, A., González, M.R., Martín, P., 2013a. Relationships between net
3214 photosynthesis and steady-state chlorophyll fluorescence retrieved from airborne hyperspectral imagery.
3215 Remote Sens. Environ. 136, 247-258.

- 3216 Zarco-Tejada, P.J., González-Dugo, V., Berni, J.A.J., 2012. Fluorescence, temperature and narrow-band
3217 indices acquired from a UAV platform for water stress detection using a micro-hyperspectral imager and
3218 a thermal camera. *Remote Sens. Environ.* 117, 322-337.
- 3219 Zarco-Tejada, P.J., Miller, J.R., Mohammed, G.H., Noland, T.L., Sampson, P.H., 1999a. Canopy optical
3220 indices from infinite reflectance and canopy reflectance models for forest condition monitoring:
3221 Application to hyperspectral CASI data, in: Proc. IEEE International Geoscience and Remote Sensing
3222 Symposium (IGARSS), 28 June-2 July 1999, Hamburg, Germany, Vol. 3, pp. 1878-1881.
- 3223 Zarco-Tejada, P.J., Miller, J.R., Mohammed, G.H., Noland, T.L., Sampson, P.H., 1999b. Optical indices
3224 as bioindicators of forest condition from hyperspectral CASI data, in: Proceedings 19th EARSeL
3225 Symposium on Remote Sensing in the 21st Century, 31 May-2 June 1999, Valladolid, Spain.
- 3226 Zarco-Tejada, P.J., Miller, J.R., Mohammed, G.H., Noland, T.L., 2000a. Chlorophyll fluorescence effects
3227 on vegetation apparent reflectance: I. Leaf-level measurements and model simulation. *Remote Sens.*
3228 *Environ.* 74, 582-595.
- 3229 Zarco-Tejada, P.J., Miller, J.R., Mohammed, G.H., Noland, T.L., Sampson, P.H., 2000b. Chlorophyll
3230 fluorescence effects on vegetation apparent reflectance: II. Laboratory and airborne canopy-level
3231 measurements with hyperspectral data. *Remote Sens. Environ.* 74, 596-608.
- 3232 Zarco-Tejada, P.J., Miller, J.R., Mohammed, G.H., Noland, T.L., Sampson, P.H., 2001. Estimation of
3233 chlorophyll fluorescence under natural illumination from hyperspectral data. *Int. J. Appl. Earth Obs.*
3234 *Geoinf.* (Special Issue on Applications of Imaging Spectroscopy) 3, 321-327.
- 3235 Zarco-Tejada, P.J., Miller, J.R., Mohammed, G.H., Noland, T.L., Sampson, P.H., 2002. Vegetation stress
3236 detection through chlorophyll a+b estimation and fluorescence effects on hyperspectral imagery. *J.*
3237 *Environ. Qual.* 31, 1433-1441.
- 3238 Zarco-Tejada, P.J., Miller, J.R., Pedrós, R., Verhoef, W., Berger, M., 2006. FluorMODgui V3.0: A
3239 graphic user interface for the spectral simulation of leaf and canopy chlorophyll fluorescence. *Computers*
3240 *& Geosciences* 32, 577-591.
- 3241 Zarco-Tejada, P.J., Morales, A., Testi, L., Villalobos, F.J., 2013b. Spatio-temporal patterns of chlorophyll
3242 fluorescence and physiological and structural indices acquired from hyperspectral imagery as compared
3243 with carbon fluxes measured with eddy covariance. *Remote Sens. Environ.* 133, 102-115.
- 3244 Zarco-Tejada, P.J., Pushnik, J.C., Dobrowski, S., Ustin, S.L., 2003. Steady-state chlorophyll *a*
3245 fluorescence detection from canopy derivative reflectance and *double-peak* red-edge effects. *Remote*
3246 *Sens. Environ.* 84, 283-294.
- 3247 Zhang, Y., Guanter, L., Berry, J.A., Joiner, J., Van der Tol, C., Huete, A., Gitelson, A., Voigt, M., Köhler,
3248 P., 2014. Estimation of vegetation photosynthetic capacity from space-based measurements of chlorophyll
3249 fluorescence for terrestrial biosphere models. *Glob. Chang. Biol.* 20, 3727-3742.
- 3250 Zhang, Y., Guanter, L., Berry, J.A., Van der Tol, C., Yang, X., Tang, J., Zhang, F., 2016a. Model-based
3251 analysis of the relationship between sun-induced chlorophyll fluorescence and gross primary production
3252 for remote sensing applications. *Remote Sens. Environ.* 187, 145-155.
- 3253 Zhang, Y., Guanter, L., Joiner, J., Song, L., Guan, K., 2018a. Spatially-explicit monitoring of crop
3254 photosynthetic capacity through the use of space-based chlorophyll fluorescence data. *Remote Sens.*
3255 *Environ.* 210, 362-374.

- 3256 Zhang, Y., Joiner, J., Alemohammad, S.H., Zhou, S., Gentine, P., 2018b. A global spatially Continuous
3257 Solar Induced Fluorescence (CSIF) dataset using neural networks. *Biogeosciences* 15, 5779-5800.
- 3258 Zhang, Y., Joiner, J., Gentine, P., Zhou, S., 2018c. Reduced solar-induced chlorophyll fluorescence from
3259 GOME-2 during Amazon drought caused by dataset artifacts. *Glob. Change Biol.* 24,
3260 <https://doi.org/10.1111/gcb.14134>.
- 3261 Zhang, Y., Xiao, X., Guanter, L., Zhou, S., Ciais, P., Joiner, J., Sitch, S., Wu, X., Nabel, J., Dong, J.,
3262 Kato, E., Jain, A.K., Wiltshire, A., Stocker, B.D., 2016b. Precipitation and carbon-water coupling jointly
3263 control the interannual variability of global land gross primary production. *Sci. Rep.* 6, 39748.
- 3264 Zhang, Y., Xiao, X., Jin, C., Dong, J., Zhou, S., Wagle, P., Joiner, J., Guanter, L., Zhang, Y., Zhang, G.,
3265 Qin, Y., Wang, J., Moore III, B., 2016c. Consistency between sun-induced chlorophyll fluorescence and
3266 gross primary production of vegetation in North America. *Remote Sens. Environ.* 183, 154-169.
- 3267 Zhang, Y., Xiao, X., Zhang, Y., Wolf, S., Zhou, S., Joiner, J., Guanter, L., Verma, M., Sun, Y., Yang, X.,
3268 Paul-Limoges, E., Gough, C.M., Wohlfahrt, G., Gioli, B., Van der Tol, C., Yann, N., Lund, M., De
3269 Grandcourt, A., 2018d. On the relationship between sub-daily instantaneous and daily total gross primary
3270 production: Implications for interpreting satellite-based SIF retrievals. *Remote Sens. Environ.* 205, 276-
3271 289.
- 3272 Zhang, Y.J., Liu, L.Y., Hou, M.Y., Liu, L.T., Li, C.D., 2009. Progress in remote sensing of vegetation
3273 chlorophyll fluorescence. *Journal of Remote Sensing* 13, 963-978.
- 3274 Zhang, Z., Zhang, Y., Joiner, J., Migliavacca, M., 2018e. Angle matters: Bidirectional effects impact the
3275 slope of relationship between gross primary productivity and sun-induced chlorophyll fluorescence from
3276 Orbiting Carbon Observatory-2 across biomes. *Glob. Change Biol.* 24, 5017-5020.
- 3277 Zhao, F., Dai, X., Verhoef, W., Guo, Y., Van der Tol, C., Li, Y., Huang, Y., 2016. FluorWPS: A Monte
3278 Carlo ray-tracing model to compute sun-induced chlorophyll fluorescence of three-dimensional canopy.
3279 *Remote Sens. Environ.* 187, 385-399.
- 3280 Zhao, F., Guo, Y., Verhoef, W., Gu, X., Liu, L., Yang, G., 2014. A method to reconstruct the solar-
3281 induced canopy fluorescence spectrum from hyperspectral measurements. *Remote Sens.* 6, 10171-10192.
- 3282 Zhao, F., Li, R., Verhoef, W., Cogliati, S., Liu, X., Huang, Y., Guo, Y., Huang, J., 2018. Reconstruction
3283 of the full spectrum of solar-induced chlorophyll fluorescence: Intercomparison study for a novel method.
3284 *Remote Sens. Environ.* 219, 233-246.
- 3285 Zhou, X., Liu, Z., Xu, S., Zhang, W., Wu, J., 2016. An automated comparative observation system for
3286 sun-induced chlorophyll fluorescence of vegetation canopies. *Sensors* 16, 775.
- 3287 Zoogman, P., Liu, X., Suleiman, R.M., Pennington, W.F., Flittner, D.E., Al-Saadi, J.A., Hilton, B.B.,
3288 Nicks, D.K., Newchurch, M.J., Carr, J.L., Janz, S.J., Andraschko, M.R., Arola, A., Baker, B.D., Canova,
3289 B.P., Miller, C.C., Cohen, R.C., Davis, J.E., Dussault, M.E., Edwards, D.P., Fishman, J., Ghulam, A.,
3290 González Abad, G., Grutter, M., Herman, J.R., Houck, J., Jacob, D.J., Joiner, J., Kerridge, B.J., Kim, J.,
3291 Krotkov, N.A., Lamsal, L., Li, C., Lindfors, A., Martin, R.V., McElroy, C.T., McLinden, C., Natraj, V.,
3292 Neil, D.O., Nowlan, C.R., O'Sullivan, E.J., Palmer, P.I., Pierce, R.B., Pippin, M.R., Saiz-Lopez, A.,
3293 Spurr, R.J.D., Szykman, J.J., Torres, O., Veeffkind, J.P., Veihelmann, B., Wang, H., Wang, J., Chance, K.,
3294 2016. Tropospheric emissions: Monitoring of pollution (TEMPO). *J. Quant. Spectrosc. Radiat. Transfer*
3295 186, 17-39.

3296 Zuromski, L.M., Bowling, D.R., Köhler, P., Frankenberg, C., Goulden, M.L., Blanken, P.D., Lin, J.C.,
3297 2018. Solar-induced fluorescence detects interannual variation in gross primary production of coniferous
3298 forests in the western United States. *Geophys. Res. Lett.* 45, 7184-7193.